THE NONMESONIC WEAK DECAY OF HYPERNUCLEI

A. PARREÑO

Departament d'Estructura i Constituents de la Matèria
Facultat de Física
Universitat de Barcelona

Maig, 1997

A la meva costella...

Agraïments

Quan vaig acabar la carrera el Ferran em va parlar d'una noia jove que tot just havia aconseguit una plaça de professora titular al Departament. Llavors, no podia imaginar tot el que acabaria aprenent sota la direcció de l'Àngels. M'ha contagiat part del seu entusiasme i m'ha ensenyat a ser crítica, fent ús d'unes bones dosis de paciència, però a més, hem passat moltes estones entranyables i divertides juntes, dins i fora de la Universitat. Per tot el que m'has donat durant aquest temps, gràcies *jefa*.

Són moltes les persones que m'han ajudat al llarg dels últims anys i que han contribuït d'alguna forma a la confecció d'aquesta tesi doctoral. A totes elles els hi voldria fer arribar un sincer sentiment d'agraïment. Per descomptat, no ho hauria pogut fer sense el suport de la meva família, i en especial del Bernat, pacient i increiblement comprensiu.

Vull donar les gràcies als companys del Departament, als que hi són ara i als que van marxar. Al Ferran, al $|JM\rangle$, al Druida, a la Cristina, a J.M. *el vasco*, a F.X. *efectos mortales*, al Víctor, al Wens... els quals, a més d'ajudar-me a resoldre *dubtes existencials*, han fet que els dies al Departament fossin més alegres. Especialment, estic en deute amb el Jordi, pel seu suport. Espero seguir gaudint amb ell i amb la seva futura dona, l'Anna, de moments tant divertits i emotius com els que hem passat fins ara. Gràcies també al J. Rovira i a la Marien per la seva amistat incondicional i per saber comprendre tots els canvis d'ànim que he patit durant els últims dies. A la Sus, tan apassionada a la vida com a la feina. I al meu cunyat Jordi, que tant d'afecte m'ha mostrat des de que el vaig conèixer.

Agraïr a la *Srta. Volpe* i al Luis les bones estones que em van fer passar durant aquell agost plujós del 96.

I would like to deeply thank Cornelius Bennhold for his constant help and guidance during my doctoral studies and for his kind hospitality during my stays in Washington DC.

I also want to express my gratitude to Mona, Henrik, JC, Levant, W. Glöckle, J. Golak and H. Kamada, for their valuable help and the nice time we spent together.

Voldria fer arribar la meva gratitud a tots aquells membres del Departament que em van proporcionar el seu suport quan ho vaig necessitar, així com agraïr-los totes aquelles contribucions científiques a la meva formació.

Also I acknowledge the Center of Nuclear Studies of the GWU, the TRIUMF Theory Group and the University of Bochum, for providing me with all the facilities I needed in my Research Stays.

Por útimo, quisiera agradecer al Ministerio de Educación y Ciencia el apoyo económico que me ha proporcionado y sin el cual la confección de esta tesis no hubiera sido posible.

Contents

Introduction

The strangeness quantum number, S, which is conserved by the strong and electromagnetic interactions but not by the weak one, allows one to label the particles belonging to the octet baryon family in such a way that $S = 0$ for nucleons and $-2 \leq S \leq -1$ for particles with strangeness (Λ, Σ, Ξ). The mass of the lightest strange baryon, the Λ-particle, is 1115.684 ± 0.006 MeV and its mean life is $\tau_\Lambda = (2.632 \pm 0.020) \times 10^{-10}$ s. The Λ can be considered a stable particle once one compares the value of its lifetime with the time scale of strong interactions ($10^{-20} - 10^{-24}$ s.). The weak decay of the Λ can proceed via two different modes. In the mesonic mode ($\Lambda \rightarrow N\pi$) a meson and a nucleon are detected in the final state. This decay is 10^3 times larger than the leptonic one ($\Lambda \rightarrow p + e^- + \nu_e$), due to the three body final state. The free Λ decays almost totally into a pion and a nucleon following the approximate ratio of 64% for $\Lambda \rightarrow n\pi^-$ and 36% for $\Lambda \rightarrow p\pi^0$.

A hypernucleus is a bound system of conventional non-strange baryons (neutrons and protons) plus one or more strange baryons. Traditionally, the Λ and the Σ particles were referred to as "hyperons". Nowadays, and in the context of hypernuclear physics, this notation has been extended to any baryon with non-zero strangeness. Hypernuclear physics has received a lot of attention since the early emulsion and bubble chamber experiments [Ju73,Ca74,Pn85] aimed at establishing how the presence of the new flavor (strangeness) broadens the knowledge achieved by the conventional field of nuclear physics and helps in understanding the breaking of SU(3) symmetry. One of the goals of hypernuclear research is to relate the hypernuclear observables to the

bare hyperon-nucleon interaction. Experimental data for the lightest Λ-hypernuclear systems show that the ΛN interaction has quite a different behavior than the NN interaction. For instance, there exists an indication of a more attractive behavior for a singlet spin state compared to a triplet one by about 1 MeV for the ΛN system, just the opposite than in the NN case. We can use hypernuclei to explore such problems as the origin of the nuclear spin-orbit force, short-range correlations, relativistic aspects of many-body nuclear dynamics and their extension to hypernuclei, the role of flavor symmetry and the chiral limit, extended models of the strong interaction, weak interactions in the nuclear medium, or possible modifications of baryon properties in the nuclear environment. Many of the phenomena involving strangeness can only be studied using bound hypernuclear systems, as the short lifetime of hyperons and low intensity fluxes make it difficult to have free hyperon targets or hyperon beams.

Although major achievements in hypernuclear physics have taken place at a slow pace due to limited statistics, the in-flight (K^-,π^-) counter experiments carried out at CERN [Be79,Br75] and Brookhaven [Ch79] revealed a considerable amount of hypernuclear features, such as small spin-orbit strength, increased validity of single-particle motion of the Λ, narrow widths of Σ-hypernuclei (though recent experiments could not verify those), etc., injecting a renewed interest in the field. Since then, the experimental facilities have been upgraded and experiments using the (π^+,K^+) and ($K^-_{stopped}$,π^0) reactions are being conducted at the Brookhaven AGS and KEK accelerators with higher beam intensities and improved energy resolution. Moreover, the photo- and electro-production of strangeness will be studied at TJNL [Sc95] and the low energy K^- beam from ϕ decay will be exploited at DAΦNE for studies of both high resolution hypernuclear spectroscopy and weak decay of hypernuclei [FI95]. It is expected that new improved experimental data will bring the field of hypernuclear physics to a stage in which major advances can be made.

Hypernuclei are typically produced in some excited state through hadronic reactions such as (K^-,π^-) or (π^+,K^+), but can reach their ground state through electromagnetic gamma and/or nucleon emission. Hypernuclei that are stable against strong decay modes (such as particle emission) can decay via weak interaction mechanisms which are nonleptonic in nature, involving the emission of pions and nucleons. This is the case of the ground state of Λ-hypernuclei ($_\Lambda$A), which are the only bound nuclear systems (stable in the time scale of strong interaction) with strangeness $S = -1$. Note that, unlike the Λ hyperon, the Σ in the nucleus decays via the strong interaction due to the

$\Sigma N \rightarrow \Lambda N$ conversion.

When the Λ is embedded in the nuclear medium the mesonic decay mode ($\Lambda \rightarrow N\pi$) becomes Pauli blocked due to the value of the final nucleon momentum (approximately 100 MeV/c), which lies below the Fermi momentum. The rate of this decay mode is suppressed with respect to the free value by several orders of magnitude and a new mechanism shows up, the nonmesonic weak decay ($\Lambda N \rightarrow NN$), in which no mesons are detected in the final state. This mode is dominant for heavier hypernuclei (A greater than 5). Experimentally, the lifetimes of hypernuclei are found to be more or less independent of A [BM90]. This is due to a compensating effect between the decrease of the mesonic channel as A increases, because of the stronger Pauli blocking, and an increase of the nonmesonic channel due to the larger number of nucleons. When A is large the decay proceeds mainly through the nonmesonic mode, which shows a saturation behavior due to the short-range character of the ΛN interaction. There is another possible nonmesonic decay channel, the two-nucleon induced process $\Lambda NN \rightarrow NNN$, where the virtual pion emitted at the weak vertex can be viewed as being absorbed by a pair of nucleons which are correlated through the strong force. This mechanism was first investigated in Ref. [AP91] where it was suggested that its magnitude could be comparable to the $\Lambda N \rightarrow NN$ one. However, a reanalysis with more realistic assumptions [RO94,RO95] reduced its contribution to 10 - 15% of the total nonmesonic decay rate.

The nonmesonic weak interaction does not conserve parity, isospin and strangeness. One of the most interesting points in the study of the nonmesonic weak decay channel is to gain insight into the fundamental aspects of the four-fermion, strangeness changing weak interaction. In this two-body weak process one can obtain information from both the parity-conserving (PC) and the parity-violating (PV) amplitudes, by taking advantage of the strangeness change ($\Delta S = 1$) as a signature. This is in contrast to the NN weak interaction where it is actually impossible to see the parity-conserving component, as it is masked by the strong NN interaction.

Many theoretical efforts have been made in the understanding of the underlying weak dynamics which governs the nonmesonic weak decay of hypernuclei. A number of theoretical approaches to the nonmesonic $\Lambda N \rightarrow NN$ decay mode have been developed over the last thirty years, which are extensively reviewed in Ref. [Co90]. The interpretation of the available data has been done with the use of different models, namely, the usual meson-exchange model, the description in terms of quarks or a combination

of a meson-exchange description for the long range of the interaction and the quark description for the short-range one.

The early phenomenological analyses by Dalitz *et al.* [DR62] provided the general nonrelativistic structure of the $\Lambda N \rightarrow NN$ amplitude which was then related to decay rates of s-shell hypernuclei using certain simplifying assumptions. The $\Delta S = 0$ weak nucleon-nucleon interaction at low and intermediate energies has generally been described in a meson-exchange model involving one strong interaction vertex and one weak one; the same basic assumption has been used by some authors for a microscopic description of the $\Delta S = 1$ $\Lambda N \rightarrow NN$ mechanism. The virtual pion emitted at the weak $\Lambda N\pi$ vertex is interpreted as being absorbed by one nucleon bound in the hypernucleus. Early calculations based on the one-pion exchange (OPE) mechanism were due to Adams [Ad67]. Modifications of the OPE due to strong interactions in the nuclear medium were suggested in Ref. [OS85] to account for many-body nuclear structure effects. At the very least, the OPE mechanism can be expected to adequately describe the long-range part of the $\Lambda N \rightarrow NN$ interaction. Due to the Λ - N mass difference, the $\Lambda N \rightarrow NN$ process involves large momentum transfers and, therefore, it is expected to be quite insensitive to nuclear structure details. Furthermore, this large momentum leads to a mechanism where short distance effects are very important and thus raises the possibility of receiving contributions from more massive mesons, apart from the pion, in the nonmesonic hyperon decay process. The production threshold of these mesons is too high for the free space Λ decay, but they can contribute through virtual exchange in a two-baryon decay channel. The first attempts to include heavier mesons, at first the ρ meson —again in complete analogy to the $\Delta S = 0$ NN interaction —, were presented in Refs. [MG84,Na88,TT85]. There were several conference papers by Dubach *et al.* [Du86] showing results of preliminary calculations with a full meson-exchange potential; a more detailed account of their calculations has recently become available [DF96]. Finally, there have been recent attempts to construct the weak transition potential incorporating the exchange of the ρ and σ mesons, in addition to the OPE mechanism, from the point of view of a correlated 2π-exchange. Refs. [IU95,Sh94] obtained the weak vertex through the coupling of the two pions to the ρ and σ mesons and intermediate N and Σ baryon states.

Apart from the meson-exchange models, there exist other works based on the use of quark degrees of freedom in the description of the $\Lambda N \rightarrow NN$ transition potential. In Refs. [CH83,HK86] the process was separated into a long-range region, to be described

by OPE, and a short-range region, modelled by a six-quark interaction with suitable adjusted parameters. This idea was revived in Ref. [IT96], where the weak transition amplitude is considered at quark level and the baryon transition potential is evaluated in lowest-order perturbation theory. Although promising, these lines of study are still at an early stage, since the connection between the effective quark hamiltonian and the empirical $\Lambda \rightarrow N\pi$ vertex remains to be established.

In recent years, a series of counter experiments carried out at BNL (USA) and KEK (Japan) improved the quality of data on the nonmesonic decay modes, using pion and kaon beams. Total and partial hypernuclear decay rates for ${}^{5}_{\Lambda}$He, ${}^{11}_{\Lambda}$B and ${}^{12}_{\Lambda}$C have been measured at Brookhaven [Sz91]. More recently, new data from the weak decay of ${}^{12}_{\Lambda}$C and ${}^{11}_{\Lambda}$B were obtained at KEK [No95]. Also at KEK, the asymmetry of the angular distribution of protons coming from the decay of polarized ${}^{12}_{\Lambda}$C and ${}^{11}_{\Lambda}$B, produced via the (π^+,K^+) reaction, was obtained [Aj92], determining for the first time the difference in the number of protons emitted along the axis of polarization compared to the number ejected in the opposite direction.

This introduction of polarization observables into the field of hypernuclear decay calls for a new consideration of the theoretical efforts, the reason being that the asymmetry is related to an interference of PV and PC amplitudes and thus might pose further constraints than those provided by total and partial rates, which are dominated by the PC piece of the weak transition.

While all the theoretical approaches mentioned above describe reasonably well the lifetimes of the hypernuclear states, they fail to reproduce the ratio of neutron- to proton-stimulated Λ decay, Γ_n/Γ_p.

The present work is an attempt to describe the nonmesonic weak decay mechanism within the one-boson-exchange model, including as few approximations as possible in order to reproduce the available experimental data and to propose new experiments for the near future. The motivation of this work is two-fold. First, in contrast to most previous investigations performed in nuclear matter, where only the ΛN L=0 relative motion is retained, this study analyses the $\Lambda N \rightarrow NN$ decay in hypernuclei using a shell-model framework. The Λ particle can interact with nucleons in s-shell, p-shell or higher orbits thus giving rise to a substantial amount of ΛN pairs having a $L \neq 0$ relative motion. Secondly, this calculation includes not only the long-ranged pion but also contributions from the other pseudoscalar mesons, the η and the K, as well as the vector mesons ρ, ω and K^*. Due to the large momentum carried by

the emitted nucleons, nuclear structure uncertainties are minimal and one can use the present framework to draw conclusions regarding the sensitivity to the underlying weak baryon-baryon-meson couplings. In this way, one may extract, via the comparison with the experiment, the theoretical ingredients that are not yet well known.

The nonmesonic weak decay taking place in several hypernuclei (${}^{12}_{\Lambda}$C, ${}^{11}_{\Lambda}$B, ${}^{5}_{\Lambda}$He and ${}^{3}_{\Lambda}$H) will be studied. For the description of the initial hypernucleus, a shell-model approach will be used, except for the case of the hypertriton for which the Faddeev equations using realistic ΛN and NN interactions have been solved. In order to take into account short-range effects, which have been demonstrated to be of great importance, appropriate short-range correlations for the initial ΛN system as well as for the final NN system will be considered. SU(6) symmetry and soft-meson theorems have been used for the evaluation of the parity-violating vertices of the weak baryon-baryon-meson interaction, as well as the pole model to obtain the parity-conserving ones. The different models one can use by now for obtaining the weak coupling constants will be explored, with the goal of extracting a good set of constants from the study of the weak mechanism.

In Chapter 1, the nonmesonic decay rate of a hypernucleus, Γ_{nm}, is expressed in terms of two-body amplitudes corresponding to the ΛN → NN transition. Also derived is an expression for the asymmetry in the distribution of protons coming from the weak decay of polarized hypernuclei.

In Chapter 2, the formalism used for obtaining the two-body decay is presented and developed with all the realistic ingredients necessary for this study.

Chapter 3 is devoted to the discussion of the results obtained for the different shell-model hypernuclei studied throughout this work. These results include the nonmesonic decay rate in units of the free Λ decay rate, $\Gamma_{nm}/\Gamma_{\Lambda}$, the intrinsic lambda asymmetry parameter, a_{Λ}, and the neutron-to-proton induced decay ratio, Γ_n/Γ_p. A comparison with other calculations and experimental data is also given within this chapter.

In Chapter 4, a brief study of the decay of the hypertriton, ${}^{3}_{\Lambda}$H, is made. Here, all the nuclear structure ingredients are derived from the same baryon-baryon interaction.

To conclude this work, Chapter 5 gives an overview and an outlook of this topic and presenting, from our point of view, the experimental and theoretical requirements that are needed for future improvements in this field.

Chapter 1

Decay Rate and Asymmetry

In the first section of this chapter the nonmesonic decay rate of a hypernucleus, $\Gamma_{\rm nm}$, is expressed in terms of two-body amplitudes corresponding to the $\Lambda N \rightarrow NN$ transition. Following a weak coupling scheme for the Λ-particle to the $(A-1)$-particle core and employing the technique of coefficients of fractional parentage, the Λ and a nucleon belonging to the hypernucleus are separated from the residual $(A-2)$-particle system in order to express the hypernuclear transition amplitude in terms of the two-body $t_{\Lambda N \rightarrow NN}$ amplitude.

In § 1.2, an expression for the asymmetry in the distribution of protons coming from the weak decay of polarized hypernuclei is also given.

1.1 Decay Rate

Assuming the initial hypernucleus to be at rest, the nonmesonic decay rate is given by:

$$\Gamma_{\rm nm} = \int \frac{d^3k_1}{(2\pi)^3} \int \frac{d^3k_2}{(2\pi)^3} \sum_{\substack{M_i \{R\} \\ \{1\}\{2\}}} (2\pi)\, \delta(M_H - E_R - E_1 - E_2)\, \frac{1}{(2J+1)}\, \mid \mathcal{M}_{fi} \mid^2 , \quad (1.1)$$

where the quantities M_H, E_R, E_1 and E_2 are the mass of the hypernucleus, the energy of the residual $(A-2)$-particle system, and the total asymptotic energies of the emitted nucleons, respectively. The integration variables $\vec{k}_1$ and $\vec{k}_2$ stand for the momenta of the

two nucleons in the final state. Note that the momentum conserving delta function has been used to integrate over the momentum of the residual nucleus. The sum, together with the factor $1/(2J+1)$, indicates an average over the initial hypernucleus spin projections, M_i, and a sum over all quantum numbers of the residual $(A-2)$-particle system, $\{R\}$, as well as the spin and isospin projections of the exiting nucleons, $\{1\}$ and $\{2\}$.

The nuclear transition amplitude $\mathcal{M}_{fi} =< F \mid \mathcal{M} \mid I >$ can be expressed in terms of the elementary two-body amplitudes. In order to do that, the A-particle final state, $\mid F >$, needs to be decomposed in products of antisymmetric two-particle and residual $(A-2)$-particle wave functions

$$\mid F >= \mathcal{A} \left\{ \Psi_{k_1 m_{s_1} t_{3_1}, k_2 m_{s_2} t_{3_2}} \cdot \Psi_R^{A-2} \right\} , \tag{1.2}$$

where R stands for the quantum numbers of the residual $(A-2)$ nuclear state, $\{R\} = \{E_R J_R M_R T_R T_{3R}\}$. The operator $\mathcal{A}$ antisymmetrizes the nucleons belonging to different wave functions. When a transformation to the total momentum, $\vec{P} = \vec{k}_1 + \vec{k}_2$, and relative momentum, $\vec{k} = (\vec{k}_1 - \vec{k}_2)/2$, of the two outgoing nucleons is performed, the expression for $\Gamma_{\rm nm}$ becomes:

$$\Gamma_{\rm nm} = \int \frac{d^3P}{(2\pi)^3} \int \frac{d^3k}{(2\pi)^3} \overline{\sum} \, (2\pi) \, \delta(M_H - E_R - E_1 - E_2) \mid \mathcal{M}_{fi} \mid^2 , \tag{1.3}$$

with $\mathcal{M}_{fi} = \left\langle \Psi_R; \vec{P}\vec{k} \; S \, M_S \; T \, M_T \right| \mathcal{M} \left| {}_\Lambda A \right\rangle = \left\langle \Psi_R; \vec{P}\vec{k} \; S \, M_S \; T \, M_T \right| \hat{O}_{\Lambda N \to NN} \left| {}_\Lambda A \right\rangle$ the amplitude for the transition from an initial hypernuclear state to a final state which is divided into a two-nucleon state and a residual $(A-2)$-particle state Ψ_R. The two-nucleon state is characterized by the total momentum $\vec{P}$, the relative momentum $\vec{k}$, the spin and spin projection SM_S and the isospin and isospin projection TM_T. In Eq. (1.3) the sum $\overline{\sum}$ stands for the averaged sum explained above, and $\hat{O}_{\Lambda N \to NN}$ is a two-body operator acting on all possible ΛN pairs.

For the decomposition of the initial state we follow Ref. [RM92] and assume a weak coupling scheme where the isoscalar Λ in an orbit $\alpha_\Lambda = \{n_\Lambda l_\Lambda s_\Lambda j_\Lambda m_\Lambda\}$ couples only to the ground state wave function of the nuclear $(A-1)$-core with total angular momentum J_C and projection M_C

$$\begin{aligned} \mid {}_\Lambda A)^{J_I M_I}_{T_I T_{3_I}} &= \mid \alpha_\Lambda \rangle \times \mid A-1 \rangle \\ &= \sum_{m_\Lambda M_C} \langle j_\Lambda m_\Lambda \, J_C M_C \mid J_I M_I \rangle \mid (n_\Lambda l_\Lambda s_\Lambda) j_\Lambda m_\Lambda \rangle \mid J_C M_C \, T_I T_{3_I} \rangle \end{aligned} \tag{1.4}$$

Table 1.1. Possible quantum numbers for the initial hypernucleus and the residual system for ${}^{5}_{\Lambda}$He, ${}^{11}_{\Lambda}$B and ${}^{12}_{\Lambda}$C.

A	J_I	T_I	T_{3I}	J_C	$T_R^{\min}$	$T_R^{\max}$	$J_R^{\min}$	$J_R^{\max}$
5	1/2	0	0	0	1/2	1/2	1/2	1/2
11	5/2	0	0	3	1/2	1/2	3/2	9/2
12	1	1/2	1/2	3/2	0	1	0	3

Note that the Λ-particle has isospin equal to zero, so the values of the $(A-1)$-core isospin and its projection are the same as those of the initial hypernucleus.

The nonmesonic decay of hypernuclei, proceeding through a two-body mechanism, requires the decomposition of the $\mid A-1 >$ core wave function into a set of states where a nucleon in a certain orbit $\alpha_{\rm N} = \{n_{\rm N} l_{\rm N} s_{\rm N} j_{\rm N} m_{\rm N}\}$ is coupled to the residual $(A-2)$-particle state via the technique of coefficients of fractional parentage (c.f.p.) [BG77]. The c.f.p. are defined by [CK67]:

$$\begin{aligned}\Psi_{\rm as}^{J_C T_C \alpha}(1....N) &= \sum_{J_{R_0} T_{R_0} \alpha_0 j_{\rm N}} \langle J_C T_C \alpha \{\mid J_{R_0} T_{R_0} \alpha_0, j_{\rm N}\rangle \\ &\times \; [\Psi_{\rm as}^{J_{R_0} T_{R_0} \alpha_0}(1....N-1) \times \phi^{j_{\rm N}}(N)]^{J_C T_C} \;, \end{aligned} \tag{1.5}$$

which relates the wave function for N active nucleons to the wave functions for (N-1) nucleons. The quantum numbers refer to angular momentum J, isospin T and the energy eigenvalue α. The subscript "0" always refers to the residual states of (N-1) nucleons and the subscript "as" recalls that the (N-1)-particle as well as the N-particle states are antisymmetrized. The bracket around the wave functions on the right implies vector coupling to form a state with total angular momentum J_C and isospin T_C. The expression for the hypernuclear decay rate will be given in terms of spectroscopic factors defined by:

$$S(J_C T_C \alpha; J_{R_0} T_{R_0} \alpha_0, j_{\rm N}) = N \cdot \langle J_C T_C \alpha \{\mid J_{R_0} T_{R_0} \alpha_0, j_{\rm N}\rangle^2 \;, \tag{1.6}$$

where the factor N comes in since the decoupled nucleon can be any of the N particles in the antisymmetric initial state. Following this technique one is able to separate one nucleon from the $(A-1)$-particle core, and write the wave function in terms of the antisymmetric wave function of the $(A-2)$ residual nucleus.

The core wave function is then finally written as:

$$
\begin{aligned}
\mid J_C M_C T_I T_{3_I}\rangle &= \sum_{J_R T_R j_N} \langle J_C\, T_I \{\mid J_R\, T_R, j_N\, t_N\rangle [\mid J_R,\, T_R\rangle \times \mid (n_N l_N s_N) j_N,\, t_N\rangle]^{J_C M_C}_{T_I T_{3_I}} \\
&= \sum_{J_R T_R j_N} \langle J_C\, T_I \{\mid J_R\, T_R, j_N\, t_N\rangle \\
&\times \sum_{M_R m_N} \sum_{T_{3_R} t_{3_t}} \langle J_R M_R\, j_N m_N \mid J_C M_C\rangle \langle T_R T_{3_R}\, t_N t_{3_t} \mid T_I T_{3_I}\rangle \\
&\times \mid J_R M_R\rangle \mid T_R T_{3_R}\rangle \mid (n_N l_N s_N) j_N m_N\rangle \mid t_N t_{3_t}\rangle \,, \qquad (1.7)
\end{aligned}
$$

where $t_N = 1/2$. In Table 1.1 the values of the total angular momentum (J_I) and the isospin and isospin projection (T_I,T_{3I}) are shown for the different hypernuclei studied throughout this work ($^{5}_{\Lambda}$He, $^{11}_{\Lambda}$B and $^{12}_{\Lambda}$C). Also listed is the corresponding value of the core total angular momentum, J_C, as well as the minimum and maximum quantum numbers of the residual system, J_R and T_R, which are obtained when an s- or p-shell nucleon is decoupled from the core wave function.

The present work is restricted to p-shell nuclei, so only the $s_{1/2}$, $p_{3/2}$ and $p_{1/2}$ orbits will be treated. For s-shell pick-up the c.f.p. can be evaluated following Ref. [BG77]. Using Cohen and Kurath's spectroscopic factors for p-shell pick-up [CK67] removes the limitation to only the extreme shell-model $p_{3/2}$ configuration. In Ref. [CK67] the factors for $1p_{3/2}$ and $1p_{1/2}$ nucleons are given separately. In this work, the energy dependence (α_0) of the spectroscopic factors will be disregarded and those corresponding to states of the residual nucleus with the same quantum numbers will be summed up. These sums include contributions from all the higher excited states, however, very little strength lies in these states. The summed spectroscopic factors, $S = (A-1)\ \langle J_C T_I \{\mid J_R T_R, j_N t_N\rangle$, appropriate for the decay of $^{12}_{\Lambda}$C, are shown in Table 1.2.

The results of pick-up reactions are usually interpreted in the independent-particle model which does not satisfy translational invariance. It is important to correct for the lack of this invariance by projecting out the spurious components of the many-body wave function. Thus, following Ref. [DF74], for p-shell pick-up one multiplies the spectroscopic factors by $A/(A-1)$ while the s-shell pick-up corrections are $1/2\ [2 - (N-2)/(A-1)]$ for neutrons and $1/2\ [2 - (Z-2)/(A-1)]$ for protons, corrections which effectively shift some strength from the s-shell to the p-shell contribution. When working in p-shell nuclei, one can check these correction factors by imposing:

$$N = N_0 S_0^n + (N - N_0) S_1 \qquad (1.8)$$

$$Z = Z_0 S_0^{\rm p} + (Z - Z_0) S_1 \ , \tag{1.9}$$

where N (Z) is the total number of neutrons (protons), N_0 (Z_0) the number of neutrons (protons) in the s-shell and S_i^α the corrected spectroscopic factor for the i^{th}-shell being α =n (p) for neutrons (protons). The corrected spectroscopic factors for ${}^{12}_{\Lambda}$C are shown in Table 1.2.

Table 1.2. Spectroscopic factors for s-shell and p-shell pick-up from ${}^{12}_{\Lambda}$C. $S^{\rm n}$ and $S^{\rm p}$ stand for the corrected spectroscopic factors for neutrons and protons, respectively.

	J_R	T_R	S	$S^{\rm n}$	$S^{\rm p}$
s-shell	1	0	0.375	0.319	0.300
	1	1	1.125	0.956	0.900
	2	0	0.625	0.531	0.500
	2	1	1.875	1.594	1.500
$p_{3/2}$-shell	0	0	0.000	0.000	0.000
	0	1	0.653	0.718	0.718
	1	0	0.606	0.667	0.667
	1	1	0.129	0.142	0.142
	2	0	0.097	0.107	0.107
	2	1	3.038	3.341	3.341
	3	0	1.239	1.363	1.363
	3	1	0.125	0.137	0.137
$p_{1/2}$-shell	1	0	0.312	0.343	0.343
	1	1	0.104	0.115	0.115
	2	0	0.246	0.271	0.271
	2	1	0.451	0.496	0.496

The previous considerations take the full details of hypernuclear structure into account, within a shell-model picture, and allow us to write the hypernuclear decay rate in terms of the two-body ΛN$\rightarrow$NN amplitudes.

In general, hypernuclei with Λ's in excited orbitals will rapidly decay into the ground state through electromagnetic or strong deexcitation processes which are orders of

magnitude faster than the weak interaction. We will therefore assume the Λ to decay from the $l_\Lambda = 0$ state. Working in a coupled two-body spin and isospin basis, the nonmesonic decay rate in Eq. (1.3) can be written as:

$$\Gamma_{\rm nm} = \Gamma_{\rm n} + \Gamma_{\rm p} \ , \tag{1.10}$$

where $\Gamma_{\rm n}$ and $\Gamma_{\rm p}$ stand for the neutron- ($\Lambda {\rm n} \rightarrow {\rm nn}$) and proton-induced ($\Lambda {\rm p} \rightarrow {\rm np}$) decay rate, respectively, given by:

$$\begin{aligned}
\Gamma_{\rm t} \ = \ & \int \frac{d^3P}{(2\pi)^3} \int \frac{d^3k}{(2\pi)^3} (2\pi)\delta(M_H - E_R - E_1 - E_2) \sum_{SM_S} \sum_{J_R M_R} \sum_{T_R T_{3_R}} \frac{1}{2J_I + 1} \\
& \times \ \sum_{M_I} \mid \langle T_R T_{3_R} \frac{1}{2} t_{3_{\rm t}} \mid T_I T_{3_I} \rangle \mid^2 \\
& \times \ \Bigg| \sum_{TT_3} \langle TT_3 \mid \frac{1}{2} t_1 \, \frac{1}{2} t_2 \rangle \sum_{m_\Lambda M_C} \langle j_\Lambda m_\Lambda \, J_C M_C \mid J_I M_I \rangle \sum_{J{\rm N}} \sqrt{S\,(J_C\,T_I\,;J_R\,T_R\,,j_{\rm N}\,t_{3_{\rm t}})} \\
& \times \ \sum_{M_R m_{\rm N}} \langle J_R M_R \, j_{\rm N} m_{\rm N} \mid J_C M_C \rangle \sum_{m_{l_{\rm N}} m_{s_{\rm N}}} \langle j_{\rm N} m_{\rm N} \mid l_{\rm N} m_{l_{\rm N}} \frac{1}{2} m_{s_{\rm N}} \rangle \\
& \times \ \sum_{m_{l_\Lambda} m_{s_\Lambda}} \langle j_\Lambda m_\Lambda \mid l_\Lambda m_{l_\Lambda} \frac{1}{2} m_{s_\Lambda} \rangle \\
& \times \ \sum_{S_0 M_{S_0}} \langle S_0 M_{S_0} \mid \frac{1}{2} m_{s_\Lambda} \, \frac{1}{2} m_{s_{\rm N}} \rangle \sum_{T_0 T_{3_0}} \langle T_0 T_{3_0} \mid \frac{1}{2} \ -\frac{1}{2} \ \frac{1}{2} t_{3_{\rm t}} \rangle \\
& \times \ t_{\Lambda{\rm N}\rightarrow{\rm NN}}(S, M_S, T, M_T, S_0, M_{S_0}, T_0, T_{3_0}, l_\Lambda, l_{\rm N}, \vec{P}, \vec{k}) \Bigg|^2 \ ,
\end{aligned} \tag{1.11}$$

with $t_{3_{\rm t}} = 1/2$, $t_1 = -1/2$, $t_2 = 1/2$ for the p-induced rate and $t_{3_{\rm t}} = -1/2$, $t_1 = -1/2$, $t_2 = -1/2$ for the n-induced rate. Equation (1.11) is written in terms of the elementary amplitude $t_{\Lambda{\rm N}\rightarrow{\rm NN}}$, which accounts for the transition from an initial ΛN state with spin (isospin) S_0 (T_0) to a final antisymmetric NN state with spin (isospin) S (T). The details on how this two-body amplitude is calculated are given in the next chapter. Note that the Λ has been assumed to act as a $\mid 1/2 \ -1/2 \rangle$ isospin state which is coupled to the nucleon to total isospin T_0. As it will be explained in the next chapter, this is the way to incorporate the change in isospin, $\Delta T = 1/2$, induced by the weak transition operator.

Let us briefly discuss what is meant by the $\Delta T = 1/2$ rule. In the mesonic decay of the free Λ ($t_\Lambda = 0$) into a pion ($t_\pi = 1$) and a nucleon ($t_{\rm N} = 1/2$), both values of the total isospin, $T = 1/2$ and $T = 3/2$, are possible in the final state. Denoting by Γ_{π^0} the

mesonic $\Lambda \rightarrow n\pi^0$ decay and by Γ_{π^-} the mesonic $\Lambda \rightarrow p\pi^-$ decay, experimentally one observes a ratio of $\Gamma_{\pi^-}/\Gamma_{\pi^0}$ close to 2. Using isospin coupling algebra and neglecting the difference in mass of the final states, it is simple to show that assuming a change in isospin of 1/2 the value of the ratio $\Gamma_{\pi^-}/\Gamma_{\pi^0}$ is 2. Note that $\Gamma_{\pi^-}/\Gamma_{\pi^0}$ will involve a ratio of two Clebsch-Gordan coefficients, $\langle\ 1/2\ t_{3i}\ 1\ t_{3\pi}\ \mid\ T\ -1/2\ \rangle$, such that:

$$\begin{aligned} \frac{\Gamma_{\pi^-}}{\Gamma_{\pi^0}} &\approx \frac{|\ \langle\ \frac{1}{2}\ \frac{1}{2}\ 1\ -1\ \mid\ \frac{3}{2}\ -\frac{1}{2}\ \rangle\ |^2}{|\ \langle\ \frac{1}{2}\ -\frac{1}{2}\ 1\ 0\ \mid\ \frac{3}{2}\ -\frac{1}{2}\ \rangle\ |^2} \\ &= \frac{|\ \sqrt{\frac{1}{3}}\ |^2}{|\ \sqrt{\frac{2}{3}}\ |^2} = \frac{1}{2} \end{aligned} \tag{1.12}$$

for $T = 3/2$ in the final state, and

$$\begin{aligned} \frac{\Gamma_{\pi^-}}{\Gamma_{\pi^0}} &\approx \frac{|\ \langle\ \frac{1}{2}\ \frac{1}{2}\ 1\ -1\ \mid\ \frac{1}{2}\ -\frac{1}{2}\ \rangle\ |^2}{|\ \langle\ \frac{1}{2}\ -\frac{1}{2}\ 1\ 0\ \mid\ \frac{1}{2}\ -\frac{1}{2}\ \rangle\ |^2} \\ &= \frac{|\ -\sqrt{\frac{2}{3}}\ |^2}{|\ \sqrt{\frac{1}{3}}\ |^2} = 2 \end{aligned} \tag{1.13}$$

for $T = 1/2$. Only in the second case seems the experimental prediction to be recovered. Note, however, that the experimental decay fractions for $\Lambda \rightarrow p\pi^-$ and $\Lambda \rightarrow n\pi^0$ yield a ratio 1.8 [PRD96], which allows for some contributions of $\Delta T = 3/2$ amplitudes.

1.2 Asymmetry

When working with polarized hypernuclei one can obtain interesting information about the decay mechanism or, for example, the magnetic moments of hypernuclei. For instance, one can work with these hypernuclei in combination with coincidence measurements of the decay particles and study the angular distribution of particles coming from the nonmesonic weak decay.

The experiments carried out at Brookhaven (USA) [Sz91] and KEK (Japan) [Aj92] have obtained experimental information on total and partial rates as well as asymmetries of the exiting protons. The hypernuclear systems produced with either the (K^-, π^-) or the (π^+, K^+) reaction were two s-shell, ${}^{4}_{\Lambda}$He and ${}^{5}_{\Lambda}$He, and two p-shell, ${}^{12}_{\Lambda}$C and ${}^{11}_{\Lambda}$B, hypernuclei.

At the kinematic conditions of the (π^+, K^+) reaction performed at KEK the hypernucleus is created with a substantial amount of polarization in the ground state. Due

to the interference between the parity-conserving and parity-violating amplitudes, the distribution of the emitted protons in the weak decay displays an angular asymmetry with respect to the polarization axis. The (π^+, K^+) reaction produced hypernuclear states with large spin polarization aligned preferentially along the axis normal to the reaction plane. In particular, the KEK experiment measured the angular asymmetry in the distribution of protons from the nonmesonic weak decay of polarized ${}^{12}_{\Lambda}\mathrm{C}$ and ${}^{11}_{\Lambda}\mathrm{B}$.

In Fig. 1.1 a simplified picture of the (π^+, K^+) reaction is shown, where a polarized ${}^{A}_{\Lambda}\mathrm{Z}$ hypernucleus is produced. This picture has been represented in the S_{M} frame, where the Madison convention [BH71] has been chosen. According to this convention, the state of spin orientation of an assembly of particles, referred to as polarization, should be referred to a right handed coordinate system in which the positive z-axis is directed along the direction of momentum of the incoming beam, and the positive y-axis along $\vec{k}_{\mathrm{in}} \times \vec{k}_{\mathrm{out}}$ for the nuclear reaction from which the polarized particles emerge. For the (π^+, K^+) case, in the S_{M} frame, the positive z_{M}-axis is aligned along $\vec{k}_{\pi}$ (beam of incident pions) and the y_{M}-axis is along the $\vec{k}_{\pi} \times \vec{k}_{\mathrm{K}}$ direction, perpendicular to the (π^+, K^+)-plane.

A brief outline on how to calculate the angular asymmetry of the protons is presented in this section, but a more detailed calculation can be found in the Appendix B of Ref. [RM92]. The starting point for the evaluation of the asymmetry parameter is the intensity of the outgoing nucleons, given by:

$$\begin{aligned} I(\chi) &= Tr(\mathcal{M}\rho_i\mathcal{M}^+) \\ &= \sum_{FM_iM_i'} < F \mid \mathcal{M} \mid M_i >< M_i \mid \rho_i \mid M_i' >< M_i' \mid \mathcal{M}^+ \mid F > \end{aligned} \qquad (1.14)$$

where χ is the angle between the direction of the proton and the polarization axis, y_{M}. $\mathcal{M}$ represents the transition operator characteristic of the weak decay, F the final state, M_i the initial hypernucleus spin projection and ρ_i the density matrix for the polarized spin-J hypernucleus. Relating this expression with our problem, the transition matrix element $< F \mid \mathcal{M} \mid M_i >$ will be a function of $\vec{k}_1 m_1, \vec{k}_2 m_2, \vec{K}_R J_R M_R, J M_i$, where $\vec{k}_i m_i$ $(i = 1, 2)$ represent each of the outgoing nucleons, the subindex R stands for the residual nucleus and $\{JM_i\}$ for the initial hypernucleus.

For pure vector polarization perpendicular to the plane of the (π^+, K^+) reaction,

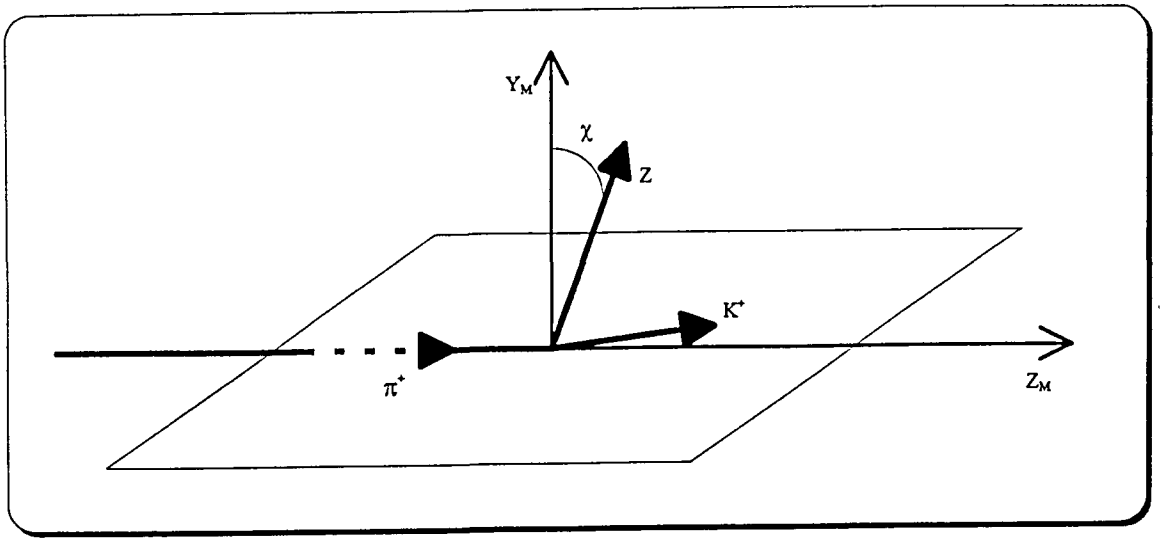

Figure 1.1. Schematic illustration of the (π^+, K^+) reaction producing a polarized ${}^{A}_{\Lambda}Z$ hypernucleus.

the density matrix is given by the expression:

$$\rho_i(J) = \frac{1}{2J+1}\left(1 + \frac{3}{J+1} P_y S_y\right) , \tag{1.15}$$

with S_y being the J-spin operator along the y_{M}-axis and P_y the hypernuclear polarization created in the production reaction. Introducing Eq. (1.15) in the expression of $I(\chi)$ one obtains:

$$\begin{aligned} I(\chi) &= I_0 \left(1 + \frac{3}{J+1} P_y \frac{Tr(\mathcal{M} S_y \mathcal{M}^+)}{Tr(\mathcal{M}\mathcal{M}^+)}\right) \\ &= I_0 \,(1 + \mathcal{A}) , \end{aligned} \tag{1.16}$$

where I_0 is the isotropic intensity for the unpolarized hypernucleus,

$$I_0 = \frac{Tr(\mathcal{M}\mathcal{M}^+)}{2J+1} , \tag{1.17}$$

and $\mathcal{A}$ the asymmetry, defined as:

$$\mathcal{A} = P_y \frac{3}{J+1} \frac{Tr(\mathcal{M} S_y \mathcal{M}^+)}{Tr(\mathcal{M}\mathcal{M}^+)} . \tag{1.18}$$

In Ref. [RM92] it is shown that, for pure vector polarization, the asymmetry $\mathcal{A}$ follows a simple $\cos\chi$ dependence. First, the trace in the numerator of Eq. (1.18) needs to be evaluated in the proton helicity frame (S) in which the transition amplitudes have been calculated. For each direction (θ, ϕ) the matrix elements of the S_y operator need to be transformed using the rotation matrices that bring the Madison frame $S_{\rm M}$ to the helicity frame S. Then, using the Wigner-Eckart theorem and the rotation matrix properties, the trace $Tr(\mathcal{M}S_y\mathcal{M}^+)$ can be expressed as a function of the intensity of protons exiting along the quantization axis z ($\hat{k}_1$) for a spin projection M_i of the hypernucleus, $\sigma(M_i)$, and the cosine of the angle χ

$$Tr(\mathcal{M}S_y\mathcal{M}^+) = \sum_{M_i} \sigma(M_i)M_i \cos\chi \ . \tag{1.19}$$

With these ingredients, the asymmetry finally writes as:

$$\begin{aligned} \mathcal{A} &= P_y \frac{3}{J+1} \frac{\sum_{M_i} \sigma(M_i)M_i}{\sum_{M_i} \sigma(M_i)} \cos\chi \\ &= P_y A_p \cos\chi \ , \end{aligned} \tag{1.20}$$

where the hypernuclear asymmetry parameter, characteristic of the hypernuclear weak decay process, has been defined as:

$$A_p = \frac{3}{J+1} \frac{\sum_{M_i} \sigma(M_i)M_i}{\sum_{M_i} \sigma(M_i)} \ . \tag{1.21}$$

At $\chi = 0°$ the asymmetry in the distribution of protons is thus determined by the product $P_y A_p$. In the weak coupling scheme, simple angular momentum algebra relations relate the hypernuclear polarization to the Λ polarization

$$p_\Lambda = \begin{cases} -\dfrac{J}{J+1} P_y & \text{if } J = J_C - \frac{1}{2} \\ P_y & \text{if } J = J_C + \frac{1}{2} \end{cases} \ , \tag{1.22}$$

where J_C is the spin of the nuclear core. It is convenient to introduce an intrinsic Λ asymmetry parameter

$$a_\Lambda = \begin{cases} -\dfrac{J+1}{J} A_p & \text{if } J = J_C - \frac{1}{2} \\ A_p & \text{if } J = J_C + \frac{1}{2} \end{cases} \ , \tag{1.23}$$

such that $P_y A_p = p_\Lambda a_\Lambda$, which is then characteristic of the elementary Λ decay process, $\vec{\Lambda}$N$\rightarrow$NN, taking place in the nuclear medium.

The asymmetry parameter can be thought in terms of an interference between the isospin $I_{NN} = 1$ parity-violating amplitude of the transition and the $I_{NN} = 0$ parity-conserving one [BM90]. In order to understand how this interference pattern comes about from Eq. (1.21), it is convenient to rewrite the intensity of protons $\sigma(M_i)$ for a spin projection M_i as:

$$\begin{aligned} \sigma(M_i) &= \sum_F |\langle F \mid \mathcal{M} \mid M_i\rangle|^2 \\ &= \sum_F \langle M_i \mid \mathcal{M}^\dagger \mid F\rangle\langle F \mid \mathcal{M} \mid M_i\rangle \\ &= \langle M_i \mid \mathcal{M}^\dagger\mathcal{M} \mid M_i\rangle \ . \end{aligned} \tag{1.24}$$

Now it must be recalled that the transition operator $\mathcal{M}$ is composed by spin non-flip parity-conserving terms and spin-flip parity-violating terms. Since the complete spin structure of $\mathcal{M}$ is complicated, let us work out the expression of the asymmetry for a simplified model in which $\mathcal{M}$ has the following schematic form:

$$\mathcal{M} = f + g\,\vec{\sigma}\cdot\hat{r} \ , \tag{1.25}$$

acting on spin 1/2-particles and where f and g are the spin non-flip and spin-flip amplitudes, respectively. From (1.25) it follows:

$$\mathcal{M}^\dagger = f^* + g^*\,\vec{\sigma}\cdot\hat{r} \tag{1.26}$$

and, using standard properties of the Pauli matrices, the product $\mathcal{M}^\dagger\mathcal{M}$ can be expressed as the sum of four terms:

$$\mathcal{M}^\dagger\mathcal{M} = |f|^2 + |g|^2 + (fg^* + f^*g)\,\vec{\sigma}\cdot\hat{r} \ . \tag{1.27}$$

The sum

$$\sum_{m_i} \sigma(m_i)\,m_i = \sum_{m_i} \langle m_i \mid \mathcal{M}^\dagger\mathcal{M} \mid m_i\rangle\, m_i \tag{1.28}$$

can be written as $\sigma(+) - \sigma(-)$, where $+(-)$ stands for the $m_i = +1/2(-1/2)$ values of the spin-1/2 projection. The two first terms in Eq. (1.27) cancel out once the sum is performed, and the two remaining terms contain the interference between the spin non-flip amplitudes and the spin-flip ones

$$\begin{aligned} \sum_{m_i} \sigma(m_i)\,m_i &= \sum_{m_i} \langle m_i \mid \mathcal{M}^\dagger\mathcal{M} \mid m_i\rangle\, m_i \\ &= (fg^* + f^*g) - (fg^* + f^*g)(-1) = 2(fg^* + f^*g) \ . \end{aligned} \tag{1.29}$$

This schematic and simplified result allows us to understand why the asymmetry is related to the interference between the parity-violating amplitudes (which contain spin-flip terms) and the parity-conserving ones (which do not flip spin).

Chapter 2

Model for the ΛN→NN Transition

The aim of this chapter is to present the formalism for evaluating the two-body weak decay ΛN→NN transition amplitudes in Λ hypernuclei. The transition potential for the decay is a strangeness-changing potential, $\Delta S = 1$, based on one-boson-exchange. In § 2.1, this transition potential is constructed considering the exchange of up to six mesons, the pseudoscalar π, η and K mesons and the vector ρ,ω, and K* mesons. A general expression for the regularized potential, containing the effect of form factors, is also given. In order to obtain the parity-violating weak coupling constants for the exchange of pseudoscalar mesons, § 2.2 makes use of SU(3) symmetry and soft-meson theorems, while $SU(6)_w$ symmetry allows the extraction of the corresponding couplings for vector mesons. The parity-conserving couplings are obtained with the help of a pole model. Based in a shell-model framework for the hypernuclear wave function, § 2.3 presents the two-body transition amplitude, $t_{\Lambda N\to NN}$, taking into account that the Λ-particle can interact with nucleons in arbitrary shells. The transition matrix elements include different ingredients, such as realistic ΛN short-range correlations and NN final state interactions based on the Nijmegen baryon-baryon potential. These ingredients are discussed in § 2.4 and § 2.5, respectively.

2.1 The Meson-Exchange Potential

The transition ΛN→NN is assumed to proceed via the exchange of virtual mesons belonging to the ground-state pseudoscalar and vector meson octets. As displayed in Figs. 2.1(a) and 2.1(b), the transition amplitude involves a strong and a weak vertex, the later being denoted by a hatched circle. For non-strange mesons the weak vertex (where the strangeness changing takes place) is placed on the left side of the diagram (Fig. 2.1(a)) while for the exchange of strange mesons it is placed on the right side (Fig. 2.1(b)).

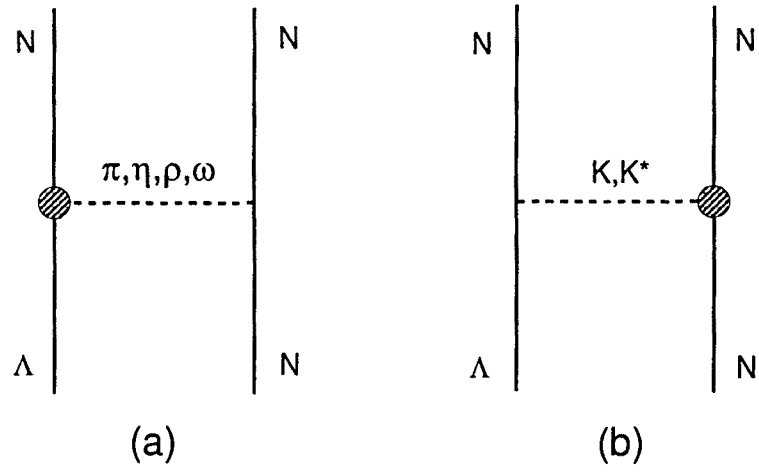

Figure 2.1. Non-strange (a) and strange (b) meson-exchange contribution to the ΛN→NN weak transition potential. The weak vertex is indicated by the circle.

In order to obtain the meson-exchange potential mediating the ΛN→NN transition, one should start from the free Feynman amplitude corresponding to the diagram shown in Fig. 2.2, using pion-exchange as an example. The expression for the Feynman diagram depicted in Fig. 2.2 is:

$$\mathcal{M}_{\rm M} = \int d^4x\, d^4y\, \overline{\Psi}_{p_3}(x)\, \Gamma_1\, \Psi_{p_1}(x)\, \Delta_{\rm M}(x-y)\, \overline{\Psi}_{p_4}(y)\, \Gamma_2\, \Psi_{p_2}(y)\,, \qquad (2.1)$$

where

$$\Psi_p(x) = \mathrm{e}^{-\mathrm{i}p_\mu x_\mu} u(p) \qquad (2.2)$$

is the free baryon field of positive energy, Γ_i the Dirac operator characteristic of the baryon-baryon-meson vertex and $\Delta_M(x-y)$ the meson propagator, which for one pion-exchange reads:

$$\Delta_\pi(x-y) = \int \frac{d^4q}{(2\pi)^4} \frac{e^{iq(x-y)}}{(q^0)^2 - \vec{q}^{\,2} - \mu^2} , \tag{2.3}$$

with μ being the pion mass. Using Eqs. (2.2) and (2.3), performing a change to center-of-mass (c.m.) and relative variables and integrating over the c.m., time and energy variables, one obtains (ignoring the momentum and energy conservation delta functions):

$$\begin{aligned} \mathcal{M}(p_1,p_3) &= \int d^3r\ e^{i(\vec{p}_1-\vec{p}_3)\vec{r}} \\ &\times \int \frac{d^3q}{(2\pi)^3}\, \overline{u}(p_3)\,\Gamma_1\, u(p_1)\, \frac{e^{-i\vec{q}\,\vec{r}}}{(q^0)^2 - \vec{q}^{\,2} - \mu^2}\, \overline{u}(p_4)\,\Gamma_2\, u(p_2) \end{aligned} \tag{2.4}$$

with $q^0 = p_1^0 - p_3^0 = p_4^0 - p_2^0$ and $\vec{q} = \vec{p}_1 - \vec{p}_3 = \vec{p}_4 - \vec{p}_2$ being the components of the four-momentum carried by the exchanged meson. The vertex $\overline{u}(p')\,\Gamma\,u(p)$ comes from the matrix element between fields $\overline{\Psi}(x)\,\Gamma\,\Psi(x)$ when only the parts of the field corresponding to the positive energy states are considered.

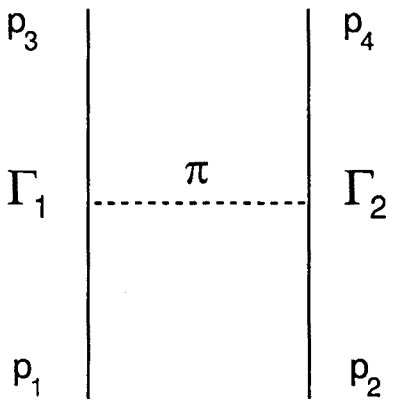

Figure 2.2. Illustration of the Feynman diagram for the two-body transition amplitude $B_1B_2 \to B_3B_4$.

Going to the nonrelativistic limit of the vertices (and assuming $q^0 = 0$) gives the nonrelativistic reduction of Eq. (2.4), $\mathcal{M}(\vec{q}) \equiv V(\vec{q})$, which is the Fourier transform

of the transition potential in coordinate space, $V(\vec{r})$. In the next two subsections, the expressions for the weak and the strong hamiltonians for each meson, pseudoscalar and vector mesons separately, are given as well as the form of their corresponding nonrelativistic potential in momentum space and in coordinate space.

One has to note that the nonrelativistic approach of the present work differs from other previous studies [RB91,RM92] based on a relativistic formalism. It was found that the suppression of the matrix elements due to short-range correlations was larger by about a factor of two to what was obtained in standard nonrelativistic calculations [OS85,MG84,Du86,DF96]. In Ref. [PR94] it was shown that, if one uses the same nonrelativistic correlation function, the relativistic and nonrelativistic schemes were not giving the same correlated potential obtained through the standard nonrelativistic reduction. In the relativistic approach, the correlation function was applied to the Feynman amplitude before the nonrelativistic reduction was carried out, whereas in the nonrelativistic procedure the correlation function was applied after the reduction of the free Feynman amplitude was obtained. The difference between the two methods was studied in Ref. [PR95], where it was shown explicitly that the relativistic framework together with a standard nonrelativistic correlation function lead to additional contributions in the correlated transition potential, which produced the larger suppression of the decay rates reported in Refs. [RB91,RM92]. The basic ideas of the study of Ref. [PR95] are elaborated in § 2.4, which is devoted to the initial ΛN correlations. Due to the lack of a better understanding for treating short-range correlations in a relativistic framework, the present work uses the standard nonrelativistic formalism.

2.1.1 Pseudoscalar Mesons

While there exist many strong NN meson-exchange potentials which, through fits to NN scattering data, provide information on the different strong NN-meson vertices, only the ΛNπ vertex is known experimentally in the weak sector. In this section the ΛN→NN transition potential mediated by the exchange of the π, η and K mesons is presented. The starting point is the expression for their corresponding strong and weak hamiltonians. For the π-meson the weak hamiltonian is parametrized in the form:

$$\mathcal{H}^{\rm W}_{\Lambda {\rm N}\pi} = {\rm i} G_F m_\pi^2 \overline{\psi}_{\rm N} (A_\pi + B_\pi \gamma_5) \vec{\tau}\, \vec{\phi}^{\,\pi} \psi_\Lambda \begin{pmatrix} 0 \\ 1 \end{pmatrix} , \tag{2.5}$$

where $G_F m_\pi^2 = 2.21 \times 10^{-7}$ is the weak coupling constant. The empirical constants $A_\pi = 1.05$ and $B_\pi = -7.15$, adjusted to the observables of the free Λ decay, determine

the strength of the parity-violating and parity-conserving amplitudes, respectively. The nucleon, lambda and pion fields are given by $\psi_{\rm N}$, ψ_Λ and $\vec{\phi}^{\,\pi}$, respectively, while the isospin spurion $\binom{0}{1}$ is included to enforce the empirical $\Delta T = 1/2$ rule observed in the decay of a free Λ. The Bjorken and Drell convention for the definition of γ_5 [BD64] has been taken.

For the strong vertex, one takes the usual pseudoscalar coupling

$$\mathcal{H}^{\rm S}_{{\rm NN}\pi} = {\rm i}\, g_{{\rm NN}\pi}\, \overline{\psi}_{\rm N} \gamma_5 \vec{\tau}\, \vec{\phi}^{\,\pi} \psi_{\rm N} \ , \tag{2.6}$$

which is equivalent to the pseudovector coupling when free spinors are used in the evaluation of the transition amplitude. As it has been already commented, the non-relativistic reduction of the free space Feynman amplitude is then associated with the transition potential. In momentum space, one obtains:

$$V_\pi(\vec{q}) = -G_F m_\pi^2 \frac{g}{2M} \left(\hat{A} + \frac{\hat{B}}{2\overline{M}} \vec{\sigma}_1\, \vec{q} \right) \frac{\vec{\sigma}_2\, \vec{q}}{\vec{q}^{\,2} + \mu^2} \ , \tag{2.7}$$

where $\vec{q}$ is the momentum carried by the pion directed towards the strong vertex, $g = g_{{\rm NN}\pi}$ the strong coupling constant for the NNπ vertex, μ the pion mass, M the nucleon mass and $\overline{M}$ the average between the nucleon and Λ masses. The operators $\hat{A}$ and $\hat{B}$, which contain the isospin dependence of the potential, read:

$$\hat{A} = A_\pi\, \vec{\tau}_1\, \vec{\tau}_2 \tag{2.8}$$

$$\hat{B} = B_\pi\, \vec{\tau}_1\, \vec{\tau}_2 \ . \tag{2.9}$$

The other mesons of the pseudoscalar octet are the isosinglet eta (η) and the isodoublet kaon (K). The strong and weak vertices for these mesons are

$$\mathcal{H}^{\rm S}_{{\rm NN}\eta} = {\rm i}\, g_{{\rm NN}\eta}\, \overline{\psi}_{\rm N} \gamma_5 \phi^\eta \psi_{\rm N} \tag{2.10}$$

$$\mathcal{H}^{\rm W}_{\Lambda{\rm N}\eta} = {\rm i}\, G_F m_\pi^2\, \overline{\psi}_{\rm N}\, (A_\eta + B_\eta \gamma_5) \phi^\eta \psi_\Lambda \binom{0}{1} \tag{2.11}$$

$$\mathcal{H}^{\rm S}_{\Lambda{\rm NK}} = {\rm i}\, g_{\Lambda{\rm NK}}\, \overline{\psi}_{\rm N} \gamma_5\, \phi^{\rm K} \psi_\Lambda \tag{2.12}$$

$$\begin{aligned} \mathcal{H}^{\rm W}_{\rm NNK} = {\rm i}\, G_F m_\pi^2 \Big[& \overline{\psi}_{\rm N} \binom{0}{1} \left(C^{\rm PV}_{\rm K} + C^{\rm PC}_{\rm K} \gamma_5\right) (\phi^{\rm K})^\dagger \psi_{\rm N} \\ & + \overline{\psi}_{\rm N} \psi_{\rm N} \left(D^{\rm PV}_{\rm K} + D^{\rm PC}_{\rm K} \gamma_5\right) (\phi^{\rm K})^\dagger \binom{0}{1} \Big] \ , \end{aligned} \tag{2.13}$$

where the weak coupling constants cannot be taken directly from experiment. In the present work one adopts the approach of Refs. [DF96,To82], presented in § 2.2. The values of the coupling constants corresponding to the strong and weak sectors are listed

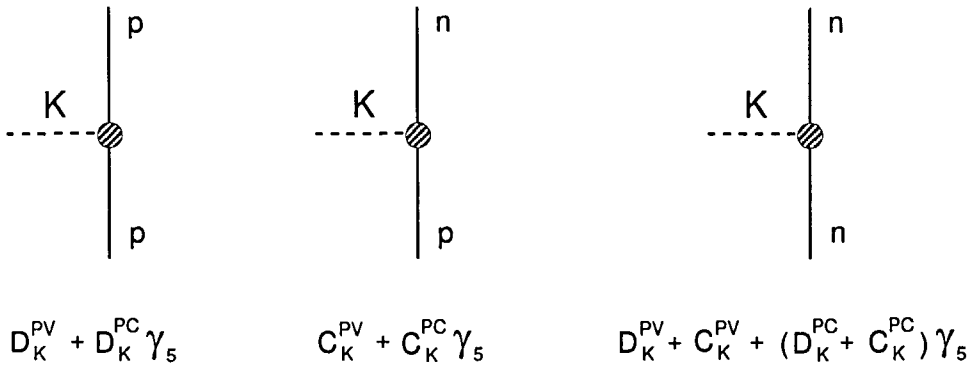

Figure 2.3. K-meson weak vertices for $p\bar{p}K^0$ (a), $p\bar{n}K^+$ (b), and $n\bar{n}K^0$ (c).

in Table 2.2 of § 2.2. The particular structure of the K weak couplings corresponds to the vertices shown in Fig. 2.3.

The corresponding nonrelativistic potentials for the exchange of these mesons in the ΛN→NN transition are analogous to Eq. (2.7) but making the following replacements:

$$g \rightarrow g_{NN\eta} \tag{2.14}$$

$$\mu \rightarrow m_\eta \tag{2.15}$$

$$\hat{A} \rightarrow A_\eta \tag{2.16}$$

$$\hat{B} \rightarrow B_\eta \tag{2.17}$$

in the case of η-exchange, and

$$g \rightarrow g_{\Lambda NK} \tag{2.18}$$

$$\mu \rightarrow m_K \tag{2.19}$$

$$\hat{A} \rightarrow \left(\frac{C_K^{PV}}{2} + D_K^{PV} + \frac{C_K^{PV}}{2}\vec{\tau}_1\vec{\tau}_2\right)\frac{M}{\overline{M}} \tag{2.20}$$

$$\hat{B} \rightarrow \left(\frac{C_K^{PC}}{2} + D_K^{PC} + \frac{C_K^{PC}}{2}\vec{\tau}_1\vec{\tau}_2\right) \tag{2.21}$$

in the case of K-exchange, where the factor $M/\overline{M}$ corrects for the fact that the nonrelativistic reduction of the strong ΛNK vertex gives a factor $1/\overline{M}$ instead of $1/M$ (in

contrast to the π and η cases where the strong vertex involves two nucleons). Performing a Fourier transform of the general expression given in Eq. (2.7) and introducing the tensor operator $S_{12}(\hat{r}) = 3\,\vec{\sigma}_1\,\hat{r}\vec{\sigma}_2\,\hat{r} - \vec{\sigma}_1\,\vec{\sigma}_2$, it is easy to obtain the corresponding transition potential in coordinate space, which can be divided into central, tensor and parity-violating pieces. The explicit expressions are given in the next section.

2.1.2 Vector Mesons

In recent years, a number of theoretical studies have investigated the contribution of the ρ-meson to the ΛN$\rightarrow$NN process [MG84,Na88,TT85]. The weak ΛNρ and strong NNρ vertices are given by [MG84]:

$$\mathcal{H}^{\rm W}_{\Lambda{\rm N}\rho} = G_F m_\pi^2\,\overline{\psi}_{\rm N}\left(\alpha_\rho\gamma^\mu - \beta_\rho {\rm i}\frac{\sigma^{\mu\nu}q_\nu}{2\overline{M}} + \varepsilon_\rho\gamma^\mu\gamma_5\right)\vec{\tau}\,\vec{\rho}_\mu\,\psi_\Lambda\,\binom{0}{1} \tag{2.22}$$

$$\mathcal{H}^{\rm S}_{{\rm NN}\rho} = \overline{\psi}_{\rm N}\left(g^{\rm V}_{{\rm NN}\rho}\gamma^\mu + {\rm i}\frac{g^{\rm T}_{{\rm NN}\rho}}{2M}\sigma^{\mu\nu}q_\nu\right)\vec{\tau}\,\vec{\rho}_\mu\,\psi_{\rm N}\,, \tag{2.23}$$

respectively, where the four-momentum transfer q is directed towards the strong vertex. The values of the strong and weak coupling constants are given in Table 2.2 of § 2.2.

The nonrelativistic reduction of the Feynman amplitude gives the following ρ-meson transition potential:

$$\begin{aligned} V_\rho(\vec{q}) = G_F m_\pi^2 \Bigg(& F_1\hat{\alpha} - \frac{(\hat{\alpha}+\hat{\beta})(F_1+F_2)}{4M\overline{M}}(\vec{\sigma}_1\times\vec{q})(\vec{\sigma}_2\times\vec{q}) \\ & + {\rm i}\frac{\hat{\varepsilon}(F_1+F_2)}{2M}(\vec{\sigma}_1\times\vec{\sigma}_2)\vec{q}\Bigg)\frac{1}{\vec{q}^{\,2}+\mu^2}\,, \end{aligned} \tag{2.24}$$

with $\mu = m_\rho$, $F_1 = g^{\rm V}_{{\rm NN}\rho}$, $F_2 = g^{\rm T}_{{\rm NN}\rho}$ and the operators $\hat{\alpha}$, $\hat{\beta}$ and $\hat{\varepsilon}$, defined by:

$$\hat{\alpha} = \alpha_\rho\,\vec{\tau}_1\,\vec{\tau}_2 \tag{2.25}$$

$$\hat{\beta} = \beta_\rho\,\vec{\tau}_1\vec{\tau}_2 \tag{2.26}$$

$$\hat{\varepsilon} = \varepsilon_\rho\,\vec{\tau}_1\,\vec{\tau}_2\,, \tag{2.27}$$

contain the isospin structure. Using the relation $(\vec{\sigma}_1\times\vec{q})(\vec{\sigma}_2\times\vec{q}) = (\vec{\sigma}_1\,\vec{\sigma}_2)\,\vec{q}^{\,2} - (\vec{\sigma}_1\,\vec{q})(\vec{\sigma}_2\,\vec{q})$ and performing a Fourier transform of $V_\rho(\vec{q},)$, one obtains the corresponding transition potential in coordinate space, which, as in the π-exchange case, can be divided into central, tensor and parity-violating pieces. Furthermore, the ρ-meson central potential can be further decomposed into a spin-independent (due to the $F_1\hat{\alpha}$

term) and a spin-dependent part [PR96]. Due to the different models employed for the weak ΛNρ-vertex [MG84,Na88,TT85], different calculations have yielded widely varying results. However, all studies until now have only included the tensor piece of the parity-conserving ρ-exchange term motivated, in part, by the observation that this is the most important contribution to the π-exchange potential. In Ref. [PR96] it has been demonstrated that the central piece of the ρ-exchange is in fact larger than its tensor interaction, an observation that can be traced to the fact that the ρ-exchange diagram has a much shorter range than the π-exchange potential. In view of a number of theoretical efforts that increase the complexity of the ΛN→NN reaction mechanism by calculating correlated 2π-exchange, through the coupling to σ and ρ mesons [IU95] or via strange ΛN→ ΣN mixing [Sh94], it is important to explicitly keep all pieces of the potential for the vector mesons first.

The other vector mesons considered in this work are the isoscalar ω and the isodoublet K*, for which the weak and strong vertices can be written as:

$$\mathcal{H}^{\rm S}_{\rm NN\omega} = \overline{\psi}_{\rm N}\left(g^{\rm V}_{\rm NN\omega}\gamma^{\mu} + {\rm i}\frac{g^{\rm T}_{\rm NN\omega}}{2M}\sigma^{\mu\nu}q_{\nu}\right)\phi^{\omega}_{\mu}\psi_{\rm N} \tag{2.28}$$

$$\mathcal{H}^{\rm W}_{\rm \Lambda N\omega} = G_F m_{\pi}^2\,\overline{\psi}_{\rm N}\left(\alpha_{\omega}\gamma^{\mu} - \beta_{\omega}{\rm i}\frac{\sigma^{\mu\nu}q_{\nu}}{2\overline{M}} + \varepsilon_{\omega}\gamma^{\mu}\gamma_5\right)\phi^{\omega}_{\mu}\psi_{\Lambda}\begin{pmatrix}0\\1\end{pmatrix} \tag{2.29}$$

$$\mathcal{H}^{\rm S}_{\rm \Lambda NK^*} = \overline{\psi}_{\rm N}\left(g^{\rm V}_{\rm \Lambda NK^*}\gamma^{\mu} + {\rm i}\frac{g^{\rm V}_{\rm \Lambda NK^*}}{2\overline{M}}\sigma^{\mu\nu}q_{\nu}\right)\phi^{\rm K^*}_{\mu}\psi_{\Lambda} \tag{2.30}$$

$$\begin{aligned}\mathcal{H}^{\rm W}_{\rm NNK^*} = G_F m_{\pi}^2\,\Big(&\left[C^{\rm PC,V}_{\rm K^*}\overline{\psi}_{\rm N}\begin{pmatrix}0\\1\end{pmatrix}(\phi^{\rm K^*}_{\mu})^{\dagger}\,\gamma^{\mu}\psi_{\rm N} + D^{\rm PC,V}_{\rm K^*}\overline{\psi}_{\rm N}\gamma^{\mu}\psi_{\rm N}(\phi^{\rm K^*}_{\mu})^{\dagger}\,\begin{pmatrix}0\\1\end{pmatrix}\right]\\ &+\left[C^{\rm PC,T}_{\rm K^*}\overline{\psi}_{\rm N}\begin{pmatrix}0\\1\end{pmatrix}(\phi^{\rm K^*}_{\mu})^{\dagger}\,(-{\rm i})\frac{\sigma^{\mu\nu}q_{\nu}}{2M}\psi_{\rm N} + D^{\rm PC,T}_{\rm K^*}\overline{\psi}_{\rm N}(-{\rm i})\frac{\sigma^{\mu\nu}q_{\nu}}{2M}\psi_{\rm N}(\phi^{\rm K^*}_{\mu})^{\dagger}\,\begin{pmatrix}0\\1\end{pmatrix}\right]\\ &+\left[C^{\rm PV}_{\rm K^*}\overline{\psi}_{\rm N}\begin{pmatrix}0\\1\end{pmatrix}(\phi^{\rm K^*}_{\mu})^{\dagger}\,\gamma^{\mu}\gamma_5\psi_{\rm N} + D^{\rm PV}_{\rm K^*}\overline{\psi}_{\rm N}\gamma^{\mu}\gamma_5\psi_{\rm N}(\phi^{\rm K^*}_{\mu})^{\dagger}\,\begin{pmatrix}0\\1\end{pmatrix}\right]\Big)\ .\end{aligned} \tag{2.31}$$

Note that the K* weak vertex has the same structure as the K one, the only difference being the parity-conserving contribution which has two terms, related to the vector and tensor couplings. The nonrelativistic potential can be obtained from the general expression given in Eq. (2.24) making the following replacements:

$$\mu \rightarrow m_{\omega} \tag{2.32}$$

$$F_1 \rightarrow g^{\rm V}_{\rm NN\omega} \tag{2.33}$$

$$F_2 \rightarrow g^{\rm T}_{\rm NN\omega} \tag{2.34}$$

$$\hat{\alpha} \rightarrow \alpha_{\omega} \tag{2.35}$$

$$\hat{\beta} \rightarrow \beta_{\omega} \tag{2.36}$$

$$\hat{\varepsilon} \;\rightarrow\; \varepsilon_\omega \tag{2.37}$$

in the case of ω-exchange, and

$$\mu \;\rightarrow\; m_{\mathrm{K}^*} \tag{2.38}$$

$$F_1 \;\rightarrow\; g^{\mathrm{V}}_{\Lambda\mathrm{N}\mathrm{K}^*} \tag{2.39}$$

$$F_2 \;\rightarrow\; g^{\mathrm{T}}_{\Lambda\mathrm{N}\mathrm{K}^*} \tag{2.40}$$

$$\hat{\alpha} \;\rightarrow\; \frac{C^{\mathrm{PC,V}}_{\mathrm{K}^*}}{2} + D^{\mathrm{PC,V}}_{\mathrm{K}^*} + \frac{C^{\mathrm{PC,V}}_{\mathrm{K}^*}}{2}\vec{\tau}_1\,\vec{\tau}_2 \tag{2.41}$$

$$\hat{\beta} \;\rightarrow\; \frac{C^{\mathrm{PC,T}}_{\mathrm{K}^*}}{2} + D^{\mathrm{PC,T}}_{\mathrm{K}^*} + \frac{C^{\mathrm{PC,T}}_{\mathrm{K}^*}}{2}\vec{\tau}_1\,\vec{\tau}_2 \tag{2.42}$$

$$\hat{\varepsilon} \;\rightarrow\; \left(\frac{C^{\mathrm{PV}}_{\mathrm{K}^*}}{2} + D^{\mathrm{PV}}_{\mathrm{K}^*} + \frac{C^{\mathrm{PV}}_{\mathrm{K}^*}}{2}\vec{\tau}_1\,\vec{\tau}_2\right)\frac{M}{\overline{M}} \tag{2.43}$$

for the exchange of a K*-meson.

2.1.3 General Form of the Potential

The Fourier transform of the general Eqs. (2.7) and (2.24) leads to a potential in configuration space which can be cast into the form:

$$\begin{aligned} V(\vec{r}) &= \sum_i \sum_\alpha V^{(i)}_\alpha(\vec{r}) = \sum_i \sum_\alpha V^{(i)}_\alpha(r)\,\hat{O}_\alpha\,\hat{I}^{(i)}_\alpha \\ &= \sum_i \Big[V^{(i)}_{\mathrm{C}}(r)\hat{I}^{(i)}_C + V^{(i)}_{\mathrm{SS}}(r)\vec{\sigma}_1\,\vec{\sigma}_2\,\hat{I}^{(i)}_{\mathrm{SS}} + V^{(i)}_{\mathrm{T}}(r)S_{12}(\hat{r})\hat{I}^{(i)}_{\mathrm{T}} + \\ &\quad + \left(n^i\vec{\sigma}_2\cdot\hat{r} + (1-n^i)\,[\vec{\sigma}_1\times\vec{\sigma}_2\,]\cdot\hat{r}\right)V^{(i)}_{\mathrm{PV}}(r)\hat{I}^{(i)}_{\mathrm{PV}}\Big]\,, \end{aligned} \tag{2.44}$$

where the index i runs over the different mesons exchanged ($i = 1,\ldots,6$ represents π,ρ,K,K*,η,ω) and α over the different spin operators denoted by C (central spin-independent), SS (central spin-dependent), T (tensor) and PV (parity-violating). In the above expression, particle 1 refers to the Λ and $n^i = 1(0)$ for pseudoscalar (vector) mesons. In the case of isovector mesons (π, ρ) the isospin factor, $\hat{I}^{(i)}_\alpha$, is $\vec{\tau}_1\,\vec{\tau}_2$ and for isoscalar mesons (η,ω) this factor is just $\hat{1}$ for all spin structure pieces of the potential. In the case of isodoublet mesons (K,K*) there are contributions proportional to $\hat{1}$ and to $\vec{\tau}_1\,\vec{\tau}_2$ that depend on the coupling constants and, therefore, on the spin structure piece of the potential denoted by α. For K-exchange one has:

$$\hat{I}^{(3)}_{\mathrm{C}} \;=\; 0 \tag{2.45}$$

Table 2.1. Constants appearing in the weak transition potential for the different mesons.

μ_i	$K_C^{(i)}$	$K_{SS}^{(i)}$	$K_T^{(i)}$	$K_{PV}^{(i)}$
π	0	$\frac{B_\pi}{2\overline{M}}\frac{g_{\rm NN\pi}}{2M}$	$\frac{B_\pi}{2\overline{M}}\frac{g_{\rm NN\pi}}{2M}$	$A_\pi\frac{g_{\rm NN\pi}}{2M}$
η	0	$\frac{B_\eta}{2\overline{M}}\frac{g_{\rm NN\eta}}{2M}$	$\frac{B_\eta}{2\overline{M}}\frac{g_{\rm NN\eta}}{2M}$	$A_\eta\frac{g_{\rm NN\eta}}{2M}$
K	0	$\frac{1}{2M}\frac{g_{\Lambda\rm NK}}{2\overline{M}}$	$\frac{1}{2M}\frac{g_{\Lambda\rm NK}}{2\overline{M}}$	$\frac{g_{\Lambda\rm NK}}{2M}$
ρ	$g^{\rm V}_{\rm NN\rho}\alpha_\rho$	$2\frac{\alpha_\rho+\beta_\rho}{2\overline{M}}\frac{g^{\rm V}_{\rm NN\rho}+g^{\rm T}_{\rm NN\rho}}{2M}$	$-\frac{\alpha_\rho+\beta_\rho}{2\overline{M}}\frac{g^{\rm V}_{\rm NN\rho}+g^{\rm T}_{\rm NN\rho}}{2M}$	$-\varepsilon_\rho\frac{g^{\rm V}_{\rm NN\rho}+g^{\rm T}_{\rm NN\rho}}{2M}$
ω	$g^{\rm V}_{\rm NN\omega}\alpha_\omega$	$2\frac{\alpha_\omega+\beta_\omega}{2\overline{M}}\frac{g^{\rm V}_{\rm NN\omega}+g^{\rm T}_{\rm NN\omega}}{2M}$	$-\frac{\alpha_\omega+\beta_\omega}{2\overline{M}}\frac{g^{\rm V}_{\rm NN\omega}+g^{\rm T}_{\rm NN\omega}}{2M}$	$-\varepsilon_\omega\frac{g^{\rm V}_{\rm NN\omega}+g^{\rm T}_{\rm NN\omega}}{2M}$
K*	$g^{\rm V}_{\Lambda\rm NK^*}$	$2\frac{1}{2M}\frac{g^{\rm V}_{\Lambda\rm NK^*}+g^{\rm T}_{\Lambda\rm NK^*}}{2\overline{M}}$	$-\frac{1}{2M}\frac{g^{\rm V}_{\Lambda\rm NK^*}+g^{\rm T}_{\Lambda\rm NK^*}}{2\overline{M}}$	$-\frac{g^{\rm V}_{\Lambda\rm NK^*}+g^{\rm T}_{\Lambda\rm NK^*}}{2M}$

$$\hat{I}^{(3)}_{\rm SS} = \hat{I}^{(3)}_{\rm T} = \frac{C^{\rm PC}_{\rm K}}{2} + D^{\rm PC}_{\rm K} + \frac{C^{\rm PC}_{\rm K}}{2}\vec{\tau}_1\,\vec{\tau}_2 \tag{2.46}$$

$$\hat{I}^{(3)}_{\rm PV} = \frac{C^{\rm PV}_{\rm K}}{2} + D^{\rm PV}_{\rm K} + \frac{C^{\rm PV}_{\rm K}}{2}\vec{\tau}_1\,\vec{\tau}_2\ , \tag{2.47}$$

and for K*-exchange:

$$\hat{I}^{(6)}_{\rm C} = \frac{C^{\rm PC,V}_{\rm K^*}}{2} + D^{\rm PC,V}_{\rm K^*} + \frac{C^{\rm PC,V}_{\rm K^*}}{2}\vec{\tau}_1\,\vec{\tau}_2 \tag{2.48}$$

$$\hat{I}^{(6)}_{\rm SS} = \hat{I}^{(6)}_{\rm T} = \frac{(C^{\rm PC,V}_{\rm K^*}+C^{\rm PC,T}_{\rm K^*})}{2} + (D^{\rm PC,V}_{\rm K^*}+D^{\rm PC,T}_{\rm K^*}) + \frac{(C^{\rm PC,V}_{\rm K^*}+C^{\rm PC,T}_{\rm K^*})}{2}\vec{\tau}_1\,\vec{\tau}_2 \tag{2.49}$$

$$\hat{I}^{(6)}_{\rm PV} = \frac{C^{\rm PV}_{\rm K^*}}{2} + D^{\rm PV}_{\rm K^*} + \frac{C^{\rm PV}_{\rm K^*}}{2}\vec{\tau}_1\,\vec{\tau}_2\ . \tag{2.50}$$

The different pieces $V^{(i)}_\alpha$, with α=C,SS,T,PV, are given by:

$$V^{(i)}_{\rm C}(r) = K^{(i)}_{\rm C}\frac{{\rm e}^{-\mu_i r}}{4\pi r} \equiv K^{(i)}_{\rm C}\,V_{\rm C}(r,\mu_i) \tag{2.51}$$

$$V_{\rm SS}^{(i)}(r) = K_{\rm SS}^{(i)} \frac{1}{3} \left[{\mu_i}^2 \frac{{\rm e}^{-\mu_i r}}{4\pi r} - \delta(r) \right] \equiv K_{\rm SS}^{(i)} V_{\rm SS}(r, \mu_i) \tag{2.52}$$

$$V_{\rm T}^{(i)}(r) = K_{\rm T}^{(i)} \frac{1}{3} \mu_i^2 \frac{{\rm e}^{-\mu_i r}}{4\pi r} \left(1 + \frac{3}{\mu_i r} + \frac{3}{(\mu_i r)^2} \right) \equiv K_{\rm T}^{(i)} V_{\rm T}(r, \mu_i) \tag{2.53}$$

$$V_{\rm PV}^{(i)}(r) = K_{\rm PV}^{(i)} \mu_i \frac{{\rm e}^{-\mu_i r}}{4\pi r} \left(1 + \frac{1}{\mu_i r} \right) \equiv K_{\rm PV}^{(i)} V_{\rm PV}(r, \mu_i) \ , \tag{2.54}$$

where μ_i denotes the mass of the different mesons. The expressions for $K_\alpha^{(i)}$, which contain factors and coupling constants, are given in Table 2.1 (omitting the $G_F m_\pi^2$ factor). A monopole form factor $F_i(\vec{q}^{\,2}) = (\Lambda_i^2 - \mu_i^2)/(\Lambda_i^2 + \vec{q}^{\,2})$ is used at each vertex, where the value of the cut-off, Λ_i, depends on the meson. The values of the Jülich YN interaction [HH89], displayed in Table 2.2 of the next section, have been chosen for the cut-off's since the Nijmegen model distinguishes form factors only in terms of the transition channel. The use of form factors leads to the following regularization for each meson:

$$V_{\rm C}(r;\mu_i) \rightarrow V_{\rm C}(r;\mu_i) - V_{\rm C}(r;\Lambda_i) - \Lambda_i \frac{{\Lambda_i}^2 - {\mu_i}^2}{2} \frac{{\rm e}^{-\Lambda_i r}}{4\pi} \left(1 - \frac{2}{\Lambda_i r} \right) \tag{2.55}$$

$$V_{\rm SS}(r;\mu_i) \rightarrow V_{\rm SS}(r;\mu_i) - V_{\rm SS}(r;\Lambda_i) - \Lambda_i \frac{{\Lambda_i}^2 - {\mu_i}^2}{2} \frac{{\rm e}^{-\Lambda_i r}}{4\pi} \left(1 - \frac{2}{\Lambda_i r} \right) \tag{2.56}$$

$$V_{\rm T}(r;\mu_i) \rightarrow V_{\rm T}(r;\mu_i) - V_{\rm T}(r;\Lambda_i) - \Lambda_i \frac{{\Lambda_i}^2 - {\mu_i}^2}{2} \frac{{\rm e}^{-\Lambda_i r}}{4\pi} \left(1 + \frac{1}{\Lambda_i r} \right) \tag{2.57}$$

$$V_{\rm PV}(r;\mu_i) \rightarrow V_{\rm PV}(r;\mu_i) - V_{\rm PV}(r;\Lambda_i) - \frac{{\Lambda_i}^2 - {\mu_i}^2}{2} \frac{{\rm e}^{-\Lambda_i r}}{4\pi} \ , \tag{2.58}$$

where $V_\alpha(r;\Lambda_i)$ has the same structure as $V_\alpha(r;\mu_i)$, defined in Eqs. (2.51)-(2.54), but replacing the meson mass, μ_i, by the corresponding cut-off mass, Λ_i.

2.2 The Weak Coupling Constants

The starting point for describing the weak decay of strange particles has been the fundamental Cabbibo Hamiltonian based on the Current $\otimes$ Current assumption

$$H = \frac{G_F}{\sqrt{2}} \int d^3x J^\alpha(x) J_\alpha^\dagger(x) + \text{h.c.} \ , \tag{2.59}$$

with

$$\begin{aligned} J_\alpha(x) &= \overline{\Psi}_e(x)\gamma_\alpha(1-\gamma_5)\Psi_{\nu_e}(x) + \overline{\Psi}_\mu(x)\gamma_\alpha(1-\gamma_5)\Psi_{\nu_\mu}(x) \\ &+ \overline{u}(x)\gamma_\alpha(1-\gamma_5)\left(d(x)\cos\theta_{\rm C} + s(x)\sin\theta_{\rm C}\right) \ , \end{aligned} \tag{2.60}$$

where θ_C is the Cabbibo angle and G_F the weak coupling constant. As it is well known, terms proportional to $\cos\theta_C$ describe, for instance, the neutron β-decay while the contributions proportional to $\sin\theta_C$ lead to the semileptonic decay of hyperons and kaons. The $\Delta S = 1$ nonleptonic decays are governed by terms proportional to $\sin\theta_C\cos\theta_C$ which consist of products of a current between u and d quarks ($\Delta T = 1$) and a current betwen u and s quarks ($\Delta T = 1/2$). Thus, since terms in $\sin\theta_C\cos\theta_C$ describe transitions with $\Delta T = 1/2$ and $3/2$ with equal probability, the empirical $\Delta T = 1/2$ rule indicates the presence of some dynamical effect related to QCD corrections that enhances the $\Delta T = 1/2$ components of the Hamiltonian.

In order to obtain hadronic weak matrix elements of the kind $\langle \mathrm{MB}'|H_w|\mathrm{B}\rangle$, where M can stand for pseudoscalar or vector mesons and B for baryons, it has been convenient to express the effective weak Hamiltonian in terms of the $\mathrm{SU}(6)_w$ symmetry that unites them.

The $\Delta S = 1$ weak nonleptonic Hamiltonian can be written in SU(3) tensor notation:

$$H_w = \frac{G_F}{2\sqrt{2}}\cos\theta_C\sin\theta_C\{J^2_{\mu 1}, J_3^{\mu 1}\} + \mathrm{h.c.} \tag{2.61}$$

where $J^i_{\mu j} = (V_\mu - A_\mu)^i_j$ is the weak hadronic current with SU(3) indices i and j. As shown in Ref. [DF96,To82,Ba67] the weak vector and axial currents can be expressed in terms of $\mathrm{SU}(6)_w$ currents. Since the Hamiltonian is the product of two currents, each belonging to the **35** representation, one can expand

$$35 \otimes 35 = 1_s \oplus 35_s \oplus 189_s \oplus 405_s \oplus 35_a \oplus 280_a \oplus \overline{280_a}\ , \tag{2.62}$$

which allows extraction of the parity-violating (PV) and parity-conserving (PC) pieces of the Hamiltonian:

$$H_{\mathrm{PC}} : 1_s \oplus 35_s \oplus 189_s \oplus 405_s \tag{2.63}$$

$$H_{\mathrm{PV}} : 35_a \oplus 280_a \oplus \overline{280_a}\ . \tag{2.64}$$

Each of the possible ways of coupling baryons to mesons within the $\mathrm{SU}(6)_w$ symmetry introduces a reduced matrix element that can either be fitted to experimental data or calculated microscopically from quark models. Below, the PV and PC amplitudes are discussed separately.

2.2.1 The Parity-Violating Amplitudes

The traditional approximation employed to obtain the PV amplitudes for the nonleptonic decays $B \to B' + M$ has been the use of the soft-meson reduction theorem:

$$\lim_{q\to 0}\langle B' M_i(q)|H_{pv}|B\rangle = -\frac{i}{F_\pi}\langle B'|[F_i^5, H_{pv}]|B\rangle = -\frac{i}{F_\pi}\langle B'|[F_i, H_{pc}]|B\rangle \ , \tag{2.65}$$

where q is the momentum of the meson and F_i is an SU(3) generator whose action on a baryon B_j gives:

$$F_i|B_j\rangle = if_{ijk}|B_k\rangle \ . \tag{2.66}$$

Since the weak Hamiltonian H_w is assumed to transform like the sixth component of an octet, a term like $\langle B_k|H_w^6|B_j\rangle$ can be expressed as:

$$\langle B_k|H_w^6|B_j\rangle = iFf_{6jk} + Dd_{6jk} \ , \tag{2.67}$$

where f_{ijk} and d_{ijk} are the SU(3) coefficients and F and D the reduced matrix elements.

With the use of these soft-meson techniques and the SU(3) symmetry one can now relate the physical amplitudes of the nonleptonic hyperon decays into a pion plus a nucleon or a hyperon, $B \to B' + \pi$, with the unphysical amplitudes of the other pseudoscalar members of the meson octet, the kaon and the eta. One obtains relations such as [To82]:

$$\langle nK^0|H_{pv}|n\rangle = \sqrt{\frac{3}{2}}\Lambda_-^0 - \frac{1}{\sqrt{2}}\Sigma_0^+ \tag{2.68}$$

$$\langle pK^0|H_{pv}|p\rangle = -\sqrt{2}\Sigma_0^+ \tag{2.69}$$

$$\langle nK^+|H_{pv}|p\rangle = \sqrt{\frac{3}{2}}\Lambda_-^0 + \frac{1}{\sqrt{2}}\Sigma_0^+ \tag{2.70}$$

$$\langle n\eta|H_{pv}|\Lambda\rangle = \sqrt{\frac{3}{2}}\Lambda_-^0 \ , \tag{2.71}$$

where Σ_0^+ stands for $\langle p\pi^0|H_{pv}|\Sigma^+\rangle$, the PV amplitude of the decay $\Sigma^+ \to p\pi^0$, which is experimentally accessible. In all these expressions the standard notation has been used, according to which the hyperon and meson charges appear as superscript and subscript, respectively. As an example of how to use these techniques, the Appendix B shows the explicit calculation of the parity-violating $\langle nK^+|H_{pv}|p\rangle$ amplitude. Using the isospin structure of the potential defined in the previous section, the $\langle NK|H_{pv}|N\rangle$

matrix elements are connected to the coupling constants C_K^{PV} and D_K^{PV} of Eq. (2.13) via the following identities:

$$\langle nK^0|H_{pv}|n\rangle = C_K^{PV} + D_K^{PV} \tag{2.72}$$

$$\langle pK^0|H_{pv}|p\rangle = D_K^{PV} \tag{2.73}$$

$$\langle nK^+|H_{pv}|p\rangle = C_K^{PV} . \tag{2.74}$$

As shown above, the symmetry of SU(3) allows connecting the amplitudes of the physical pionic decays with those of the unphysical decays involving etas and kaons. $SU(6)_w$, on the other hand, furthermore permits relating the amplitudes involving pseudoscalar mesons with those of the vector mesons. Refs. [DF96,To82] give more details of the calculation, here just the final relations in terms of the coupling constants given in the previous section, rather than matrix elements, are shown,

$$A_\pi = \frac{1}{\sqrt{2}}\Lambda_-^0 \tag{2.75}$$

$$A_\eta = \sqrt{\frac{3}{2}}\Lambda_-^0 \tag{2.76}$$

$$C_K^{PV} = \sqrt{\frac{3}{2}}\Lambda_-^0 + \frac{1}{\sqrt{2}}\Sigma_0^+ \tag{2.77}$$

$$D_K^{PV} = -\sqrt{2}\Sigma_0^+ \tag{2.78}$$

$$A_\rho = \varepsilon_\rho = \frac{2}{3}\Lambda_-^0 - \frac{1}{\sqrt{3}}\Sigma_0^+ + \sqrt{3}a_T \tag{2.79}$$

$$A_\omega = \varepsilon_\omega = \Sigma_0^+ - \frac{1}{3}a_T \tag{2.80}$$

$$C_{K^*}^{PV} = -\sqrt{3}\Lambda_-^0 + \frac{1}{3}\Sigma_0^+ + \frac{10}{3}a_T \tag{2.81}$$

$$D_{K^*}^{PV} = -\frac{2}{3}\Sigma_0^+ + \frac{8}{9}a_T . \tag{2.82}$$

The numerical values of the constants are given in Table 2.2. Note, that an additional parameter, a_T, is present in the coupling constants for the vector mesons. This coupling, which is very small in the case of pion emission due to PCAC, can be calculated in the factorization approximation, where the vector meson is coupled to the vacuum by one of the weak currents. The numerical value is $a_T = -0.953 \times 10^{-7}$ taken from Ref. [To82].

2.2.2 The Parity-Conserving Amplitudes

A description of the physical nonleptonic decay amplitudes $B \rightarrow B' + \pi$ can also be performed by using a lowest-order chiral analysis. Employing a chiral lagrangian truncated at lowest order in the energy expansion for the PV (or s-wave) amplitudes, yields results identical to those discussed above for pseudoscalar mesons. However if one defines the lowest-order chiral lagrangian for PC (or p-wave) amplitudes, one finds that such an operator has to vanish since it has the wrong transformation properties under CP. Thus, the only allowed chiral lagrangian at lowest order can generate PV but not PC terms.

The standard method to compute the PC amplitudes is the so-called pole model. As shown in Ref. [Do86], this approach can be motivated by considering the transition amplitude for the nonleptonic emission of a meson

$$\langle B' M_i(q)|H_w|B\rangle = \int d^4x e^{iqx}\theta(x^0)\langle B'|[\partial A_i(x), H_w(0)]|B\rangle \ . \tag{2.83}$$

Inserting a complete set of intermediate states, $\{|n\rangle\}$, one can show that

$$\langle B' M_i(q)|H_w|B\rangle = -\int d^3x e^{iqx}\langle B'|[A_i^0(x,0), H_w(0)]|B\rangle - q_\mu M_i^\mu \ , \tag{2.84}$$

where

$$\begin{aligned} M_i^\mu &= (2\pi)^3 \sum_n \left[\delta(\vec{p}_n - \vec{p}_{B'} - \vec{q}) \frac{\langle B'|A_i^\mu(0)|n\rangle\langle n|H_w(0)|B\rangle}{p_B^0 - p_n^0} \right. \\ &+ \left. \delta(\vec{p}_B - \vec{p}_n - \vec{q}) \frac{\langle B'|H_w(0)|n\rangle\langle n|A_i^\mu(0)|B\rangle}{p_B^0 - q^0 - p_n^0} \right] \ . \end{aligned} \tag{2.85}$$

While the first term in Eq. (2.84) becomes the commutator introduced in Eq. (2.65), the second term contains contributions from the $\frac{1}{2}^+$ ground state baryons which are singular in the SU(3) soft-meson limit. These pole terms become the leading contribution to the PC amplitudes. Note in passing that in principle, such baryon-pole terms can also contribute to the PV amplitudes, however, more detailed studies [Do86] showed that their magnitude is only several per cent of the leading current algebra contribution.

The first step is to compute the p-wave amplitude of the $\Lambda \rightarrow N\pi$ decay since here one can compare with experiment. The contribution to the PC weak vertex coming from the baryon-pole diagrams shown in Figs. 2.4(a) and (b) are given by:

$$B_\pi = g_{NN\pi} \frac{1}{m_\Lambda - m_N} A_{N\Lambda} + g_{\Lambda\Sigma\pi} \frac{1}{m_N - m_\Sigma} A_{N\Sigma} \ , \tag{2.86}$$

Table 2.2. Nijmegen [NR77] (Jülich [HH89]) strong coupling constants, weak coupling constants [DF96] and cut-off parameters for the different mesons. The weak couplings are in units of $G_F m_\pi{}^2 = 2.21 \times 10^{-7}$. For the kaon and the ρ-meson we also quote the weak couplings obtained by Ref. [SS96] and Ref. [Na88], respectively.

Meson	Strong c.c.	Weak c.c.		Λ_i
		PC	PV	(GeV)
π	$g_{NN\pi} = 13.3$	B_π=−7.15	A_π=1.05	1.30
	$g_{\Lambda\Sigma\pi} = 12.0(9.8)$			
η	$g_{NN\eta} = 6.40(0.)$	B_η=−14.3	A_η=1.80	1.30
	$g_{\Lambda\Lambda\eta} = -6.56(0.)$			
K	$g_{\Lambda NK} = -14.1(-13.5)$	C_K^{PC}=−18.9	C_K^{PV}=0.76	1.20
		=−14.0 [SS96]	=0.40 [SS96]	
	$g_{N\Sigma K} = 4.28(3.55)$	D_K^{PC}=6.63	D_K^{PV}=2.09	
		=3.20 [SS96]	=1.50 [SS96]	
ρ	$g^V_{NN\rho} = 3.16(3.25)$	α_ρ=−3.50	ϵ_ρ=1.09	1.40
		=−3.39 [Na88]	=3.84 [Na88]	
	$g^T_{NN\rho} = 13.3(19.8)$	β_ρ=−6.11		
		=−7.11 [Na88]		
	$g^V_{\Lambda\Sigma\rho} = 0(0)$			
	$g^T_{\Lambda\Sigma\rho} = 11.2(16.0)$			
ω	$g^V_{NN\omega} = 10.5(15.9)$	α_ω=−3.69	ϵ_ω= −1.33	1.50
	$g^T_{NN\omega} = 3.22(0)$	β_ω=−8.04		
	$g^V_{\Lambda\Lambda\omega} = 7.11(10.6)$			
	$g^T_{\Lambda\Lambda\omega} = -4.04(-9.91)$			
K*	$g^V_{\Lambda NK^*} = -5.47(-5.63)$	$C_{K^*}^{PC,V}$=−3.61	$C_{K^*}^{PV}$=−4.48	2.20
	$g^T_{\Lambda NK^*} = -11.9(-18.4)$	$C_{K^*}^{PC,T}$=−17.9		
	$g^V_{N\Sigma K^*} = -3.16(-3.25)$	$D_{K^*}^{PC,V}$=−4.89	$D_{K^*}^{PV}$=0.60	
	$g^T_{N\Sigma K^*} = 6.00(7.87)$	$D_{K^*}^{PC,T}$=9.30		

where $A_{N\Lambda}$ and $A_{N\Sigma}$ are weak baryon → baryon transition amplitudes that can be

related to the process $\Lambda \to N\pi$ and $\Sigma \to N\pi$. These quantities can be determined via current algebra/PCAC as before

$$\lim_{q\to 0}\langle \pi^0 n|H_{pv}|\Lambda\rangle = \frac{-i}{F_\pi}\langle n|[F^5_{\pi^0}, H_{pv}]|\Lambda\rangle = \frac{i}{2F_\pi}\langle n|H_{pc}|\Lambda\rangle \tag{2.87}$$

$$\lim_{q\to 0}\langle \pi^0 p|H_{pv}|\Sigma^+\rangle = \frac{-i}{F_\pi}\langle p|[F^5_{\pi^0}, H_{pv}]|\Sigma^+\rangle = \frac{i}{2F_\pi}\langle p|H_{pc}|\Sigma^+\rangle\ . \tag{2.88}$$

Then assuming no momentum dependence for the baryon s-wave decay amplitude and absorbing the i factor in the definitions of $A_{N\Lambda}$ and $A_{N\Sigma}$, one gets:

$$\begin{aligned} A_{N\Lambda} &= i\langle n|H_{pc}|\Lambda\rangle = 2F_\pi\langle \pi^0 n|H_{pv}|\Lambda\rangle = -\sqrt{2}F_\pi\langle \pi^- p|H_{pv}|\Lambda\rangle \qquad (2.89)\\ &= -4.32\times 10^{-5}\ \text{MeV}\\ A_{N\Sigma} &= \frac{i}{\sqrt{2}}\langle p|H_{pc}|\Sigma^+\rangle = \sqrt{2}F_\pi\langle \pi^0 p|H_{pv}|\Sigma^+\rangle\\ &= -4.35\times 10^{-5}\ \text{MeV}. \qquad (2.90)\end{aligned}$$

With these values, obtained from the physical $\Lambda \to p\ \pi^-$ and $\Sigma^+ \to p\ \pi^0$ parity-violating amplitudes, and using the Nijmegen strong coupling constants $g_{NN\pi}$ and $g_{\Lambda\Sigma\pi}$ listed in Table 2.2, we derive $B_\pi = -11.98\times 10^{-7}$, which is within 24% of the experimental value ($B_\pi^{exp} = -7.15\times G_F m_\pi^2 = -15.80\times 10^{-7}$). If one chooses the Jülich B strong couplings rather than the Nijmegen ones, also listed in Table 2.2, the new value for B_π is -15.74×10^{-7}, closer to the experimental one. In the calculations, the experimental value has been used.

In view of this result, it seems reasonable to take the Jülich B strong coupling constants to work out the weak PC couplings for the other mesons contributing to the decay mechanism. However, no arguments of the same kind as for the pion can be made for the five mesons left. There are no experimental values of the couplings to compare the predicted constants obtained within this model. Furthermore, taking into account the breaking of the SU(3) symmetry leads already to an uncertainty in the value of the strong constants of at least 30%. As a consequence, our results will implicitly carry the effect of such uncertainty. In § 3 results using the Nijmegen set of constants as well as the Jülich one in the strong sector will be given.

For the η contribution the PC $\Lambda N\eta$ term, shown in Figs. 2.4(c) and (d), can be written as:

$$B_\eta = g_{NN\eta}\frac{1}{m_\Lambda - m_N}A_{N\Lambda} + g_{\Lambda\Lambda\eta}\frac{1}{m_N - m_\Lambda}A_{N\Lambda}\ , \tag{2.91}$$

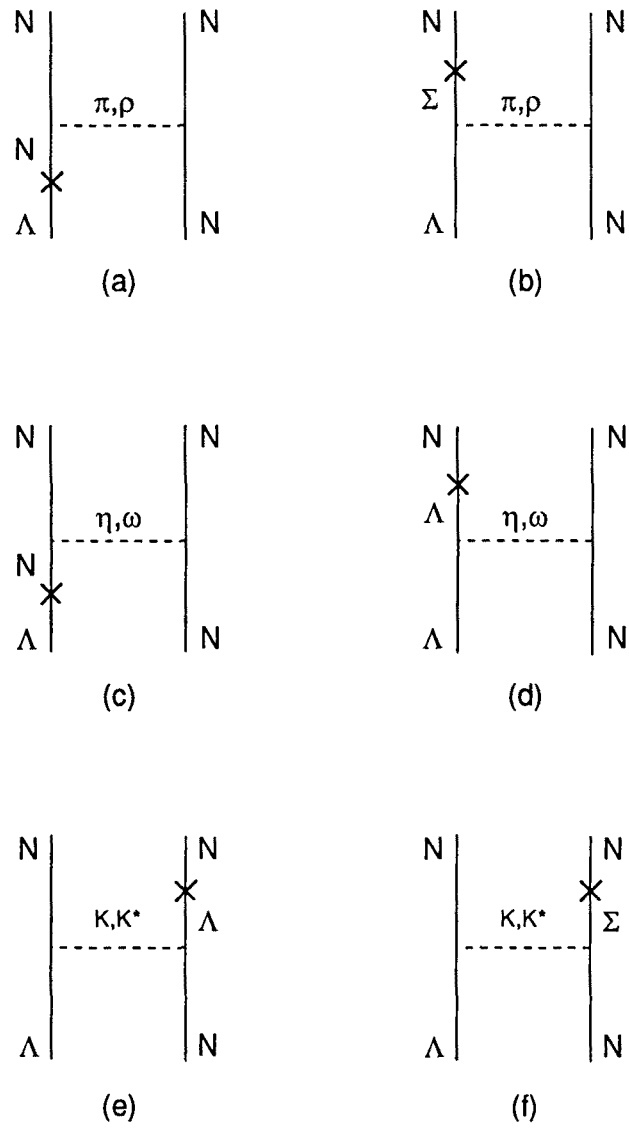

Figure 2.4. Baryon-pole diagrams contributing to the PC weak vertices in the ΛN→NN transition amplitude.

while for the kaon (Figs. 2.4(e) and (f)), the expressions are:

$$\langle \mathrm{nK}^+|H_{\mathrm{pc}}|\mathrm{p}\rangle = C_{\mathrm{K}}^{\mathrm{PC}} = g_{\Lambda \mathrm{pK}^+}\frac{1}{m_{\mathrm{n}}-m_{\Lambda}}A_{\mathrm{n}\Lambda} + g_{\mathrm{p}\Sigma^0\mathrm{K}^+}\frac{1}{m_{\mathrm{n}}-m_{\Sigma}^0}A_{\mathrm{n}\Sigma^0}$$

$$= g_{\Lambda NK}\frac{1}{m_N - m_\Lambda}A_{N\Lambda} - g_{N\Sigma K}\frac{1}{m_N - m_\Sigma}A_{N\Sigma} \tag{2.92}$$

$$\langle pK^0|H_{pc}|p\rangle = D_K^{PC} = g_{p\Sigma^+K^0}\frac{1}{m_p - m_\Sigma^+}A_{p\Sigma^+}$$

$$= 2g_{N\Sigma K}\frac{1}{m_N - m_\Sigma}A_{N\Sigma}\ , \tag{2.93}$$

where the relations $A_{n\Sigma^0} = -A_{N\Sigma}$ and $A_{p\Sigma^+} = \sqrt{2}A_{N\Sigma}$ have been used.

The expressions for the vector mesons are similar:

$$\alpha_\rho = g^V_{NN\rho}\frac{1}{m_\Lambda - m_N}A_{N\Lambda} + g^V_{\Lambda\Sigma\rho}\frac{1}{m_N - m_\Sigma}A_{N\Sigma} \tag{2.94}$$

$$\alpha_\omega = g^V_{NN\omega}\frac{1}{m_\Lambda - m_N}A_{N\Lambda} + g^V_{\Lambda\Lambda\omega}\frac{1}{m_N - m_\Lambda}A_{N\Lambda} \tag{2.95}$$

$$C_{K^*}^{PC,V} = g^V_{\Lambda NK^*}\frac{1}{m_N - m_\Lambda}A_{N\Lambda} - g^V_{N\Sigma K^*}\frac{1}{m_N - m_\Sigma}A_{N\Sigma} \tag{2.96}$$

$$D_{K^*}^{PC,V} = 2g^V_{N\Sigma K^*}\frac{1}{m_N - m_\Sigma}A_{N\Sigma}\ , \tag{2.97}$$

and the tensor coupling constants β_ρ, β_ω, $C_{K^*}^{PC,T}$ and $D_{K^*}^{PC,T}$ are obtained from the previous relations by replacing the strong vector couplings with the tensor ones. The numerical values of all these coupling constants can be found in Table 2.2.

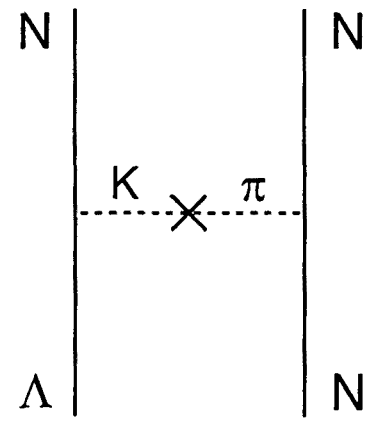

Figure 2.5. Meson-pole diagram contributing to the ΛN→NN transition amplitude.

Some studies have included meson-pole diagrams of the form shown in Fig. 2.5 whose contribution would be given by:

$$g_{\Lambda NK}\frac{1}{m_K^2 - m_\pi^2}A_{K\pi} \ , \tag{2.98}$$

where the meson → meson weak transition amplitude $A_{K\pi}$ can also be related via PCAC to the experimental amplitude for K→ $\pi\pi$ decay, yielding $A_{K\pi} = -2.5 \times 10^{-3}$ MeV^2 [Do86]. There is considerable uncertainty regarding the phase between the meson and the baryon poles which lead some studies to adjust it to better reproduce the data. It has been argued [Do86] that the presence of these meson-pole diagrams is important to fulfil the requirements of the so-called Feinberg-Kabir-Weinberg theorem in the nonleptonic decays. On the other hand, counting powers of energy in a chiral analysis, one finds that while the baryon-pole terms are of order q^{-1} the meson poles enter at next order, along with higher-order chiral lagrangians. In general, it has been found that these contributions are very small and have therefore been neglected in the following. In principle, SU(6)$_w$ can be used as well to relate the weak meson → meson pseudoscalar transition amplitudes with those of the vector mesons. The results, given here for completeness, are:

$$A_{K\eta} = -\frac{1}{\sqrt{3}}A_{K\pi} \tag{2.99}$$

$$A_{K^*\rho} = A_{K\pi} \tag{2.100}$$

$$A_{K^*\omega} = -\frac{1}{\sqrt{3}}A_{K\pi} \ . \tag{2.101}$$

2.3 Two-Body Amplitudes

In this section the elementary two-body transition amplitude $t_{\Lambda N\to NN}$ which describes the one-nucleon induced decay of the Λ-particle in hypernuclei, will be derived. This amplitude contains the dynamics of the weak decay process, as it is shown in Eq. (1.11). In the first place, it is necessary to rewrite the product of two single-particle wave functions, $\langle \vec{r}_1 \mid \alpha_\Lambda \rangle$ and $\langle \vec{r}_2 \mid \alpha_N \rangle$, in terms of relative, $\vec{r}$, and center-of-mass coordinates, $\vec{R}$. Via the Moshinsky brackets [Mo59] one may connect the wave functions for two particles in a common harmonic oscillator potential with the wave functions given in terms of the relative and center-of-mass coordinates of the two particles. In the present work, the single-particle Λ and N orbits are taken to be solutions of harmonic oscillator mean

field potentials with parameters b_Λ and b_N, respectively, that have been adjusted to experimental separation energies and charge form factor of the hypernucleus under study. Assuming an average size parameter $b = (b_\Lambda + b_N)/2$ and working in the LS representation, the product of the two harmonic oscillator single-particle states, $\Phi^\Lambda_{nlm}(\vec{r}_1\,/b)$ and $\Phi^N_{n'l'm'}(\vec{r}_2\,/b)$, can be transformed to a linear combination of products of relative and center-of-mass wave functions, $\Phi^{\rm rel}_{N_r L_r M_{L_r}}(\vec{r}\,/\sqrt{2}b)$ and $\Phi^{\rm CM}_{N_R L_R M_{L_R}}(\vec{R}\,/(b/\sqrt{2}))$, respectively. Since the Λ is in a $l_\Lambda = 0$ shell, one obtains:

$$\Phi^\Lambda_{100}\left(\frac{\vec{r}_1}{b}\right)\Phi^N_{100}\left(\frac{\vec{r}_2}{b}\right) = \Phi^{\rm rel}_{100}\left(\frac{\vec{r}}{\sqrt{2}b}\right)\Phi^{\rm CM}_{100}\left(\frac{\vec{R}}{b/\sqrt{2}}\right)\,, \tag{2.102}$$

when the nucleon is in the s-shell and

$$\Phi^\Lambda_{100}\left(\frac{\vec{r}_1}{b}\right)\Phi^N_{11m}\left(\frac{\vec{r}_2}{b}\right) = \frac{1}{\sqrt{2}}\left\{\Phi^{\rm rel}_{100}\left(\frac{\vec{r}}{\sqrt{2}b}\right)\Phi^{\rm CM}_{11m}\left(\frac{\vec{R}}{b/\sqrt{2}}\right) - \Phi^{\rm rel}_{11m}\left(\frac{\vec{r}}{\sqrt{2}b}\right)\Phi^{\rm CM}_{100}\left(\frac{\vec{R}}{b/\sqrt{2}}\right)\right\} \tag{2.103}$$

when the nucleon is in the p-shell. With this decomposition, the amplitude $t_{\Lambda N\to NN}$ of Eq. (1.11) can be written in terms of amplitudes which depend on C.M. and relative orbital angular momentum quantum numbers

$$t_{\Lambda N\to NN} = \sum_{N_r L_r N_R L_R} X(N_r L_r N_R L_R, l_\Lambda l_N)\; t^{N_r L_r N_R L_R}_{\Lambda N\to NN}\,, \tag{2.104}$$

where $X(N_r L_r N_R L_R, l_\Lambda l_N)$ are the Moshinsky brackets which for l_Λ=l_N=0 are just $X(1\;0\;1\;0,\;0\;0) = 1$, and for $l_N = 1$ are $X(1\;0\;1\;1,\;0\;1) = 1/\sqrt{2}$ and $X(1\;1\;1\;0,\;0\;1) = -1/\sqrt{2}$.

As for the final NN state, the antisymmetric state of two independently moving nucleons with total momentum $\vec{P}$ and relative momentum $\vec{k}$ reads:

$$\left\langle \vec{R}\,\vec{r}\,\middle|\,\vec{P}\,\vec{k}\;S\,M_S\;T\,M_T\right\rangle = \frac{1}{\sqrt{2}}e^{i\vec{P}\vec{R}}\left(e^{i\vec{k}\vec{r}} - (-1)^{S+T}e^{-i\vec{k}\vec{r}}\right)\chi^S_{M_S}\chi^T_{M_T}\,. \tag{2.105}$$

In order to incorporate the effects of the NN interaction the plane wave describing the relative NN motion needs to be substituted by a distorted wave

$$e^{i\vec{k}\vec{r}} \to \Psi_{\vec{k}}(\vec{r})\,. \tag{2.106}$$

In § 2.5 it is shown how the distorted wave is obtained via the solution of an R-matrix scattering problem.

The matrix elements $t^{N_r L_r N_R L_R}_{\Lambda N \to NN}$ (Eq. 2.104) are given by:

$$\begin{aligned} t^{N_r L_r N_R L_R}_{\Lambda N \to NN} &= \frac{1}{\sqrt{2}} \int d^3R \int d^3r \, e^{-i\vec{P}\vec{R}} \Psi^*_{\vec{k}}(\vec{r}) \chi^{\dagger S}_{M_S} \chi^{\dagger T}_{T_3} V(\vec{r}) \, \Phi^{\rm CM}_{N_R L_R}\left(\frac{\vec{R}}{b/\sqrt{2}}\right) \\ &\times \Phi^{\rm rel}_{N_r L_r}\left(\frac{\vec{r}}{\sqrt{2}b}\right) \chi^{S_0}_{M_{S_0}} \chi^{T_0}_{T_{3_0}} \\ &= (2\pi)^{3/2} \, \Phi^{CM}_{N_R L_R}\left(\vec{P}\frac{b}{\sqrt{2}}\right) \, t_{\rm rel} \, , \end{aligned} \tag{2.107}$$

with

$$t_{\rm rel} = \frac{1}{\sqrt{2}} \int d^3r \, \Psi^*_{\vec{k}}(\vec{r}) \chi^{\dagger S}_{M_S} \chi^{\dagger T}_{T_3} V(\vec{r}) \, \Phi^{\rm rel}_{N_r L_r}\left(\frac{\vec{r}}{\sqrt{2}b}\right) \chi^{S_0}_{M_{S_0}} \chi^{T_0}_{T_{3_0}} \, , \tag{2.108}$$

where, for simplicity, only the direct amplitude corresponding to the first term of Eq. (2.105) is shown. The exchange term of the ΛN→NN diagram can be evaluated easily once one performs an expansion of the exponentials appearing in Eq. (2.105)

$$e^{i\vec{k}\vec{r}} = \sum_{LM_L} 4\pi i^L \, j_L(kr) \, Y^*_{LM_L}(\hat{k}) \, Y_{LM_L}(\hat{r}) \tag{2.109}$$

$$\begin{aligned} e^{-i\vec{k}\vec{r}} &= \sum_{LM_L} 4\pi i^L \, j_L(kr) \, Y^*_{LM_L}(-\hat{k}) \, Y_{LM_L}(\hat{r}) \\ &= \sum_{LM_L} (-1)^L 4\pi i^L \, j_L(kr) \, Y^*_{LM_L}(\hat{k}) \, Y_{LM_L}(\hat{r}) \, . \end{aligned} \tag{2.110}$$

This exchange contribution can be then easily incorporated via the correct insertion of the factor $(-1)^{L+S+T}$ in Eq. (2.105) once the expansions have been made.

The function $\Phi^{CM}_{N_R L_R}\left(\vec{P}\frac{b}{\sqrt{2}}\right)$ is the Fourier transform of the ΛN center-of-mass wave function and $t_{\rm rel}$ is the expectation value of the transition potential $V(\vec{r})$ between ΛN and NN relative wave functions. The potential $V(\vec{r})$ has the form shown in § 2.1 where it has been decomposed as:

$$V(\vec{r}) = \sum_i \sum_\alpha V^{(i)}_\alpha(r) \, \hat{O}_\alpha \, \hat{I}^{(i)}_\alpha \, , \tag{2.111}$$

where the index i runs over the different mesons exchanged and α over the different spin operators, $\hat{O}_\alpha \in (\hat{1}, \, \vec{\sigma}_1 \vec{\sigma}_2 \, , \, S_{12}(\hat{r}) = 3 \, \vec{\sigma}_1 \hat{r} \, \vec{\sigma}_2 \hat{r} - \vec{\sigma}_1 \vec{\sigma}_2, \vec{\sigma}_2 \hat{r}, \, [\vec{\sigma}_1 \times \vec{\sigma}_2] \hat{r})$, which occur in the potential $V(\vec{r})$. The isospin operator, $\hat{I}^{(i)}_\alpha$, depends on the meson and can be either $\hat{1}$ for isoscalar mesons (η, ω), $\vec{\tau}_1 \vec{\tau}_2$ for isovector mesons (π, ρ) or a linear combination of $\hat{1}$ and $\vec{\tau}_1 \vec{\tau}_2$, with the coefficients depending on the particular spin structure piece

of the potential, for isodoublet mesons (K, K*). The radial parts $V_\alpha^{(i)}(r)$, have been discussed in § 2.1.3, are given by Eqs. (2.55) - (2.58).

By performing a partial-wave expansion of the final two-nucleon wave function and working in the $(LS)J$-coupling scheme, the relative $\Lambda N \rightarrow NN$ amplitude, $t_{\rm rel}$, can be further decomposed

$$\begin{aligned} t_{\rm rel} \;=\; & \frac{1}{\sqrt{2}} \sum_i \sum_\alpha \sum_{LL'J} 4\pi i^{-L'} \, \langle LM_L SM_S | JM_J \rangle \, Y_{LM_L}(\hat{k}_r) \\ & \langle L_r M_{L_r} S_0 M_{S_0} | JM_J \rangle \, \langle (L'S) JM_J \mid \hat{O}_\alpha \mid (L_r S_0) JM_J \rangle \\ & \langle TT_3 \mid \hat{I}_\alpha^{(i)} \mid T_0 T_{3_0} \rangle \int r^2 dr \, \Psi^{*J}_{LL'}(k_r, r) \, V_\alpha^{(i)}(r) \, \Phi^{\rm rel}_{N_r L_r}(\frac{r}{\sqrt{2}b}) \, , \end{aligned} \tag{2.112}$$

where $\Phi^{\rm rel}_{N_r L_r}(r/(\sqrt{2}b))$ stands for the radial piece of the H.O. wave function. The explicit expressions for $\langle (L'S) JM_J \mid \hat{O}_\alpha \mid (L_r S_0) JM_J \rangle$, the expectation values of the spin-space pieces, can be found in Appendix A.

The function $\Psi^J_{LL'}(k_r, r)$ is the scattering solution of two nucleons moving under the influence of the strong interaction, for which the updated version of the Reid soft-core potential [Re68], given in Ref. [SK94], and the Nijmegen [SK94] NN potential have been taken. Such a wave function is obtained by solving an R-matrix equation (see § 2.5) in momentum space and using partial-wave decomposition, following the method described in Ref. [HT70]. The tensor component of the NN interaction couples relative orbital states (L and L') having the same parity and total angular momentum as, for instance, the $^3S_1$ and $^3D_1$ channels. Therefore, starting from an initial L_r orbital momentum, the weak transition potential produces a transition to a L' value, which mixes, through the subsequent action of the strong interaction, with another value of orbital angular momentum, L. In Table 2.3 one can find all the possible final states starting from initial ΛN states having either $L_r = 0$ or 1 and for the central ($\Delta\vec{S} = 0$, $\Delta\vec{L} = 0$), tensor ($\Delta\vec{S} = 2$, $\Delta\vec{L} = 2$) and parity-violating ($\Delta\vec{S} = 1$, $\Delta\vec{L} = 1$) pieces in which the transition potential can be decomposed. In the absence of final state interactions (FSI), the NN wave function in Eq. (2.112) would reduce to a spherical Bessel function

$$\Psi^J_{LL'}(k_r, r) = \delta_{L,L'} \, j_L(k_r r) \; . \tag{2.113}$$

Note that the procedure followed here to include FSI between the two emitted nucleons differs from the simplified choice taken in our previous works [PR96,BP95], where the non-interacting NN pair, represented by a Bessel function in the final state, was

multiplied by an average NN correlation function

$$f_{\rm FSI}(r) = 1 - j_0(q_c r), \tag{2.114}$$

with $q_c = 3.93$ fm^{-1}, which provides a good description of nucleon pairs in ^{4}He [We77] as calculated with the Reid soft-core interaction [Re68].

2.4 Initial State Correlations

When evaluating the matrix elements of the ΛN→NN transition in nuclei one must take into account that, simultaneously with the weak exchange of the meson, there exists the strong interaction between nucleons or between the Λ and the N. The short-range nuclear forces generate short-range correlations (SRC) which must be taken into account. As it has been already mentioned, the momentum carried by the exchanged meson in the nonmesonic weak decay of a Λ in a hypernucleus is of the order of 400 MeV/c. This leads to a short-range process, thus the influence of short-range correlations between the interacting ΛN pair in the decay is of great relevance.

To account for the ΛN correlations which are absent in the independent-particle model, we replace the harmonic oscillator ΛN wave function, $\Phi^{\rm rel}_{N_r L_r}(r/(\sqrt{2}b))$, by a correlated ΛN wave function that contains the effect of the strong ΛN interaction. Such wave functions were obtained from a microscopic finite-nucleus G-matrix calculation [Ha93] using the soft-core and hard-core Nijmegen models [NR77]. As it will be shown below, multiplying the uncorrelated harmonic oscillator ΛN wave function with the spin-independent correlation function

$$f(r) = \left(1 - {\rm e}^{-r^2/a^2}\right)^n + br^2{\rm e}^{-r^2/c^2}\ , \tag{2.115}$$

with $a = 0.5$, $b = 0.25$, $c = 1.28$, $n = 2$, yields decay rates slightly larger than those obtained with the numerical Nijmegen soft-core correlations but slightly smaller than those computed with the Nijmegen hard-core potential. Since the deviations are at most 10% the above parametrization can be used as a good approximation to the full correlation function.

One of the open problems in the study of the weak decay of hypernuclei in the early 90's was to reconcile the differences for the effect of correlations found by the nonrelativistic and relativistic approaches. The nonrelativistic calculations performed

Table 2.3. Possible $^{2S+1}L_J$ channels present in the weak decay of p-shell hypernuclei.

L_r	Weak decay channel (ΛN)	L' (NN)	Strong FSI (NN)	L
	Central			
$^1S_0$	→	$^1S_0$	→	$^1S_0$
$^3S_1$	→	$^3S_1$	→	$^3S_1, ^3D_1$
$^1P_1$	→	$^1P_1$	→	$^1P_1$
$^3P_0$	→	$^3P_0$	→	$^3P_0$
$^3P_1$	→	$^3P_1$	→	$^3P_1$
$^3P_2$	→	$^3P_2$	→	$^3P_2, ^3F_2$
	Tensor			
$^3S_1$	→	$^3D_1$	→	$^3D_1, ^3S_1$
$^3P_0$	→	$^3P_0$	→	$^3P_0$
$^3P_1$	→	$^3P_1$	→	$^3P_1$
$^3P_2$	→	$^3P_2, ^3F_2$	→	$^3P_2, ^3F_2$
	P.V.			
$^1S_0$	→	$^3P_0$	→	$^3P_0$
$^3S_1$	→	$^1P_1$	→	$^1P_1$
$^3S_1$	→	$^3P_1$	→	$^3P_1$
$^1P_1$	→	$^3S_1, ^3D_1$	→	$^3S_1, ^3D_1$
$^3P_0$	→	$^1S_0$	→	$^1S_0$
$^3P_1$	→	$^3S_1, ^3D_1$	→	$^3S_1, ^3D_1$
$^3P_2$	→	$^1D_2$	→	$^1D_2$
$^3P_2$	→	$^3D_2$	→	$^3D_2$

in nuclear matter in the past [MG84,OS85, Du86] showed a reduction of the non-mesonic rate by a factor of up to 2 once these correlations were taken into account. In finite nuclei calculations using the Local Density Approximation [OS85], where there are regions with smaller density than the normal nuclear matter density, the reduction

is smaller, of the order of 30% for a nucleus like ${}^{12}_{\Lambda}$C. On the other hand, a relativistic calculation performed in ${}^{12}_{\Lambda}$C [RB91,RM92] found twice as much reduction when including a similar correlation function. One may expect the discrepancy between both calculations to come from the new ingredients considered in Refs. [RB91,RM92], as the relativistic formalism based on Dirac phenomenology or the consideration of a finite system rather than nuclear matter.

In Ref. [PR94] there is a first attempt to explain the origin of the discrepancy, including a detailed analysis of the influence of SRC in the nonmesonic decay of Λ-hypernuclei, considering different correlation functions for the initial ΛN system and comparing their effect in both models, the relativistic and the nonrelativistic one. The study focused on s-shell nucleons of ${}^{12}_{\Lambda}$C. The correlated wave functions were obtained in r-space by solving the ΛΣ coupled channel Bethe-Goldstone equation [Ha93]. There, solutions of the hard-core model D and the soft-core Nijmegen interactions [NR77] were used. In Fig. 2.6, the correlation function, defined as the ratio $f_{LSJ}(r) = \Psi_{LSJ}(r)/\Phi_{LSJ}(r)$ between the correlated and the uncorrelated wave function, is plotted for the hard-core and soft-core potentials respectively. In this figure the spin-independent parametrization given in Eq. (2.115) is also plotted and it is the same function used in Ref. [RM92]. Looking at these plots one can see the "hole" present in the wave function produced by the strong repulsion of the hyperon-nucleon force at short distances, preventing the Λ and the N from being close.

The results obtained in Ref. [PR94] are summarized in Tables 2.4 and 2.5. Table 2.4 shows the contribution to the nonmesonic rate, divided between the parity-conserving (PC), parity-violating (PV) and total rates (Total), of the s-shell nucleons in ${}^{12}_{\Lambda}$C for the different correlations quoted above. The harmonic oscillator size parameters taken for the nucleon and the Λ-particle are $b_{\rm N} = 1.64$ fm and $b_{\Lambda} = 1.87$ fm, respectively. The first column in the table gives the uncorrelated rate (FREE), the second column represents the rate obtained when the hard-core interaction is used to obtain the correlated ΛN wave function (HARD), the third one represents the same calculation but using the soft-core interaction (SOFT) and the last one stands for the correlated rate when the correlation function of Eq. (2.115) is used ($f(r)$). In this s-shell study, the reduction factor on the rate due to the inclusion of short-range correlations, varies from 1.3 to 1.5. The results are consistent with the other nonrelativistic approaches [MG84,OS85,Du86] (which give a reduction factor close to 2), where the slightly larger reduction is due to the use of a NN correlation function which has a somewhat larger

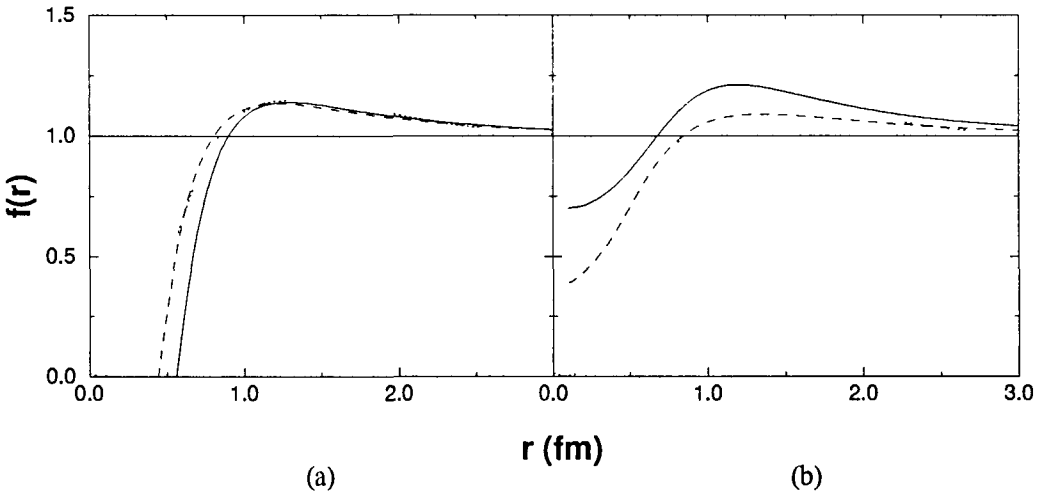

Figure 2.6. Correlation function for the ΛN channel $^1S_0$ (full line) and $^3S_1$ (dashed line) in the case of the hard-core D (a) and the soft-core (b) Nijmegen potential. The dotted line stands for the spin-independent parametrization $f(r)$ used in this work.

core than that of the ΛN system and/or the larger nuclear matter density, ρ_0, compared to an average density for $^{12}_{\Lambda}$C. It is interesting to compare the results of Table 2.4 with what is obtained in the relativistic model of Ref. [RM92], shown in Table 2.5. The reduction factor introduced by SRC is about 3, even when the same correlation function (2.115) is used.

Table 2.4. s-shell nonmesonic rate $\Gamma_{nm}/\Gamma_\Lambda$ for $^{12}_{\Lambda}$C.

	FREE	HARD	SOFT	f(r)
PC	0.479	0.307	0.343	0.324
PV	0.208	0.146	0.192	0.162
Total	0.687	0.453	0.535	0.486

The study of Ref. [PR94] was further elaborated in Ref. [PR95], where one finds a revised version of these calculations and a definite answer to the problem, showing that the explanation can be traced to the way the correlations are implemented.

To start explaining where the difference between both approaches comes from, one

Table 2.5. s-shell nonmesonic rate $\Gamma_{nm}/\Gamma_\Lambda$ for $^{12}_{\Lambda}$C from the relativistic model of Ref. [RM92].

	FREE	f(r)
PC	0.456	0.130
PV	0.177	0.058
Total	0.633	0.188

must explore the expression of the correlated Feynman amplitude. More details of the calculation can be found in Ref. [PR95]. The starting point will be the uncorrelated Feynman diagram for the ΛN→NN transition mediated by the exchange of a pion

$$\mathcal{M}_\pi = \int d^4x d^4y \overline{\Psi}_{p_3}(x)\Gamma^{\rm W}\Psi^{\Lambda}_{p_1}(x)\Delta_\pi(x-y)\overline{\Psi}_{p_4}(y)\Gamma^{\rm S}\Psi_{p_2}(y)\ , \tag{2.116}$$

where $\Psi_{p_i}(x)$ is the free baryon field of positive energy and $\Delta_\pi(x-y)$ the pion propagator. For the weak vertex the parametrization $\Gamma^{\rm W} = G_F m_\pi^2(A + B\gamma_5)$ is taken, with A=1.05 and B=−7.15 being empirical constants adjusted to the free Λ decay (see § 2.1.1). For the strong vertex, on the other hand, a pseudoscalar coupling $\Gamma^{\rm S} = g_{\rm NN\pi}\gamma_5$ is chosen.

The nonrelativistic procedure starts from the nonrelativistic reduction of the free Feynman amplitude of Eq. (2.116) to determine the transition potential $V(\vec{r})$, and defines the correlated potential by multiplying the obtained $V(\vec{r})$ with a correlation function $f(r)$,

$$\tilde{V}(\vec{r}) = V(\vec{r})\cdot f(r)\ . \tag{2.117}$$

In contrast, the relativistic approach given in Ref. [RM92] incorporates SRC by replacing in Eq. (2.116) the free pion propagator with:

$$\Delta_\pi(x-y) \to \Delta_\pi(x-y)\cdot f(|\vec{x}-\vec{y}|) \tag{2.118}$$

and computing the decay rate starting from this correlated Feynman amplitude. Although both procedures are apparently similar, it was already noted in Ref. [PR94] that the nonrelativistic limit of Eq. (2.118) was not giving the same correlated potential of Eq. (2.117).

In order to make the differences between both approaches clear, it is convenient to study the problem in momentum space, and go back to the microscopic origin of short-range correlations. In the meson-exchange model, these correlations arise because of the

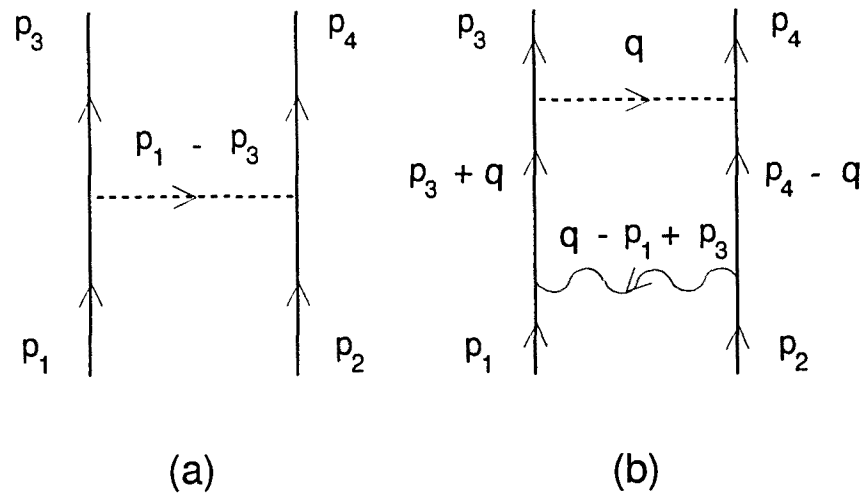

Figure 2.7. Schematic model to include correlations in the OPE potential. Bare OPE diagram (a) and OPE with simultaneous exchange of a heavy meson responsible for the short-range repulsion (b).

simultaneous exchange of heavy mesons together with one-pion exchange. A simplified picture including only one extra heavy meson is shown in Fig. 2.7. In the problem studied here, the pion-exchange (dashed line) would correspond to the weak ΛN→NN transition, while the wavy line would correspond to a strong exchange of a heavy meson, such as the omega meson. Taking into account this simultaneous exchange requires the evaluation of the loop integral:

$$\int \frac{d^3q}{(2\pi)^3} D(\vec{q})\overline{u}(\vec{p}_3)\gamma_5 u(\vec{p}_3+\vec{q})\overline{u}(\vec{p}_4)\gamma_5 u(\vec{p}_4-\vec{q})... \qquad (2.119)$$

where the parity-conserving part of the pion-exchange amplitude has been chosen for the discussion. The dots symbolize additional elements of the amplitude which are not relevant for the present discussion, such as the intermediate nucleon propagators, the propagator of the heavy meson and the vertices connecting the incoming spinors with the intermediate ones. In this expression one can see that the matrix elements of the γ_5 operators are evaluated between an external spinor and an intermediate one which depends on the loop variable $\vec{q}$. This is precisely what is obtained from the nonrelativistic procedure based in Eq. (2.117), which first builds up the transition

potential $V(r)$ and then multiplies by $f(r)$. The parity-conserving part of the correlated potential is then:

$$\tilde{V}_{\rm PC}(\vec{r}) = -\frac{G_F m_\pi^2 B}{2\overline{M}} \frac{g_{\pi {\rm NN}}}{2M} f(r) \int \frac{d^3q}{(2\pi)^3} \frac{{\rm e}^{-{\rm i}\vec{q}\vec{r}}}{\vec{q}^{\,2}+m_\pi^2} \vec{\sigma}_1\vec{q}\,\vec{\sigma}_2\vec{q}\,, \tag{2.120}$$

where the $\vec{\sigma}_i\vec{q}$ $(i=1,2)$ factors, related to the nonrelativistic reduction of the γ_5 matrix elements, depend on the momentum carried by the pion and are inside the $\vec{q}$-integration.

However, the procedure of Ref. [RM92], based on the replacement of Eq. (2.118), leads to matrix elements of γ_5 that are evaluated between spinors of the external particles and factorized out the $\vec{q}$ integral,

$$\overline{u}(\vec{p}_3)\gamma_5 u(\vec{p}_1)\overline{u}(\vec{p}_4)\gamma_5 u(\vec{p}_2) \int \frac{d^3q}{(2\pi)^3}\tilde{D}(\vec{q})\ldots\,, \tag{2.121}$$

where $\tilde{D}(\vec{q})$ stands for the Fourier transform of the modified pion propagator (Eq. (2.118)). This shows that this procedure leads to matrix elements of the γ_5 operators independent on $\vec{q}$ rather than $\vec{q}$-dependent. However, the diagram of Fig. 2.7, which gives a microscopic interpretation for the origin of correlations, shows that the bare interaction connects the final states with intermediate spinors which are $\vec{q}$-dependent. The important point is that in the construction of the correlated amplitude the vertices of the bare OPE (one-pion exchange) potential must enter the $\vec{q}$ integration as a function of $\vec{q}$ instead of factorizing out as functions of the external variables.

From the microscopic model one concludes that the form of the correlated potential given by the nonrelativistic calculations is the correct one, and that the origin of the differences between the nonrelativistic and relativistic approaches is a too simplified treatment of the correlations in Ref. [RM92] and not relativistic effects.

For completeness, and in order to illustrate more explicitly the differences between both approaches, the expression of the nonrelativistic correlated potential in r-space is given, as well as the potential corresponding to a nonrelativistic reduction of Ref. [RM92]. As it has already been pointed out, the standard nonrelativistic approach gives rise to a correlated potential of the form $\tilde{V}(\vec{r}\,) = V(\vec{r}\,)\cdot f(r)$, where $V(\vec{r}\,)$ stands for the uncorrelated potential given by Eqs. (2.51) to (2.54), and $f(r)$ is the specific correlation function used in the calculation. Within this approach, the different expressions for each radial potential channel, in the OPE case, read:

$$\tilde{V}_{\rm SS}^{(\pi)}(r) \;=\; K_{\rm SS}^{(\pi)} \frac{1}{3}\left[\mu_\pi^2 \frac{{\rm e}^{-\mu_\pi r}}{4\pi r} - \delta(r)\right] f(r) \tag{2.122}$$

$$\tilde{V}_{\rm T}^{(\pi)}(r) = K_{\rm T}^{(\pi)} \frac{1}{3} \mu_\pi^2 \frac{e^{-\mu_\pi r}}{4\pi r} \left(1 + \frac{3}{\mu_\pi r} + \frac{3}{(\mu_\pi r)^2} \right) f(r) \tag{2.123}$$

$$\tilde{V}_{\rm PV}^{(\pi)}(r) = K_{\rm PV}^{(\pi)} \mu_\pi \frac{e^{-\mu_\pi r}}{4\pi r} \left(1 + \frac{1}{\mu_\pi r} \right) f(r) \, . \tag{2.124}$$

After performing a nonrelativistic reduction and a Fourier transform of the correlated Feynman amplitude for the relativistic approach (Eq. (2.116) with the substitution (2.118)), the radial parts of the correlated potential in r-space equivalent to Ref. [RM92] are given by the following expressions:

$$\begin{aligned} \tilde{V}_{\rm SS}^{(\pi)}(r) &= K_{\rm SS}^{(\pi)} \frac{1}{3} \left\{ \left(\mu_\pi^2 \frac{e^{-\mu_\pi r}}{4\pi r} - \delta(r) \right) f(r) \right. \\ &\quad \left. - \mu_\pi^2 \frac{e^{-\mu_\pi r}}{4\pi r} \left(\frac{2}{\mu_\pi} \frac{df}{dr} - \frac{1}{\mu_\pi^2} \frac{d^2 f}{dr^2} \right) \right\} \end{aligned} \tag{2.125}$$

$$\begin{aligned} \tilde{V}_{\rm T}^{(\pi)}(r) &= K_{\rm T}^{(\pi)} \frac{1}{3} \mu_\pi^2 \frac{e^{-\mu_\pi r}}{4\pi r} \left\{ \left(1 + \frac{3}{\mu_\pi r} + \frac{3}{(\mu_\pi r)^2} \right) f(r) \right. \\ &\quad \left. - \left(\frac{3}{\mu_\pi r} + 2 \right) \frac{1}{\mu_\pi} \frac{df}{dr} + \frac{1}{\mu_\pi^2} \frac{d^2 f}{dr^2} \right\} \end{aligned} \tag{2.126}$$

$$\tilde{V}_{\rm PV}^{(\pi)}(r) = K_{\rm PV}^{(\pi)} \mu_\pi \frac{e^{-\mu_\pi r}}{4\pi r} \left\{ \left(1 + \frac{1}{\mu_\pi r} \right) f(r) - \frac{1}{\mu_\pi} \frac{df}{dr} \right\} \, . \tag{2.127}$$

In deriving these expressions, some properties involving derivatives of the delta function [PR95] have been used. By comparing Eqs. (2.124) and (2.127) one realizes that in the approach based on Eq. (2.118) one obtains new terms in the potential, involving first and second derivatives of the correlation function. This explains the different effect of SRC on the ΛN→NN decay rate discussed in this chapter.

In the same Ref. [PR95] there is a comparative study of the nonmesonic decay width for the ${}^{5}_{\Lambda}$He hypernucleus. In this hypernucleus the Λ particle, in a $s_{1/2}$ state, is coupled to the ground state of the ^{4}He (0^+). The ^{4}He core is described as four s-shell nucleons in a harmonic oscillator potential with size parameter $b_{\rm N} = 1.4$ fm (which reproduces reasonably well the ^{4}He charge form factor). For the Λ-particle one takes $b_\Lambda = 1.85$ fm, which reproduces the Λ separation energy in ${}^{5}_{\Lambda}$He, $B_\Lambda = -3.12$ MeV. For this study, three different correlation functions are used: the gaussian correlation

$$f(r) = 1 - e^{-r^2/b^2} \, , \tag{2.128}$$

with $b = 0.75$ fm, also used in nuclear matter calculations [MG84], the Bessel correlation

$$f(r) = 1 - j_0(q_c r) \, , \tag{2.129}$$

with $q_c = 3.93$ fm^{-1} [OS85], and the parametrization given by Eq. (2.115). These functions are depicted in Fig. 2.8 and in Table 2.6 a comparison of the decay rate of ${}^{5}_{\Lambda}$He between both correlated potentials, the standard nonrelativistic prescription (2.117) and the nonrelativistic reduction of the relativistic approach given by (2.118), is made (without including form factors and final state interactions). This comparison

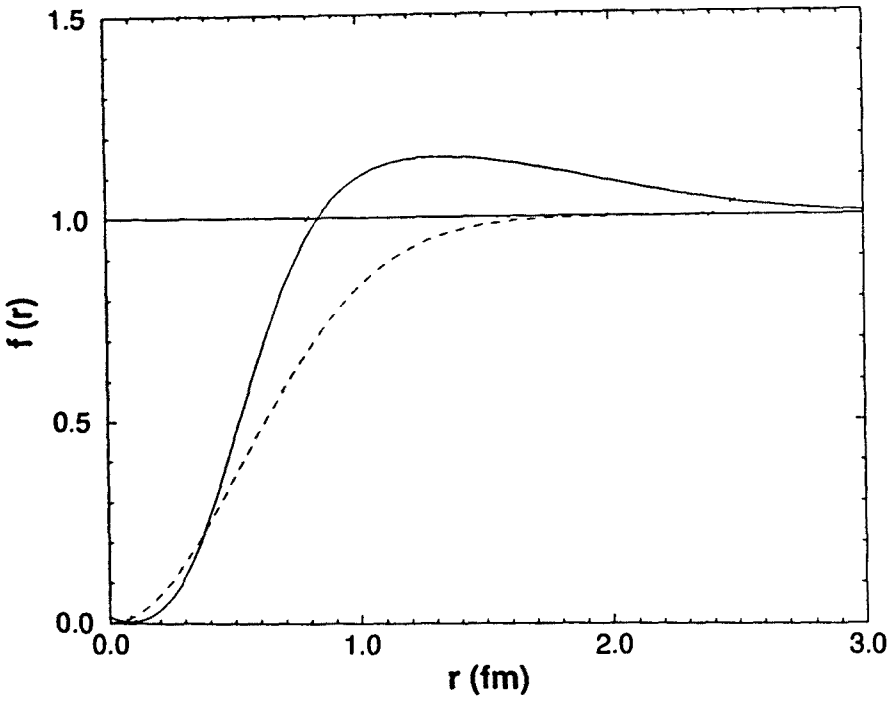

Figure 2.8. The ΛN correlation function as a function of the relative distance r. The dashed, dotted and full line correspond to the Gaussian-type of Eq. (2.128), the Bessel-type of Eq. (2.129) and the parameterization of Eq. (2.115), respectively.

is shown for the different correlation functions mentioned above. Examining the results listed in Table 2.6 one can see that in the standard nonrelativistic calculations (Eq. (2.124) in the table) the channel more drastically affected by correlations is the central SS transition, due to the fact that our correlation function is such that $f(r = 0) = 0$. Evaluating the correlated potential as $V(\vec{r}) \cdot f(r)$ completely suppresses the delta piece of the central SS part of the potential, which provides most of its contribution when SRC are turned off. Although this suppression also takes place in the prescription

given by Eq. (2.127), a larger central SS strength is obtained due to the additional derivative pieces of the correlated potential. In order to help in the understanding of these results, two figures will be shown. In Fig. 2.9, the radial integrand of the central SS transition amplitude for both correlated potentials is plotted, while in Fig. 2.10 the radial integrand corresponds to the tensor transition amplitude. These integrands have the form:

$$r^2\,\Phi_{100}(r;\sqrt{2}b)\,\tilde{V}_\alpha^{(\pi)}(r)\,j_L(k_0 r)\ , \tag{2.130}$$

where L=0,2 and α=SS,T for the central and the tensor channels, respectively. A relative momentum for the outgoing NN system of 1.97 fm^{-1} (corresponding to a back-to-back kinematics) has been chosen. Because of the change of sign in the derivative

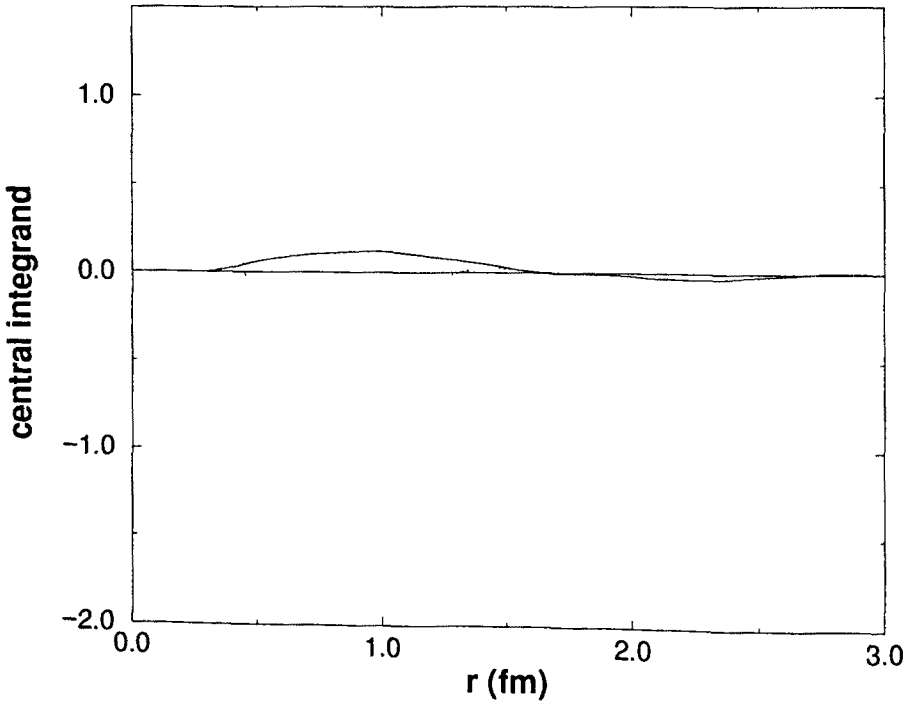

Figure 2.9. Integrand of the central transition amplitude, in arbitrary units, as a function of the relative distance r. The solid and dotted lines correspond to the correlated potentials (2.124) and (2.127) respectively, using the correlation function of Eq. (2.115).

of $f(r)$ around 0.5 fm, one can see in Fig 2.9 that the correlated transition amplitude

based on Eq. (2.127) (dotted line) shows large positive and negative contributions, which do not cancel each other completely and end up giving an integrated central SS rate much larger than that obtained from the integral of the nonrelativistic prescription (2.124) (solid line). On the other hand, it is precisely this oscillatory behavior of the correlated potential (2.127) which is the reason for the reduced tensor and parity-violating rates, as shown in the last column of Table 2.6. Let us make some comments on the tensor integrand that can be extrapolated to the parity-violating one, which is not shown here. The positive and negative parts induced by the derivative terms in Eq. (2.127) (dotted line in Fig. 2.10), tend to cancel each other giving rise to an integrated rate which is considerably smaller than the one obtained with Eq. (2.124). Depending somewhat on the correlation function used, the rates based on the correlated potential (2.127) are a factor 2-3 smaller than those obtained with (2.124).

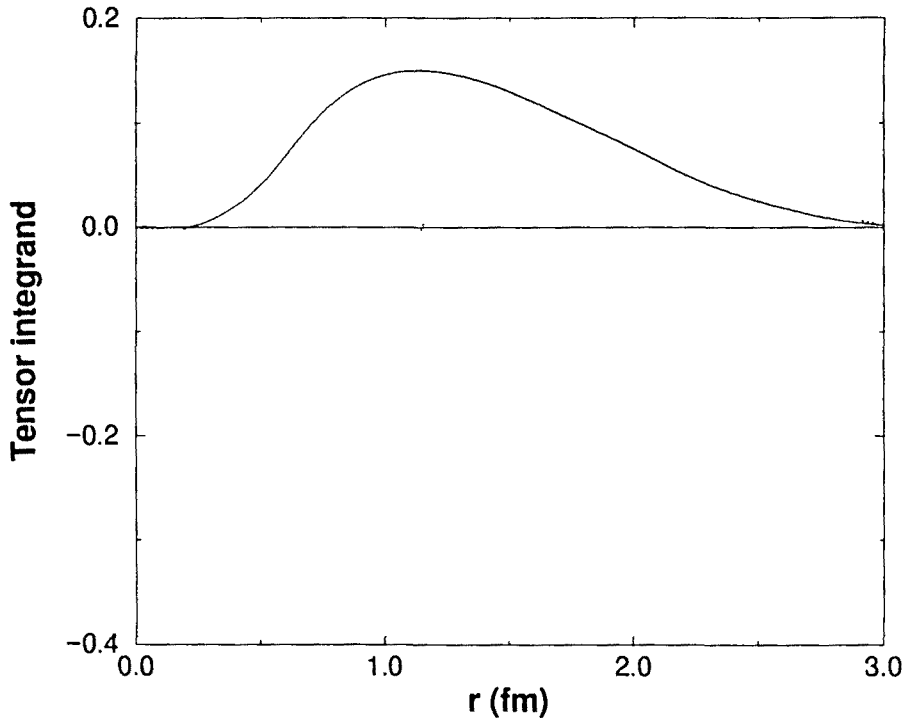

Figure 2.10. The same as Fig. 2.9 for the tensor transiton amplitude.

The numbers given in the last column for the parametrization (2.115) are very similar to the results quoted in the relativistic calculations of Ref. [RM92], where

Table 2.6. ΛN→NN decay rate of ${}^{5}_{\Lambda}$He for different correlation functions (in units of the free Λ width).

	FREE	$f(r) = 1 - e^{-r^2/b^2}$	
		Eq. (2.124)	Eq. (2.127)
SS	0.174	9.2×10^{-4}	0.028
T	0.495	0.309	0.077
PV	0.308	0.155	0.059
TOTAL	0.977	0.465	0.164
	FREE	$f(r) = 1 - j_0(q_c r)$	
		Eq. (2.124)	Eq. (2.127)
SS	0.174	2.2×10^{-3}	0.082
T	0.495	0.434	0.233
PV	0.308	0.249	0.156
TOTAL	0.977	0.685	0.471
	FREE	$f(r) = \left(1 - e^{-r^2/a^2}\right)^n + br^2 e^{-r^2/c^2}$	
		Eq. (2.124)	Eq. (2.127)
SS	0.174	1.7×10^{-3}	0.057
T	0.495	0.448	0.159
PV	0.308	0.244	0.117
TOTAL	0.977	0.694	0.333

the same correlation function is used. This fact corroborates that the origin of the discrepancies between both approaches has nothing to do with relativistic effects and is due to the prescription used to include the correlation function in the transition amplitude.

2.5 Final State Interactions

Any realistic calculation on the weak decay of Λ hypernuclei has to take into account that the two final nucleons emerging from the decay feel the influence of the medium

in which they are moving. In our case, apart from the mutual influence between both nucleons there also exists the residual interaction with the $(A-2)$-particle system. However, the most important kinematical contribution to the weak decay rate corresponds to the situation in which the nucleons emerge back-to-back with the largest possible relative momentum, which should be high enough for not being very sensitive to the possible distortions produced by the residual nucleus. This is the reason why here the effect of FSI will only take into account the mutual influence between the outgoing nucleons, through a distorted wave function for the relative two-body motion. For this purpose it is necessary to solve the reaction matrix equation in momentum space, from which the wave function corresponding to the problem of two nucleons moving under the influence of the strong interaction can be obtained. As strong interaction models, the updated version of the Reid soft-core potential [Re68] and the Nijmegen NN one, both of them given in Ref. [SK94], are used.

In § 2.3 comments on the mixing of the channels in the final relative state having the same parity and same value of the total angular momentum, due to the tensor component of the strong interaction (see Table 2.3), have already been made. We focus our attention in how to obtain the correlated wave function describing the relative motion between the two emerging nucleons. In order to obtain the correlated wave function for the final NN relative state, the procedure described in Ref. [HT70] is followed. The authors make use of a numerical matrix inversion method in order to solve the coupled channel Schrödinger equation in momentum space. The method can be applied to any nonsingular potential either local or nonlocal, central or noncentral. The starting point is the relative two-body Schrödinger equation formulated in a time-independent scattering process. Assuming the hamiltonian to be expressed as $H = H_0 + V$, where H_0 is the kinetic energy operator and V the two-body interaction, the Schrödinger equation will be given by:

$$(H_0 + V)\Psi = E\Psi \ , \tag{2.131}$$

or explicitly by:

$$\frac{\hbar^2}{M}\nabla^2\Psi_n(\vec{r}) + \int d^3r' \, V(\vec{r} \mid \vec{r}')\Psi_n(\vec{r}') = E_n\Psi_n(\vec{r}) \ , \tag{2.132}$$

where M stands for the nucleon mass, $\vec{r} = \vec{r}_1 - \vec{r}_2$ for the relative distance between the two nucleons and E_n for the total relative energy. If Φ is a plane wave solution of the

free Schrödinger equation with enery E, $H_0\Phi = E\Phi$, possible solutions for Ψ are:

$$| \Psi^{(\pm)}\rangle = | \Phi\rangle + \frac{1}{E - H_0 \pm i\epsilon} V | \Psi^{(\pm)}\rangle , \tag{2.133}$$

which in the limit $V \to 0$ must behave as $| \Psi\rangle \to | \Phi\rangle$. One can easily check Eq. (2.133) evaluating $(E - H_0) | \Psi^{(\pm)}\rangle$ and taking the limit $\epsilon \to 0$.

This is the known Lippmann-Schwinger equation, where the positive (negative) solution corresponds to a plane wave plus an outgoing (incoming) spherical wave at sufficiently large distances. If one takes the positive solution $| \Psi^{(+)}\rangle$, the infinitessimal quantity $+i\epsilon$ ensures the proper boundary conditions for obtaining a purely outgoing scattered wave function from an incident plane wave. In higher-order Born approximation for scattering processes, one uses a transition operator T defined such that

$$V | \Psi^{(+)}\rangle = T | \Phi\rangle . \tag{2.134}$$

Multiplying the Lippmann-Schwinger equation, for the positive solution, on the left by V and using Eq. (2.134) one obtains:

$$V | \Psi^{(+)}\rangle = V | \Phi\rangle + V \frac{1}{E - H_0 + i\epsilon} V | \Psi^{(+)}\rangle \tag{2.135}$$

$$T | \Phi\rangle = V | \Phi\rangle + V \frac{1}{E - H_0 + i\epsilon} T | \Phi\rangle , \tag{2.136}$$

from where one gets an equation for the T operator

$$T = V + V \frac{1}{E - H_0 + i\epsilon} T . \tag{2.137}$$

The standing solutions of Eq. (2.132) fulfill the equation:

$$| \Psi\rangle = | \Phi\rangle + P \frac{1}{E - H_0} V | \Psi\rangle , \tag{2.138}$$

where the symbol P stands for the principal value. Similar to Eqs. (2.134) to (2.137), one obtains:

$$| \Psi\rangle = | \Phi\rangle + P \frac{1}{E - H_0} R | \Phi\rangle , \tag{2.139}$$

where the reaction matrix R fulfills:

$$R = V + P \frac{1}{E - H_0} R . \tag{2.140}$$

The above equation can be solved in momentum space

$$R(\vec{k} \mid \vec{k}_0) = V(\vec{k} \mid \vec{k}_0) + \int d^3q \, \frac{V(\vec{k} \mid \vec{q}) \, R(\vec{q} \mid \vec{k}_0)}{E(k_0) - E(q)} \, , \tag{2.141}$$

where $E(k) = k^2/M$ is the kinetic energy of a pair of particles moving with relative momentum $\vec{k}$ in their center-of-mass frame. The equation giving the correlated wave function, Ψ, for standing waves reads:

$$\begin{aligned} \Psi(\vec{k}_0;\vec{r}) \, \chi_S^{M_S} &= \Phi(\vec{k}_0;\vec{r}) \, \chi_S^{M_S} \\ &- \sum_{M_S'} \int d^3k \, \frac{R(\vec{k}SM_S' \mid \vec{k}_0SM_S) \, \Phi(\vec{k};\vec{r}) \, \chi_S^{M_S'}}{E(k) - E(k_0)} \, , \end{aligned} \tag{2.142}$$

where $\Phi(\vec{k};\vec{r}) = \mathrm{e}^{\mathrm{i}\vec{k}\vec{r}}$ is the uncorrelated wave function, $\chi_S^{M_S}$ the spin function and R the reaction matrix, appropriate for the description of the scattering of two-particles leading to standing solutions for the relative wave functions. In the expressions above, the conservation of spin (S) of the strong interaction has been taken into account. In Eqs. (2.141) and (2.142), $\vec{k}_0$ stands for the relative momentum between the emerging nucleons just after the weak transition occurs. Isospin is easy to incorporate at the final step of our calculation multiplying the obtained correlated wave function by the isospinor $\chi_T^{M_T}$. For the calculation it is convenient to write an expression similar to (2.142) but using a partial-wave decomposition, working in the coupled scheme in which L and S couple to J. Using this decomposition we can write [Jo87]:

$$\begin{aligned} \Psi(\vec{k}_0;\vec{r}) \, \chi_S^{M_S} &= \sum_{J,M_J} \sum_{L,M_L} \sum_{L'} \mathrm{i}^{L'} 4\pi \, \Psi_{LL'}^J(k_0,r) Y_{LM_L}^*(\hat{k}_0) \\ &\times \langle LM_LSM_S|JM_J\rangle \, \mathcal{J}_{L',S,J}^{M_J}(\hat{r}) \end{aligned} \tag{2.143}$$

for the correlated wave function, and

$$\begin{aligned} \Phi(\vec{k}_0;\vec{r}) \, \chi_S^{M_S} &= \mathrm{e}^{\mathrm{i}\vec{k}_0\vec{r}} \chi_S^{M_S} \\ &= \sum_{L,M_L} \sum_{L',M_L'} \mathrm{i}^{L'} 4\pi \, j_L(k_0 r) \, \delta_{L,L'} \, Y_{LM_L}^*(\hat{k}_0) \, Y_{L'M_L'}(\hat{r}) \, \chi_S^{M_S} \\ &= \sum_{J,M_J} \sum_{L,M_L} \sum_{L'} \mathrm{i}^{L'} 4\pi \, j_L(k_0 r) \, \delta_{L,L'} \, Y_{LM_L}^*(\hat{k}_0) \\ &\times \langle LM_LSM_S|JM_J\rangle \, \mathcal{J}_{L'SJ}^{M_J}(\hat{r}) \end{aligned} \tag{2.144}$$

for the uncorrelated one. In the expressions above, $\mathcal{J}_{L'SJ}^{M_J}(\hat{r})$ stands for the generalized spherical harmonic which reads:

$$\mathcal{J}_{L'SJ}^{M_J}(\hat{r}) = \sum_{M_LM_S} \langle JM_J \mid L'M_L'SM_S\rangle \, Y_{L'M_L'}(\hat{r}) \, \chi_{M_S}^S \, , \tag{2.145}$$

and $j_L(k_0 r)$ represents the bessel function describing the free relative motion of two nucleons with angular momentum L and relative momentum $\vec{k}_0$.

Inside the integral of Eq. (2.142) we have two functions with an angular dependence that can be also expanded as before,

$$\begin{aligned}\Phi(\vec{k};\vec{r}) &= e^{i\vec{k}\vec{r}}\chi^S_{M'_S} \\ &= \sum_{J,M_J}\sum_{L,M_L} i^L 4\pi\, j_L(kr)\, Y^*_{LM_L}(\hat{k}) \\ &\times \langle LM_L SM'_S|JM_J\rangle\, \mathcal{J}^{M_J}_{LSJ}(\hat{r}) \end{aligned} \tag{2.146}$$

and,

$$\begin{aligned}R(\vec{k}SM'_S \mid \vec{k}_0 SM_S) &= \sum_{L'M'_L}\sum_{L''M''_L} Y_{L'M'_L}(\hat{k})\, \langle k; L'M'_L SM'_S|T|k_0; L''M''_L SM_S\rangle \\ &\times Y^*_{L''M''_L}(\hat{k}_0) \\ &= \sum_{J'M'_J}\sum_{L'M'_L}\sum_{L''M''_L} Y_{L'M'_L}(\hat{k})\, \langle L'M'_L SM'_S|J'M'_J\rangle \\ &\times \langle k; (L'S)J'M'_J|T|k_0; (L''S)J'M'_J\rangle \\ &\times \langle L''M''_L SM_S|J'M'_J\rangle\, Y^*_{L''M''_L}(\hat{k}_0)\ . \end{aligned} \tag{2.147}$$

Combining all these terms inside the integral and carrying out the angular integration, we can easily find an expression for the partial-wave decomposed two-body correlated wave function:

$$\begin{aligned}\Psi^J_{LL'}(k_0 r) &= j_L(k_0 r)\, \delta_{L,L'} \\ &- \int k^2 dk\, \frac{\langle k; (L'S)JM_J|R|k_0; (LS)JM_J\rangle}{E(k) - E(k_0)}\, j_{L'}(kr)\ . \end{aligned} \tag{2.148}$$

These correlated wave functions $\Psi^J_{LL'}(k_0, r)$ will be used in Eq. (2.112) for each channel coming from the weak transition and for each k_0 value. As an example, the correlated wave functions for several channels are displayed in Figs. 2.11 and 2.12. The relative momentum used to compute the plots is $k_0 = 1.87$ fm^{-1}. In Fig. 2.11 the $^3S_1 \rightarrow {}^3D_1$ coupled channel NN wave functions are shown, where the solid line stands for the correlated wave function obtained when the Nijmegen93 NN interaction is used, and the dashed line represents the resulting wave function for the Reid93

NN interaction. There is also plotted the phenomenological correlated wave function (dotted line), which corresponds to the use of a correlation function of the type (2.114). Fig. 2.12 represents the same as Fig. 2.11 but for the uncoupled $^1S_0$, $^3P_0$, $^1P_1$ and $^3P_1$ channels. How the different choice (Nijm93, Reid93 and phenomenological correlation) affects the decay rate and other observables will be discussed in the next chapter.

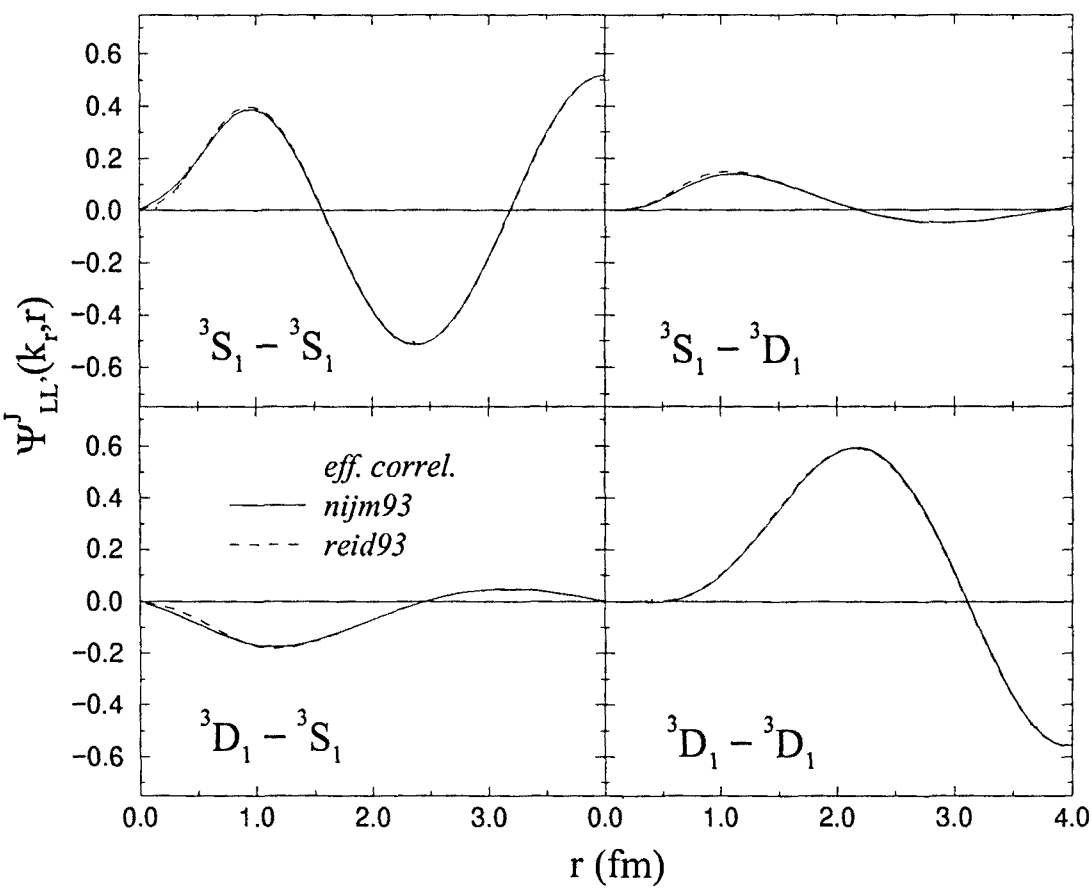

Figure 2.11. $^3S_1 - ^3D_1$ coupled channel NN wave functions for a relative momentum of $k_0 = 1.97$ fm^{-1}, obtained with the Nijmegen93 (solid line) and the Reid93 (dashed line) interactions. The dotted line represents the phenomenological correlated wave function discussed in the text.

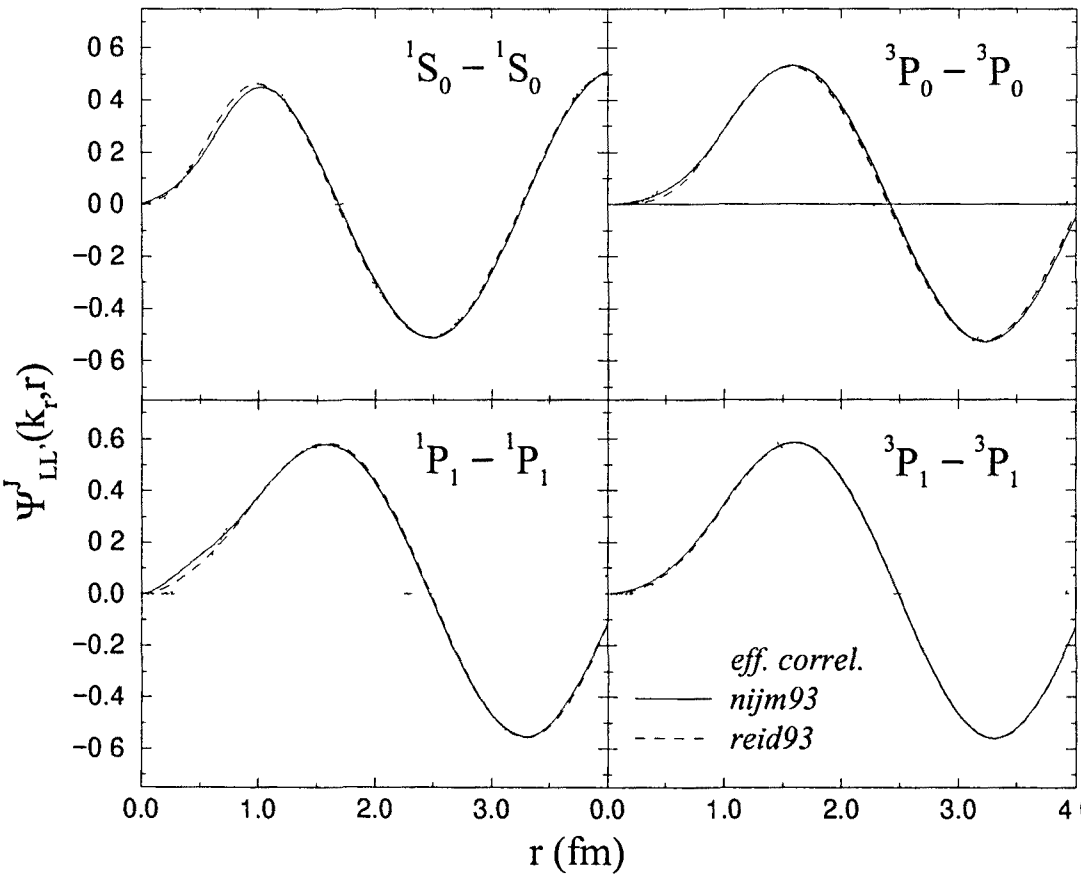

Figure 2.12. Same as Fig.2.11 for the uncoupled $^1S_0$, $^3P_0$, $^1P_1$ and $^3P_1$ channels.

Chapter 3

Results

In this chapter, the results obtained for the nonmesonic decay of several hypernuclei are presented and discussed, with special emphasis on the ${}^{12}_{\Lambda}$C hypernucleus. These results include the total nonmesonic decay rate in units of the free Λ decay Γ_Λ, Γ/Γ_Λ, as well as other observables, such as the intrinsic lambda asymmetry parameter, a_Λ, and the neutron-to-proton ratio, Γ_n/Γ_p, which are discussed separately. The contribution of the different mesons included in the decay mechanism are given, with mesons having the same isospin character being studied in pairs ((π,ρ),(K,K*) and (η,ω)). The total contribution, corresponding to the addition of all the mesons considered, is also shown. Two different sets of strong coupling constants, corresponding to the JülichB group and the Nijmegen one, have been used.

When analyzing the OPE contribution to the hypernuclear decay, two different potentials are used in order to obtain the correlated wave function for the final two-body NN state, the Reid93 and the Nijm93 NN interactions, as well as a phenomenological way to include these final state interactions via an effective correlation function. For the rest of the mesons and for the total calculation, only the results obtained with the Nijm93 NN interaction are shown. All the values have been computed taking into account correlations in the initial ΛN system (SRC), monopole form factors at each of the vertices of the meson-exchange diagram (FF) and final state interactions (FSI) in the final NN system. The rates corresponding to the different parity-conserving

(PC) and parity-violating (PV) transition channels are also shown, as well as the total nonmesonic rate Γ/Γ_Λ, the asymmetry a_Λ and the ratio Γ_n/Γ_p for hypernuclei different from the hypercarbon, ${}^{11}_{\Lambda}$B and ${}^{5}_{\Lambda}$He, where the same techniques have been used.

3.1 π-Exchange

The first meson discussed in this chapter is the pion. Results using only the OPE part of the weak $\Lambda N \rightarrow NN$ interaction are presented. On the one hand, one would expect this meson to adequately describe the long-range part of the transition potential, while on the other hand its contribution has minimal uncertainties since the weak $\Lambda N\pi$ vertex is experimentally known. It is therefore a good starting point to assess the significance of form factors as well as initial and final state correlations before including the other mesons in the potential. The results of our calculations with OPE only are shown in Table 3.1 where the nonmesonic decay rate of ${}^{12}_{\Lambda}$C is given in units of the free Λ decay rate ($\Gamma_\Lambda = 3.8 \times 10^9$). For the harmonic oscillator size parameters of the Λ and the nucleon in the ${}^{12}_{\Lambda}$C hypernucleus, the values $b_\Lambda = 1.87$ fm and $b_N = 1.64$ fm have been taken, respectively. The uncorrelated results (FREE) are compared with computations which include initial ΛN short-range correlations, form factors, and final state interactions separately for the (spin-dependent) central (SS), tensor (T) (adding to a total parity-conserving contribution) and parity-violating potentials. The free central term is reduced dramatically by the initial SRC, however, most of the uncorrelated central potential contribution is in fact due to the δ-function in the transition potential which is completely eliminated by SRC. Without the δ-function, the central part is reduced by about a factor of two. Including SRC, FF, and FSI gives a negligible central decay rate. In contrast, the contribution of the tensor interaction is reduced only 10% by SRC and by 20-35% once FF and FSI are included as well. Therefore, the contribution of the central term amounts to less than 0.5% of the total π-exchange rate. This behavior has been found and discussed by other authors as well [MG84,Du86,TT85]. Furthermore, our PV potential yields about 40% of the π-exchange rate, at variance with older nuclear matter results that reported either a 15% [Du86] or a negligible PV contribution to the rate [MG84] . The total one-pion-exchange contribution to the nonmesonic decay rate of ${}^{12}_{\Lambda}$C is 0.9 - 1.1 Γ_Λ, depending on the choice for FSI, which is a factor 1.5 - 2 smaller than the FREE value.

As discussed in previous sections, Refs. [PR94,PR95] demonstrate the sensitivity

Table 3.1. π-exchange contribution to the ΛN→NN decay rate of $^{12}_{\Lambda}$C

	FREE	SRC	SRC+FF	SRC+FF+FSI		
				phenom.	Nijm93	Reid93
				Eq. (2.114)		
C	0.282	3.4×10^{-3}	1.3×10^{-2}	4.2×10^{-3}	3.3×10^{-3}	4.0×10^{-3}
T	0.858	0.781	0.637	0.685	0.566	0.579
PC	1.140	0.785	0.650	0.689	0.531	0.547
PV	0.542	0.447	0.389	0.421	0.353	0.345
Γ/Γ_Λ	1.682	1.232	1.038	1.110	0.885	0.892
Γ_n/Γ_p	0.182	0.113	0.120	0.118	0.104	0.100
PV/PC	0.476	0.570	0.598	0.610	0.665	0.631
a_Λ	−0.594	−0.420	−0.506	−0.484	−0.238	−0.242

of the calculated decay rates to the form of the initial SRC. In particular, it was found that older calculations using a phenomenological NN correlation function [MG84,HK86] to simulate ΛN SRC in the initial state, rather than SRC based on a realistic YN meson-exchange potential as it is done here, tend to overpredict the amount of initial correlations. As shown in Table 3.1, the PV and PC rates are reduced by about 10% and 18%, respectively, when FSI are included via a correlation function based on a realistic NN potential (last two columns), rather than the 8% and 6% increase obtained with the phenomenological NN correlation function of Eq. (2.114). It is comforting to see that the variation between different realistic NN interactions, such as the soft-core Nijmegen and a modern version of the Reid potential, plays essentially no role. This behavior can also be understood from Figs. 2.11 and 2.12, shown in the previous chapter, where a comparison between the different correlated wave functions for several channels and at a relative momentum of $k_0 = 1.97$ fm^{-1} has been done. The figures demonstrate that the phenomenological correlated wave function overestimates the realistic NN wave functions at intermediate distances (0.5 − 1.5 fm) while it underestimates them at short distances. As a result, the phenomenological approach overestimates the decay rate by about 20%. Including realistic final state correlations leads to an interference between central and tensor transitions. For phenomenological FSI the central and

tensor contributions to the total rate add incoherently, as can be seen in Table 3.1. Once a realistic NN potential is used this incoherence is replaced by a destructive interference, due to the mixing of the channels by the strong force. While this is only a small effect for the pion due to the small size of the central potential term, this interference is more significant for the vector mesons, where the central transition amplitude is comparable in size and even larger than the tensor term.

The second quantity of interest displayed in Table 3.1, which is sensitive to the isospin structure of the transition amplitude, is the neutron- to proton-induced ratio Γ_n/Γ_p. Noticeable is the smallness of the ratio, which is due to the Pauli Principle that suppresses the final $T = 1$, $L = 2$, $S = 1$ state with its antisymmetrization factor $(1 - (-1)^{L+S+T})$. That excludes the tensor transition in the neutron-induced rate, which gives rise to nn ($T = 1$) pairs, and it is precisely this tensor piece which constitutes the largest part of the OPE diagram. This argument holds only for relative ΛN S-states. For nucleons in the p-shell there exits a relative ΛN P-state which contributes a small but non-zero amount of the tensor potential to the neutron-induced decay. However, only about a 10% of the total decay rate comes from this relative P-state. Note that including initial SRC, FF and realistic FSI reduces the Γ_n/Γ_p further by about 40%. This is due to the elimination of the central rate for which we obtain a value for Γ_n/Γ_p of about 1/3 (not shown in the table). In principle, one would expect Γ_n/Γ_p =1/2 for the central term due to the statistical factor of 1/2 that accounts for two identical particles in the final state. For ${}^{12}_{\Lambda}$C this number becomes 1/2.4 since we have 5 neutrons and 6 protons. The remaining difference comes from different ${}^1S_0$ ($T = 1$) and ${}^3S_1$ ($T = 0$) final state wave functions which enter the various spin-isospin channels and, therefore, lead to slightly different Λn$\rightarrow$nn and Λp$\rightarrow$np central transition amplitudes.

The suppression of the central potential term due to SRC, FF and FSI also explains the difference between the uncorrelated and the fully correlated ratio of PV to PC amplitudes, PV/PC, shown in Table 3.1 as well. More relevant than this unobservable quantity, however, is the asymmetry parameter, a_Λ, defined in Eq. (1.23). This quantity, which measures the interference between the PC and the PV part of the amplitude (see § 1.2), can be accessed experimentally in contrast to the PV/PC ratio which is merely of theoretical interest. We find that this asymmetry parameter is only mildly sensitive to initial SRC and FF but changes by more than a factor of two when realistic FSI are included. This observable thus clearly demonstrates that for its

accurate prediction the use of a realistic NN potential to describe the interactions in the final state is imperative. Below we use realistic FSI generated with the Nijmegen potential for all results that include final state correlations.

Comparing the results given in the present work with older nuclear matter computations [OS85, MG84,Du86,DF96] one can point out that the fully correlated total rate in nuclear matter is predicted to be in the range of 1.85–2.3, thus overpredicting our shell-model calculations by more than a factor of two. When a Local Density Approximation (LDA) is performed [RO94,OS85] the rate reduces to $\Gamma_{nm} = 1.45\,\Gamma_\Lambda$ for ${}^{12}_{\Lambda}$C. Although this value is further reduced when the same Λ wave function as in the present work is used, the LDA result is still larger by about 30%. However, the sensitivity to the Landau-Migdal parameter, which measures the initial state correlations, is greater than expected. The LDA calculations [RO94,OS85] used $g'_\Lambda = 0.52$, but a more appropriate choice of this parameter (around $g'_\Lambda = 0.2$) corresponding to a correlation function of the type $1 - j_0(q_c r)$ with q_c=780 MeV (used in several nuclear matter calculations), shifts the nonmesonic rate value from 1.45 Γ_Λ to 1.05 Γ_Λ, very close to the finite nucleus result given in the present work. In view of this argument one can not assert that the differences between the LDA approach and the finite nuclei results are due to the breakdown of the LDA description for s- and p-shell nuclei, but are closely related to the appropriate choice of the Landau-Migdal parameter.

We conclude the discussion of the OPE by assessing the role of the relative ΛN P-state contributions. In shell-model calculations such terms naturally arise for nucleons in p-shell and higher orbitals when one transforms from shell-model coordinates to the relative ΛN two-body system. For s-shell nucleons, where one has an s-wave in both the relative and center-of-mass (CMS) motions, the transition amplitude gives a maximum contribution at the back-to-back kinematics, $\vec{k}_1 = -\vec{k}_2$, yielding a total CMS momentum $\vec{K} = 0$. For p-shell nucleons one would expect the contribution from the initial relative ΛN S-state to be suppressed compared to that of the relative P-state since the CMS harmonic oscillator wave function is then a P-state and thus zero at $\vec{K} = 0$. Surprisingly, one finds that after integrating over all kinematics with $\vec{k}_1 \neq -\vec{k}_2$, this relative $L = 0$ term contributes about 90 % to the p-shell rate [BR92]. Thus, once the whole phase space is included, most of the total decay rate of p-shell nucleons still comes from the relative ΛN S-state. Furthermore, neglecting the relative P-state contribution leaves the ratio Γ_n/Γ_p unaltered while the asymmetry parameter a_Λ is reduced by 10%.

3.2 π- and ρ-Exchange

In this section, one starts examining the role of additional mesons and their contribution to the different observables in the weak ${}^{12}_{\Lambda}$C decay. The ρ meson is the isospin partner of the pion, so it seems to be a good choice, in summing up the contribution of mesons different than the pion, to analyze first the ρ and the $\pi + \rho$ contributions to these observables.

As is well known, in terms of hadronic degrees of freedom, the ΛN$\rightarrow$NN process initially had been described with a one-pion-exchange potential since the weak ΛNπ vertex is well constrained from the free $\Lambda \rightarrow$ Nπ decay. The fact that the final nucleons emerge with a momentum of around 400 MeV/c suggests that short-range effects may be important. As discussed above, one is faced with the immediate difficulty that none of the weak couplings involving heavier mesons can be accessed experimentally. Thus, one is required to resort to models which in this case involve considerable uncertainty. Many theoretical studies [MG84,TT85,Na88] have investigated the contribution of a more massive meson, the ρ, in the exchange mechanism yielding very different results due to the different models employed for the weak ΛNρ vertex. However, all works until now have only included the tensor part of the parity-conserving ρ-exchange term, in part motivated by the fact that the central potential of the π-exchange term gives a negligible contribution compared to the tensor one. In Ref. [PR96] it is shown that this is not the case. For this meson, the central term is not only negligible but larger than the tensor one. This can be traced to the fact that the ρ-exchange diagram has a much shorter range than the π-exchange potential.

Table 3.2 shows the present results for the ρ-meson exchange alone as well as for the π- and ρ-exchanges combined. Since both the ΛNπ- and the ΛNρ-couplings are obtained within the same model there is no sign ambiguity. As noted before (§ 2.1.2), the central potential can now be divided into a spin-independent (C) and a spin-dependent (SS) piece, which are shown separately in the table. In the SS piece it is found that, in contrast to the pion case, the factor m_ρ^2 in front of the Yukawa function of Eq. (2.52) enhances this term which then becomes comparable in magnitude to the piece containing the delta function. The two terms interfere destructively and yield a SS central part that is about half the size of the tensor contribution. We briefly point out here some of the features of the central and tensor potentials given in Ref. [PR96]. To understand the origin for the different ratio of central to tensor transiton strengths in

Table 3.2. π- and ρ-exchange contribution to the $\Lambda N \rightarrow NN$ decay rate of $^{12}_{\Lambda}C$. The values between parentheses have been calculated using the weak coupling constants by Nardulli [Na88].

	π	ρ	$\pi + \rho$
C (C)	—	0.020 (0.019)	0.020 (0.019)
C (SS)	0.003	0.014 (0.016)	0.006 (0.007)
C (Total)	0.003	0.045 (0.047)	0.028 (0.030)
T	0.566	0.027 (0.032)	0.373 (0.358)
PC	0.531	0.021 (0.023)	0.445 (0.428)
PV	0.353	0.008 (0.096)	0.414 (0.635)
Γ/Γ_Λ	0.885	0.029 (0.120)	0.859 (1.063)
Γ_n/Γ_p	0.104	0.076 (0.097)	0.095 (0.063)
a_Λ	-0.238	0.036 (0.046)	−0.100 (−0.008)

the π- and ρ-exchange mechanisms, the integrands of the SS central (without the delta function) and tensor amplitudes are shown in Fig 3.1. A fixed outgoing momentum of $k_0 = 1.97$ fm^{-1} has been chosen for the relative final wave function. These integrands have the form of Eq. (2.130) given in § 2.4, but for the case in which SRC, FF and FSI are not included. Starting from an initial ΛN relative S-state, the tensor potential amplitude is governed by the Bessel function $j_2(k_0 r)$ ($S \rightarrow D$ transitions), describing the NN motion in the final state. Since j_2 vanishes at the origin it eliminates strength from the tensor potential at short distances. Due to its shorter range, the tensor contribution of the ρ is reduced by j_2 more than in the case of the pion. On the other hand, the central piece is governed by $j_0(k_0 r)$ which is not suppressed at short distances of the potential. However, due to the smaller value of m_π, the function $j_0(k_0 r)$ oscillates once in the effective range of the pion central potential, leading to a reduction of its central contribution relative to the tensor one.

The effect of including SRC is to reduce both the C- and the SS-central parts of the ρ-meson contribution without δ-function by almost a factor of 10, compared to a factor of 2 in the π case, reflecting the much shorter range of the ρ-exchange diagram. Similarly, the tensor interaction of the ρ is reduced by a factor of 2.5, compared to a 10% reduction in the π case, as soon as SRC are included. In order to illustrate these

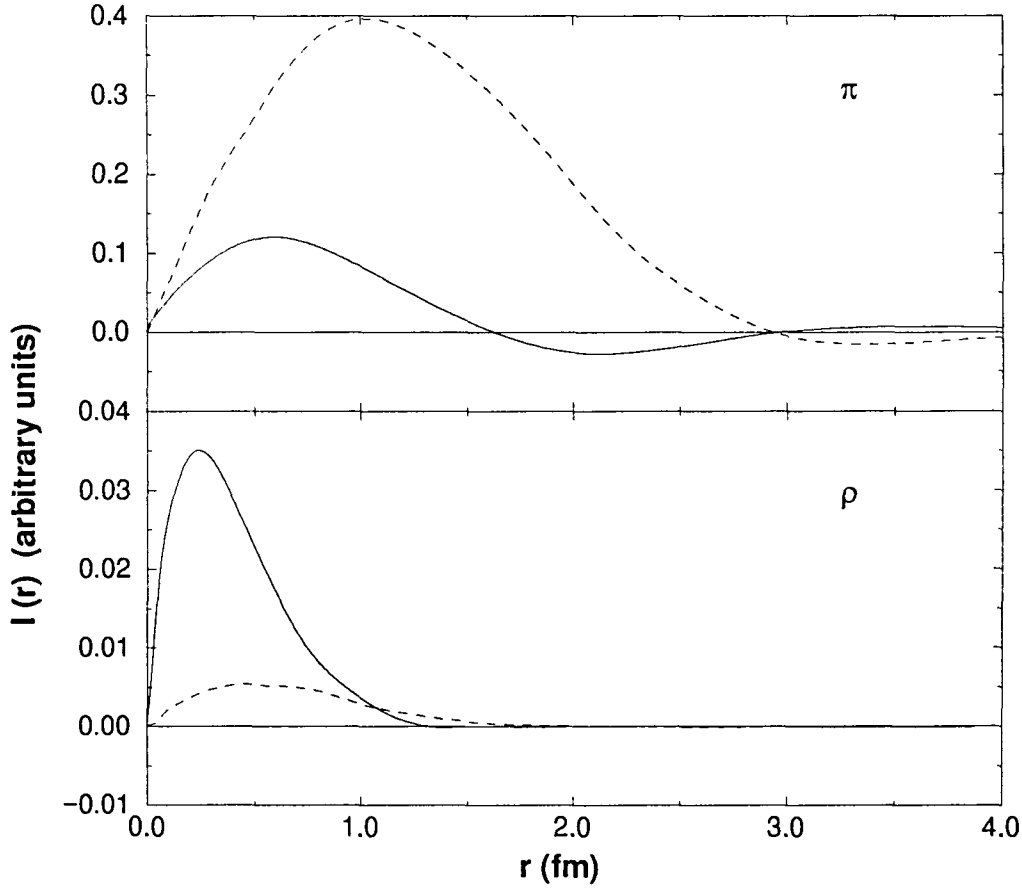

Figure 3.1. Integrand of the free transition amplitude, in arbitrary units, at fixed outgoing relative momentum ($k_0 = 1.97\ \mathrm{fm}^{-1}$) for the spin-dependent central potential (SS) without the δ function (solid line) and for the tensor potential (dashed line). Upper part: pion-exchange. Lower part: rho exchange.

results Fig. 3.2 shows the integrands of the tensor amplitudes for the π and ρ mesons separately. The fixed relative outgoing momentum is the same as in Fig. 3.1. The solid line corresponds to the free case, in which SRC, FF and FSI are ignored. Clearly, the integrand of the ρ-exchange peaks sooner (≈ 0.5 fm) and drops off faster, reaching zero at around 2 fm, compared to the integrand for the π-exchange which peaks around 1 fm and drops to zero around 3 fm. It therefore comes as no surprise that including SRC leads to a much stronger reduction for the ρ than for the π contribution. The

dotted line in Fig. 3.2 stands for the tensor integrand when all the ingredients (SRC, FF and phenomenological FSI) have been taken into account. This dotted line further confirms that including SRC, FF and FSI have different effects depending on the meson considered.

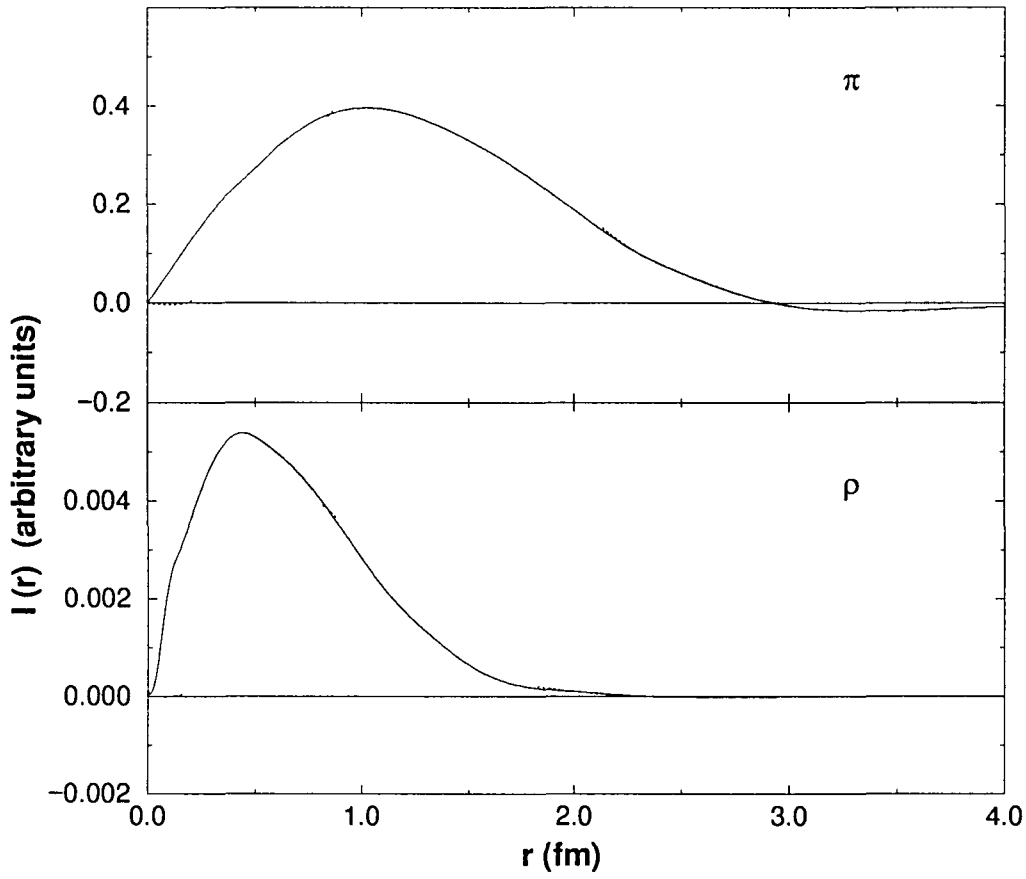

Figure 3.2. Illustration of the effects of SRC, FF and FSI in the tensor transition amplitude. The solid line shows the free tensor integrand and the dotted line includes the effects of SRC, FF and FSI. Upper part: pion-exchange. Lower part: rho-exchange.

One may think that, due to the much shorter range of the ρ potential, it would be very sensitive to the details of the short-range correlation function. This is indeed the case, so different values for the total ρ rate [PR96] are obtained when using a realistic correlation function obtained from a G-matrix calculation with the Nijmegen soft-core

or hard-core interaction. However, as soon as form factors and final state interactions (which provide further suppression at short distances) are included, the rates get closer and similar to the value obtained with our spin-independent parametrization (Eq. (2.115)).

The inclusion of FF and FSI further reduces both the central and tensor rates by substantial amounts. As it is evident from Table 3.2, the final result of the central ρ contribution exceeds the ρ tensor term by almost a factor of two. Due to the strong destructive interference induced by the FSI between the tensor and the central part, the total PC rate turns out to be smaller than either term alone.

In terms of the combined π and ρ contribution one sees a destructive interference between the two mesons for the PC rate but constructive interference for the PV decay mode. While the π-only PC rate is reduced by 16% when the ρ is added, the π-only PV rate is enhanced by about 17% even though the ρ-only PV rate is very small. These interferences lead to a combined $\pi + \rho$ total decay rate that is very similar to that of the π alone. The neutron- to proton-induced ratio Γ_n/Γ_p, on the other hand, is slightly decreased. This may at first be surprising since the tensor rate of the ρ-exchange is not as dominant as it is in the π case. As noted in Ref. [PR96], this is due to an interference pattern of the central C and SS amplitudes which is destructive for the n-induced and constructive for the p-induced mechanisms. This yields a central rate which is basically p-induced. The strongest change can be seen in the asymmetry parameter a_Λ which is reduced by more than a factor of 2. This reduction can be traced to the above mentioned interference pattern between the PV and PC rates which are measured by this observable.

The ρ-meson was the first of the heavier mesons which was included in several earlier calculations. Our results for the rates calculated with this meson are quite different from previous studies [MG84,TT85,Na88]. This is not only due to the omission of the central potential in the ρ-exchange diagram, but even more so to the different models used for the weak $\Lambda N\rho$ coupling constants. The first attempt was due to McKellar and Gibson [MG84] who performed a calculation in a nuclear matter framework. They evaluated the weak $\Lambda N\rho$ couplings using SU(6) and, alternatively, a factorization model. In their approach, which neglected the PV couplings, the phase between the π and ρ amplitudes was not determined and their final results varied dramatically with their different models for the weak coupling constants. In a more recent calculation [Na88], Nardulli obtains the PC couplings in a pole model approach similar to the one used

in the present work. Besides the ground state baryon pole the Nardulli work includes the $\frac{1}{2}^*$ baryon resonance pole terms as well as K*-pole contributions that appear in Refs. [DF96,To82] but have been omitted here. The weak baryon-baryon transition amplitudes for the resonance poles are taken from a pole model analysis of hyperon PC pion decays which uses an F/D ratio of -1 for the weak baryon transition amplitudes and adjusts the overall coupling to the experimentally measured p-wave π decay rates. As pointed out in Ref. [MS95] the most serious problem with this fit is that it employs a K$\rightarrow$ π weak transition amplitude in its K-pole graphs that is about an order of magnitude larger than the strength extracted from the weak kaon decay mode K$\rightarrow$ $\pi\pi$ [Do86]. The K*-pole contributions are calculated using a simplified factorization approach in which a number of terms are neglected [MS95]. The PV couplings of Ref. [Na88] are computed in a pole model approach that includes baryon resonance poles with negative parity, belonging to the $(70,1^-)$ multiplet of SU(6). In order to obtain the weak baryon transition amplitudes the experimental hyperon s-wave π decays are used as input. Therefore, his approach for the PV weak $\Lambda N\rho$ vertex is considerably different from the analysis used in this study. For the sake of comparison, Table 3.2 also lists the ρ term calculated with Nardulli's weak coupling constants. The PC transition potentials turn out to be very similar in magnitude while the PV rate is larger by more than a factor of 10 for the ρ alone. This increase enhances the $\pi + \rho$ total decay rate by about 25%, while the Γ_n/Γ_p and a_Λ are reduced by roughly the same amount. One should point out that the close agreement in the PC terms is fortuitous since the baryon resonance pole terms which are not present in our approach contribute about 30% to the weak $\Lambda N\rho$ tensor coupling of Ref. [Na88]. From this comparison it becomes obvious that there is considerable uncertainty in the determination of the weak vector meson vertices.

3.3 Other Mesons

In this section, the contribution of the isovector K and K* mesons, as well as the isoscalar η and ω mesons, to the different observables in the weak decay of ${}^{12}_{\Lambda}$C are explored within the same OBE model.

Most of the calculations performed until now have not included these extra mesons and have restricted the study of the hypernuclear decay to the consideration of the π and ρ exchanges in the weak transition. However, some relativistic calculations [RB94]

worked out a different study of the decay mechanism exchanging the same set of mesons in ${}^{12}_{\Lambda}$C. Furthermore, other treatments of the nonrelativistic approach in nuclear matter calculations have also considered additional meson exchanges [DF96].

3.3.1 K- and K*-Exchange

The kaon is the lightest meson after the pion with a strong coupling constant $g_{\Lambda NK}$ of comparable magnitude to $g_{NN\pi}$ but of opposite sign. Its contribution to the total decay rate is the largest one among all the heavier mesons, about 15% of the π term. The K (and the K*) can contribute to both the $T = 0$ and $T = 1$ weak $\Lambda N \rightarrow NN$ transition potential and therefore has two independent couplings, C_K and D_K (see § 2.1.1). Due to the special isospin structure of this meson, it was suggested [Gi89] that including its exchange will strongly influence the Γ_n/Γ_p ratio. Using a simple schematic model that ignores the spin structure it was shown that the ratio Γ_n/Γ_p could be estimated with the expression

$$\frac{\Gamma_n}{\Gamma_p} = \left| \frac{A_0 + A_1}{A_0 - 3A_1} \right|^2 , \tag{3.1}$$

where A_0 and A_1 are the isoscalar and isovector coupling constants, respectively, which in our case are given by:

$$A_0 = \frac{C_K}{2} + D_K \tag{3.2}$$

$$A_1 = \frac{C_K}{2} . \tag{3.3}$$

With the PV values of Table 2.2 (§ 2.2), one obtains from Eq. (3.1) the value $\Gamma_n/\Gamma_p = 4.6$, confirming the result quoted in Ref. [Gi89]. However, the value $\Gamma_n/\Gamma_p = 0.23$ is obtained when the PC coupling constants of Table 2.2 are used. The complete result, which considers the spin structure and includes both PC and PV amplitudes, turns out to be $\Gamma_n/\Gamma_p = 0.26$ as shown in Table 3.3. This much smaller result suggests that one cannot draw conclusions about the ability of the strange mesons to drastically increase the neutron-to-proton ratio. Moreover, when this ratio is calculated using PV and PC amplitudes only, but retaining the spin dependence, the values 1.69 and 0.03 are obtained, respectively, far away from the estimates made above using Eq. (3.1). Note that, as shown by Dalitz [DR62], the $\Delta T = 1/2$ rule requires the ratio Γ_n/Γ_p to be smaller than 2 for any meson exchange.

As we can see in Table 3.3, the Γ_n/Γ_p ratio for the kaon only is larger than the corresponding value for the pion by a factor of 2.5, while the asymmetry parameter is

very small. In § 2.2 it was pointed out that our framework for the weak baryon-baryon-meson coupling constants assumes the validity of SU(3) (and SU(6) in the case of the vector mesons). No attention has been paid to the effects of SU(3) symmetry breaking which is known to be of the order of 30%. These effects have been addressed in a recent work by Savage and Springer [SS96] in the framework of next-to-leading order chiral pertubation theory (χPT). They point out that understanding the weak NNK vertex could elucidate a problem regarding the nonleptonic π decay of free hyperons. While the PV (s-wave) amplitudes of these $\Delta S = 1$ decays are adequately reproduced at tree level, the corresponding PC (p-wave) amplitudes cannot be well described using coupling constants from the s-waves as input. A one-loop calculation of the leading SU(3) corrections [Je92], performed in χPT, found that these loop corrections can change the tree level prediction of the p-wave amplitudes by a disturbing 100%, thus raising questions about the validity of χPT in this sector. As an alternative it was suggested [Je92] that large cancellations may occur between tree-level p-wave π decay amplitudes which would magnify the SU(3) breaking effects. The one-loop corrections to the weak NNK vertex found in Ref. [SS96], on the other hand, modify the tree-level p-wave amplitudes by only up to 30%. If an experimental signature for these SU(3) corrections could be found in the nonmesonic decay it would provide insight into the applicability of χPT to these reactions. Table 3.3 shows the results of our calculations performed with the Savage-Springer weak NNK couplings. As expected, the kaon rates are roughly a factor of two smaller since the improved constants are reduced by about 30%. The values of the Γ_n/Γ_p ratio and the asymmetry, on the other hand, are barely affected because all pieces of the transition amplitude are reduced by about the same amount and the reduction cancels out in the ratio.

Among the vector mesons, the K* meson is the heaviest one exchanged in our weak decay mechanism, with a large value of the weak NNK* and strong ΛNK* tensor couplings, which makes its contribution more important than the rest of the vector mesons, either the ρ or the ω. The central and tensor potential contributions are very similar in size, however, due again to the interference generated by the realistic FSI that mixes S and D states, the total PC rate turns out to be of the same magnitude. The PV rate is significantly greater than the corresponding rates for the ρ- and the ω-exchange contribution. This is due to the large value of the PV coupling constant. The total K*-only decay rate (0.06) is seen to be about half of the K-only rate but twice as large as the ρ- and ω-only rates. In view of this result, the consideration of

Table 3.3. K- and K*-exchange contribution to the ΛN→NN decay rate of $^{12}_{\Lambda}$C. The values between parentheses have been calculated using the the NNK weak coupling constants obtained from next-to-leading order in χPT [SS96].

	K	K*	K + K*
C (C)	—	0.019	0.019 (0.019)
C (SS)	0.004 (0.002)	0.092	0.130 (0.122)
C (Total)	0.004 (0.002)	0.038	0.063 (0.058)
T	0.083 (0.038)	0.038	0.015 (0.005)
PC	0.093 (0.044)	0.037	0.082 (0.050)
PV	0.040 (0.018)	0.023	0.091 (0.061)
Γ/Γ_Λ	0.133 (0.062)	0.060	0.173 (0.111)
Γ_n/Γ_p	0.263 (0.272)	0.500	0.647 (0.760)
a_Λ	−0.080 (−0.090)	−0.192	−0.426 (−0.532)

other mesons different than the pion and the rho is clearly of great relevance.

For the Γ_n/Γ_p ratio we get a value of 0.5, as we can see in Table 3.3, about five times larger than that for the pion-exchange ratio. This is due to the relative magnitude of the central term in the PC rate. Both central and tensor channels give now similar contributions, despite the fact that for s-shell hypernuclei there is no n-induced channel contributing to the tensor transition. This fact illustrates in a dramatic way how the different isospin structure of the various mesons can affect the ratio Γ_n/Γ_p. With respect to the asymmetry parameter, for K*-meson exchange one finds a value which is more than twice the one corresponding to the kaon.

Next, we look at the sum of both, K and K*, contributions. As we have seen in Table 3.3, even though the K* rate is around half the K contribution, the K + K* rate is only slightly larger than the corresponding K rate. This is due to the strong interference between both mesons. We can see the effects of this interference by looking at the separated channels. For instance, the PV rate is more than twice the K-only result and, as a consequence, the asymmetry parameter is enhanced dramatically. The Γ_n/Γ_p ratio which turns to be quite large, seems to go in the favorable direction, although it remains to be seen how the interference between all the mesons actually affects the final results for the observables.

Table 3.4. η- and ω-exchange contribution to the $\Lambda N \rightarrow NN$ decay rate of ${}^{12}_{\Lambda}C$.

	η	ω	$\eta + \omega$
C (C)	—	0.045	0.045
C (SS)	0.001	0.009	0.016
C (Total)	0.001	0.036	0.036
T	0.005	0.004	1.5×10^{-4}
PC	0.006	0.024	0.035
PV	0.003	0.002	0.005
Γ/Γ_Λ	0.009	0.026	0.041
Γ_n/Γ_p	0.383	0.235	0.183
a_Λ	−0.114	−0.086	−0.134

3.3.2 η- and ω-Exchange

The η-meson exchange contribution, which is the smallest of the different mesons included, has an NNη coupling constant not well determined but much smaller than both $g_{NN\pi}$ and $g_{\Lambda NK}$. In this work, we use the value of the Nijmegen potential which is $g_{NN\eta} = 6.4$ even though the NN phase shifts are very insensitive to this coupling. In Table 3.4 our results for the exchange of this meson are shown. The general behavior of the η-meson is characterized by a negligible central term, a dominant tensor potential and a PV rate about half of the size of the tensor term. That resembles the OPE contribution, at least, at the level of the rates. The Γ_n/Γ_p ratio on the other hand, is almost a factor of four larger than the ratio corresponding to the pion. This can be understood by the fact that the η-exchange potential does not have a charge exchange term for the proton induced decay due to its isospin structure.

In general, one can see that the contribution of the η meson to the different channels of the transition is insignificant, due in part to the smaller value of the coupling constants in comparison to the other mesons and also to the absent exchange contribution for Γ_p. In any case, the results obtained for the neutron-to-proton ratio and the asymmetry parameter, justify a priori the inclusion of the η meson in the present calculation.

With respect to the ω-meson exchange we point out that the size of tensor and

vector couplings for the strong NNω vertex are opposite in comparison with the NNρ one. Here it is the tensor coupling which is relatively small and the vector one which is large. This produces a much larger central spin-independent contribution with respect to the other PC channels. Even though we obtain a different magnitude of the central and tensor channels compared to the values obtained for the ρ meson, at the end one gets a value for the PC rate which is very similar to the ρ-exchange case. A final remark about the small PV rate should be made. The same is true for the ρ-exchange contribution. The small size of the weak ΛNω coupling constant is the reason for that. No other models are available for weak vertices involving this meson.

3.4 The Full Weak One-Meson-Exchange Potential

To conclude this section, the effect of including all the mesons discussed before in the weak decay observables is explored. For this purpose and in order to begin the discussion, in Figs. 3.3 and 3.4 the contribution of the different mesons to the integrand of Eq. (2.112) for relevant transition channels are shown. Fig. 3.3 displays the tensor transition $^3S_1 \rightarrow {}^3D_1$ ($T = 0$) of the PC amplitudes since it yields the most important contribution for pseudoscalar mesons and gives rise to important interference effects when the contributions of the mesons are added in pairs of identical isospin. As is evident from the figure, the pion-exchange contribution dominates, not only in magnitude but also in range, as it should be, a consequence of the pion being the lightest meson. As expected, the kaon provides the second-largest contribution with a range somewhat less than that of the pion, followed by the heavier mesons with an even shorter range. Note that the contribution of each isospin-like pair [(π, ρ), (K,K*), (η, ω)] interferes destructively, thus the large tensor contribution of each pseudoscalar meson is partially cancelled by that of its vector meson partner, an effect that can also be explicitly seen in Tables 3.2, 3.3 and 3.4, discussed before. The integrands of the central transitions are not shown, since they are very small for the pseudoscalar mesons.

Significant interferences are also observed for the integrands of the PV transitions $^3S_1 \rightarrow {}^1P_1$ ($T = 0$) and $^3S_1 \rightarrow {}^3P_1$ ($T = 1$), shown in Fig. 3.4. Again, the pion is found to be dominant among the mesons in the $T = 0$ transition, while the contribution of the other mesons play a more important role, relative to the pion, in the $T = 1$ channel.

The different observables characteristic of the weak decay, including a comparison

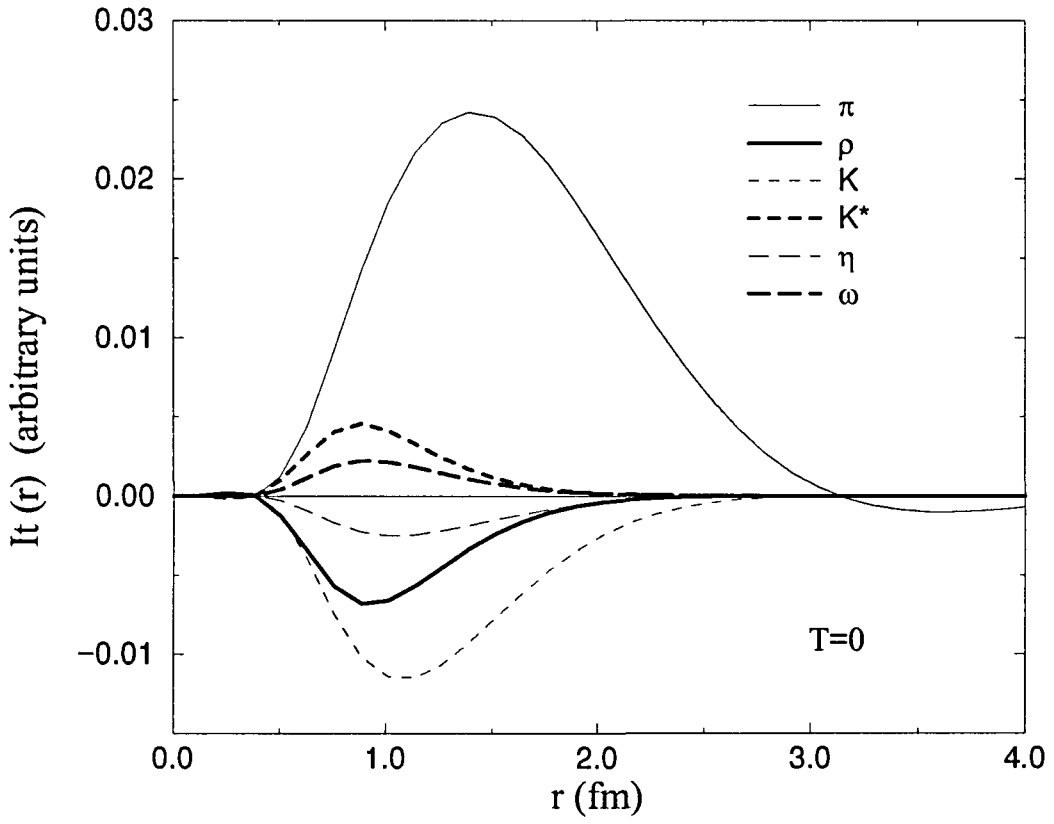

Figure 3.3. Contribution of the different mesons to the integrand of the ${}^3S_1 - {}^3D_1$ (T=0) correlated weak transition amplitude.

between the results obtained with the Nijmegen coupling constants with those obtained using the Jülich couplings at the strong vertices, are given in Tables 3.5 and 3.6. Although in principle the strong couplings also affect the PC weak vertices through the pole model, the goal here is to assess, for one particular model of weak couplings, the effect of using strong coupling constants from two different YN potentials which fit the hyperon-nucleon scattering data equally well.

The results in Table 3.5 again demonstrate the significance of the short-range correlations and form factors in the nonmesonic decay. Adding the heavier mesons without form factors, SRC and FSI (column FREE) leads to a total rate that fluctuates significantly, with the additional mesons giving an appreciable contribution to the π-exchange

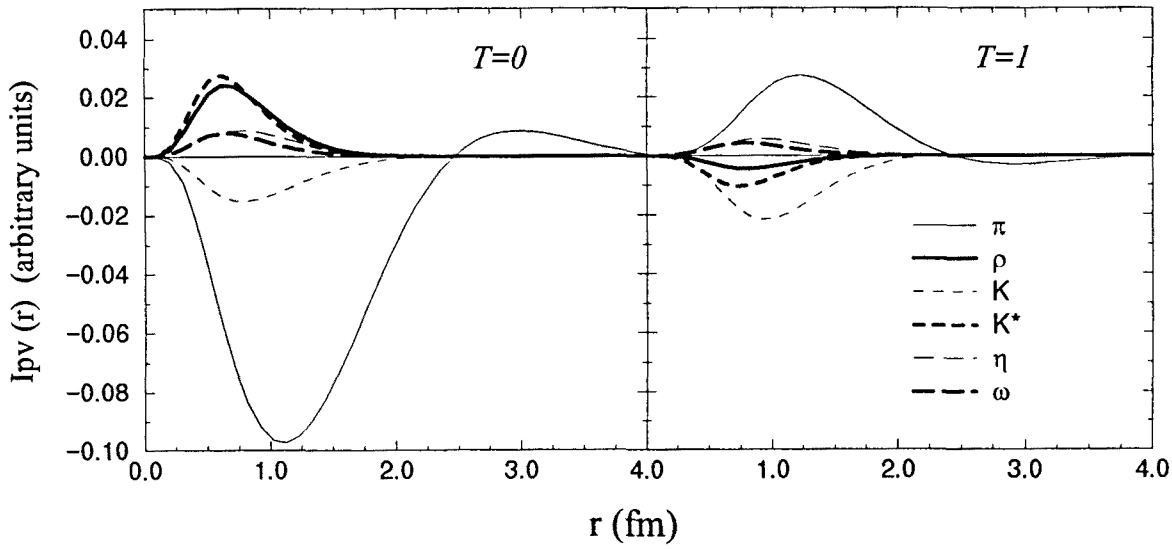

Figure 3.4. Same as Fig. 3.3 for the PV $^3S_1 - ^1P_1$ (T=0) and $^3S_1 - ^3P_1$ (T=1) transition amplitudes.

rate, specially in the case of the Jülich couplings. This behavior is considerably suppressed by short-range effects, as shown in the second column. The rate is especially sensitive to the inclusion of the strange mesons. While including the ρ-meson has almost no effect, the addition of kaon-exchange reduces the total rate by almost 50% when the Nijmegen strong couplings are used, and a little less when using the Jülich couplings. The reduction is mostly compensated by the addition of the K*, yielding, in the Nijmegen case, a rate 15% below the pion-only decay rate. The situation is similar for the η and ω mesons and their combined effect on the rate is negligible. Thus, with Nijmegen couplings adding the heavier mesons gives a reduction of only 15%. The situation is slightly different when the Jülich strong coupling constants are employed; their omission of the η and their larger K* and ω couplings lead to a total rate 15% larger than the pion-only rate. This indicates that the results are sensitive to the model used for the strong vertices, although both results are consistent with the present experimental values. This sensitivity to the strong coupling constants is unfortunate since it will certainly complicate the task of extracting weak couplings from this reaction. Improved YN potentials which narrow the range of the strong coupling

Table 3.5. Free and fully correlated nonmesonic decay rate of $^{12}_{\Lambda}$C in units of the free Λ decay rate (Γ_Λ). The values between parentheses have been calculated using the JülichB coupling constants at the strong vertex.

	FREE	SRC+FF+FSI
π	1.682 (1.682)	0.885 (0.885)
$+\rho$	2.055 (2.325)	0.859 (0.831)
+K	1.336 (1.699)	0.497 (0.506)
+K*	2.836 (3.821)	0.760 (0.902)
$+\eta$	2.467 (3.821)	0.683 (0.902)
$+\omega$	2.301 (4.338)	0.753 (1.023)
weak NNK-couplings from χPT [SS96]		0.844 (1.104)

constants are required to reduce this uncertainty. Table 3.5 also shows the results obtained when the NNK weak coupling constants derived in next-to-leading order χPT [SS96] are used. Due to the smaller value of the coupling constants, the effect of the K meson is reduced, enhancing the accumulated rate and thus increasing the total rate by about 10%.

In Table 3.6 the values for other observables in the weak decay of $^{12}_{\Lambda}$C are presented. They include the accumulated neutron-to-proton ratio, Γ_n/Γ_p, and the asymmetry parameter, a_Λ. The ratio between the PV and the PC partial rates is also given which, even though it is not an observable, may help one to understand the behavior of other quantities, such as the asymmetry, or it can be useful in the comparison with other works.

The results for the ratio of the neutron- to proton-induced partial rates Γ_n/Γ_p, shown in Table 3.6, are, as expected, quite sensitive to the isospin structure of the exchanged mesons. It has been known for a long time that pion-exchange alone produces only a small ratio [MG84]. While the role of the ρ is limited, it is again the inclusion of the two strange mesons that dramatically modifies this partial ratio. In-

Table 3.6. Weak decay observables for $^{12}_{\Lambda}$C. The values between parentheses have been calculated using the JülichB coupling constants at the strong vertex.

	Γ_n/Γ_p	PV/PC	a_Λ
π	0.104 (0.104)	0.665 (0.665)	−0.238 (−0.238)
$+\rho$	0.095 (0.096)	0.930 (1.137)	−0.100 (−0.052)
+K	0.030 (0.029)	2.413 (3.206)	−0.138 (−0.074)
+K*	0.049 (0.070)	1.797 (1.968)	−0.182 (−0.202)
$+\eta$	0.058 (0.070)	2.249 (1.968)	−0.200 (−0.202)
$+\omega$	0.068 (0.109)	2.077 (1.675)	−0.316 (−0.368)
weak NNK-couplings from χPT [SS96]	0.080 (0.108)	1.678 (1.436)	−0.302 (−0.350)

cluding the K-exchange, which interferes destructively with the pion amplitude in the neutron-induced channel (see, for example, the $T = 1$ PV transition amplitudes of Fig. 3.4), leads to a reduction of the ratio by more than a factor of three. The K*, on the other hand, adds contructively. Again, an indication of this behavior can be seen in Figs. 3.3 and 3.4. In the $T = 1$ PV channel, relevant for the n-induced rate, the K and K* amplitudes have the same sign, whereas in both $T = 0$ channels the interference between the two strange mesons is destructive and, as a consequence, the p-induced rate is lowered with respect to the n-induced rate. However, this constructive addition is not enough to restore the Γ_n/Γ_p ratio to the $\pi + \rho$ value. Using the Nijmegen strong coupling constants leads to a final ratio that is 34% smaller than the pion-only ratio, while using the Jülich couplings leaves this ratio unchanged, due again mostly to their larger K* and ω couplings. Employing the weak NNK couplings calculated with χPT has the effect of increasing the Γ_n/Γ_p ratio by 17% with Nijmegen couplings while the ratio remains unchanged for the Jülich model.

As it has been noted before, one expects the addition of the strange mesons to considerably change the value of the Γ_n/Γ_p ratio. This is indeed true and although the desired change should increase the ratio, at the end, the inclusion of both mesons, the

K and the K*, leads to a much smaller ratio than expected.

Table 3.6 also presents the unobservable ratio of PV to PC rates to aid in the comparison with other theoretical calculations. Again, adding the strange mesons produces the largest effect, specially when using the Jülich strong couplings. The final PV/PC ratio is larger by more than a factor of two compared to the pion-only ratio. The nuclear matter results quoted in Ref. [DF96] are of the order of 1 and, therefore, closer to the results obtained in this work with the Jülich model.

The intrinsic asymmetry parameter, a_Λ, shown in the same Table, is also found to be very sensitive to the different mesons included in the model. This is the only observable which is changed dramatically by the inclusion of the ρ, reducing the pion-only value by more than a factor of two (and a factor of four when strong Jülich couplings are used). Adding the other mesons increases a_Λ, leading to a result about 30% larger than for π-exchange alone in the case of the Nijmegen couplings and 50% larger for the Jülich model. The effect of using the weak NNK couplings from χPT is very small for this observable.

3.5 Other Hypernuclei and Comparison with Experiment

Our final results for various shell-model hypernuclei are presented in Table 3.7. The total nonmesonic decay rate, Γ/Γ_Λ, the neutron-to-proton ratio Γ_n/Γ_p, the fraction of the proton induced decay rate to the total decay rate, Γ_p/Γ, the intrinsic lambda asymmetry parameter, a_Λ, and the asymmetry parameter $\mathcal{A}(0°)$ (Eq. (1.20)), are shown separately for ${}^{5}_{\Lambda}$He, ${}^{11}_{\Lambda}$B and ${}^{12}_{\Lambda}$C.

An overall agreement has been found between our results for the nonmesonic rate and the experimental values, specially when the χPT weak couplings for the K meson are used, which yield somewhat larger rates. It is convenient to remind here that, the nonmesonic decay rate presented for the ${}^{5}_{\Lambda}$He hypernucleus would be slightly reduced once one considered dynamical effects tied to the short-range ΛN repulsion, which pushes the Λ wave function to the surface of the nucleus [SN93].

It has been the hope for many years that the inclusion of additional mesons would dramatically increase the ratio of neutron- to proton-induced rates. However, the opposite is found to be true. The final ratio greatly underestimates the newer central experimental values, although the large experimental error bars do not permit any defi-

Table 3.7. Weak decay observables for various hypernuclei. The values between parentheses have been calculated using the NNK weak coupling constants obtained from next-to-leading order in χPT [SS96].

	${}^{5}_{\Lambda}$He	${}^{11}_{\Lambda}$B	${}^{12}_{\Lambda}$C
Γ/Γ_Λ	0.414 (0.467)	0.611 (0.686)	0.753 (0.844)
EXP:	0.41 ± 0.14 [Sz91]	$0.95 \pm 0.13 \pm 0.04$ [No95]	1.14 ± 0.2 [Sz91]
			$0.89 \pm 0.15 \pm 0.03$ [No95]
Γ_n/Γ_p	0.073 (0.089)	0.084 (0.099)	0.068 (0.080)
EXP:	0.93 ± 0.55 [Sz91]	$1.04^{+0.59}_{-0.48}$ [Sz91]	$1.33^{1.12}_{-0.81}$ [Sz91]
		$2.16 \pm 0.58^{+0.45}_{-0.95}$ [No95]	$1.87 \pm 0.59^{+0.32}_{-1.00}$ [No95]
		0.70 ± 0.3 [Mo74]	0.70 ± 0.3 [Mo74]
		0.52 ± 0.16 [Mo74]	0.52 ± 0.16 [Mo74]
Γ_p/Γ_Λ	0.386 (0.428)	0.563 (0.624)	0.705 (0.782)
EXP:	0.21 ± 0.07 [Sz91]	$0.30^{+0.15}_{-0.11}$ [No95]	$0.31^{+0.18}_{-0.11}$ [No95]
a_Λ	-0.273 (-0.264)	-0.391 (-0.378)	-0.316 (-0.302)
$\mathcal{A}(0°)$		-0.120 (-0.116)	-0.030 (-0.029)
EXP:		-0.20 ± 0.10 [Aj92]	-0.01 ± 0.10 [Aj92]

nite conclusion at this time. Other mechanisms that have been explored to remedy this puzzle include quark-model calculations which yield a large violation of the $\Delta T = 1/2$ rule [IT96,MS94], and the consideration of the 3N emission channel (ΛNN$\rightarrow$NNN) as a result of the pion being absorbed on correlated 2N pairs [AP91,RO94]. A recent reanalysis [RV97], which includes FSI of the three nucleons on their way out of the nucleus via a Monte Carlo simulation, shows that the 2N-induced channel further increases the experimental error bars and leads to an experimental value compatible with the predictions of the OPE model. However, the same reference shows that a comparison of the calculated proton spectrum with the experimental one favors values of $\Gamma_n/\Gamma_p = 2$–3. It is therefore imperative, before speculating further about the deficiencies of the present models in reproducing this ratio, to carry out more precise experiments such as the measurement of the number of protons emitted per Λ decay, suggested in Ref. [RV97].

On the other hand, the proton-induced rate which has errors of the same magnitude

as the total rate is overpredicted by our calculations by up to a factor of two. It is the neutron-induced rate which has been very difficult to measure accurately. It is somewhat surprising that while both individual rates appear in disagreement with the data their sum conspires to a total rate which reproduces the measurements.

Regarding the asymmetry parameter, comparison with experiment can only be made at the level of the measured proton asymmetry. As discussed in § 1.2, this quantity is determined as a product of the asymmetry parameter, A_p, characteristic of the weak decay, and the polarization of the hypernucleus, P_y, which must be determined theoretically. The energy resolution of the experiment measuring the decay of polarized ${}^{12}_{\Lambda}$C produced in a (π^+, K^+) reaction [Aj92] was 5 - 7 MeV which did not allow distinguishing between the first three 1^- states. Before the weak decay occurs, the two excited states decay electromagnetically to the ground state. Therefore, in order to determine the polarization at this stage, one requires: i) the polarization of the ground and excited states, together with the corresponding formation cross sections, and ii) an attenuation coefficient to account for the loss of polarization in the transition of the excited states to the ground state. In Ref. [IM94], hypernuclear production cross sections and polarizations have been estimated for the (π^+, K^+) reaction in the distorted wave impulse approximation with configuration-mixed wave functions. One should point out that the sum of the cross sections for the two excited 1^- states amounts to 40% relative to the ground state peak, which is consistent with the $(31 \pm 8)\%$ obtained in a fit to the Brookhaven ${}^{12}\mathrm{C}(\pi^+, \mathrm{K}^+){}^{12}_{\Lambda}\mathrm{C}$ spectrum [Mi91]. Using the values of Ref. [IM94] for the polarization and cross sections of the 1^- states in ${}^{12}_{\Lambda}$C together with the spin depolarization formalism of Ref. [ET89], a value of P_y equal to -0.19 is obtained. This value, together with $A_p = 0.151$ (Nijmegen) or 0.175 (Jülich), determined from a_Λ using Eq. (1.23), leads to an asymmetry $\mathcal{A} = -0.029$ (Nijmegen) or -0.033 (Jülich), which lies within the uncertainties of the experimental result.

The hypernucleus ${}^{11}_{\Lambda}$B is created by particle emission from excited states of ${}^{12}_{\Lambda}$C in which a Λ in a $p_{1/2}$ or $p_{3/2}$ orbit is coupled to a ^{11}C core in its ground state. The window of excitation energy that spans 1.55 MeV between the (p $+{}^{11}_{\Lambda}$B) and the (Λ+^{11}C) particle decay threshold contains three positive-parity states: two 2^+ states separated by ~ 800 keV and a narrow 0^+ state just below the (Λ+^{11}C) threshold. Using the same model of Ref. [IM94], which predicts equal formation cross sections for the 2^+_1 and 2^+_2 states, and neglecting the 0^+ state because of its relatively small cross section, we obtain a polarization of $P_y = -0.29$. However, hypernuclear structure calculations

by Auerbach *et al* [AB83] predicted strong configuration mixing which reduced the cross section of the lower 2^+ state by a factor of three relative to the higher one. This prediction was verified by a reanalysis of older emulsion data [DD86]. Taking these relative weights into account, we obtain the value $P_y = -0.43$, which is the one used in Table 3.7 and leads to better agreement with the experimental asymmetry. Just as in the case of the proton- to neutron-induced ratio, the present level of uncertainty in the experiment does not yet permit using the asymmetry as an observable that differentiates between different models for the weak decay.

In order to avoid the need for theoretical input and access A_p directly, a new experiment at KEK [Ki95] is measuring the decay of polarized ${}^{5}_{\Lambda}$He, extracting both the pion asymmetry from the mesonic channel, $\mathcal{A}_{\pi^-}$, and the proton asymmetry from the nonmesonic decay, $\mathcal{A}$. The asymmetry parameter a_{π^-} of the pionic channel has been estimated to be very similar to that of the free Λ decay [Mo94], and, therefore, the hypernuclear polarization can now be obtained from the relation $P_y = \mathcal{A}_{\pi^-}/a_{\pi^-}$. This in turn can then be used as input, together with the measured value of $\mathcal{A}$, to determine the asymmetry parameter for the nonmesonic decay from the equality $A_p = \mathcal{A}/P_y$. This experiment will not only allow a clean extraction of the nonmesonic asymmetry parameter but will also check theoretical model predictions for the amount of hypernuclear polarization.

Finally, with the purpose of clarifying the present situation concerning the different available results for the nonmesonic decay rate of hypernuclei, Table 3.8 shows the calculated decay rates quoted by several publications, as well as the results exposed throughout this work to facilitate the comparison. The numbers given in this Table have been obtained using different models and prescriptions. Three models are shown: the one-boson-exchange model (OBE) in which the present work is based, the quark model (QM) and a hybrid version based in a one-pion-exchange (OPE) description for long distances and in a QM for shorter ones.

Almost all the works are completely based in a OBE mechanism (without considering the body of this thesis). The first attempt to include heavier mesons was the work of McKellar and Gibson [MG84], where the rho meson was included in addition to the pion for the nonmesonic Λ decay in nuclear matter. Guided by the smallness of the central pion rates, Ref. [MG84] took only into account the tensor transition for the ρ-meson exchange, giving the (π,ρ) rates in terms of the s $\rightarrow$ d contribution. In this calculation, ΛN correlations were treated with a stronger empirical correlation

function than the one derived from a realistic YN interaction and the final states were treated with the Reid soft-core potential. This model was later used in Ref. [TT85] to predict nonmesonic decay rates of light hypernuclei as ${}^{5}_{\Lambda}$He. Both references, [TT85] and [MG84], present the ambiguity given by the relative sign between both mesons.

The nuclear matter calculation of Oset *et al.* [OS85] considers the exchange of a pion in the transition mechanism. The pion is properly modified by its strong interaction with the nuclear medium and no final state interactions are considered. Their Local Density Approximation (LDA) results are also listed in Table 3.8 for two hypernuclei, ${}^{12}_{\Lambda}$C and ${}^{5}_{\Lambda}$He. As already discussed in § 2.4, their results depend somewhat on the choice of the Landau-Migdal parameter, g'_{Λ}, which controls the short-range ΛN correlations.

Dubach *et al* [DF96] go further and consider the exchange of the same set of mesons than in the present work. They include an initial state correlation of the form used in Ref. [MG84], a Reid soft-core potential to generate the final states but omit form factors at the vertices. Their finite nuclei results were obtained using a simple shell-model to describe the hypernuclear structure, where an extreme single-particle model with no configuration mixing and only phenomenological forms for the correlation functions are employed. However, no details of their method are presently available and the values quoted in Table 3.8 must be considered preliminary.

Shinmura [Sh97] performs a relativistic study of the nonmesonic weak decay of light s-shell hypernuclei, where, in addition to the OPE result, the effect of a typical three body mechanism (ΛNN → NNN), which yields about 30% of the calculated total nonmesonic decay rate, is also studied. No final state interactions have been considered in this work.

The Table also quotes a recent work by Itonaga *et al.* [IU95] where, in addition to the OPE potential, two new potentials are built such that two pions couple to ρ and/or σ mesons and intermediate N and Σ baryons.

The generation of a weak transition potential from a quark model point of view is the approach followed by Refs. [HK86,IT96]. Ref. [HK86] evaluates, in the framework of the hybrid-hadron model, the nonmesonic decay rate for nuclear matter as well as for the ${}^{12}_{\Lambda}$C hypernucleus using a shell-model wave function to describe the nuclear structure. An effective correlation function is used to address the problem of two-body correlations. An effective quark weak interation hamiltonian explicitly constructed to incorporate the $\Delta T = 1/2$ rule (guided by renormalization group results including the penguin diagrams) is taken. The authors in Ref. [IT96] consider a direct quark pro-

cess (DQ) via an effective contact four-quark hamiltonian (which contains the QCD corrections on the pure weak vertex) as well as the OPE for the $\Lambda N \rightarrow NN$ transition. The direct quark matrix elements are non-zero only at the short distances where the quarkwave functions overlap each other, while the meson exchanges contribute at longer distances. However, the relation between the phenomenological pionic transition hamiltonian and the effective quark hamiltonian needs to be studied further before the correct superposition of DQ and OPE processes is made. Moreover, their results carry the uncertainty of the phase between the OPE contribution and the QM one in the hybrid calculation shown in the last column of the Table.

From the results in Table 3.8 it is clear that all the nuclear matter calculations are consistent with each other. The results of Ref. [MG84] are almost a factor of two smaller due to the use of a much stronger ΛN correlation function. We note that the π-exchange result of Ref. [HK86] must be combined with the quark contribution, yielding a somewhat larger final value, although it is not clear how the matching point of their hybrid calculation should be chosen and why the amplitudes are combined constructively.

The finite nuclei calculations show a wider variety of results. The values found in the present work for the OPE mechanism seem too low when compared with the LDA approach of Ref. [OS85], but if an appropriate g'_A parameter, suitable for the ΛN correlation used in the present work, is chosen then the LDA value is reduced to 1.1, which is quite similar to the result quoted in Table 3.1 in the absence of final state interactions. The OPE value of 0.46 for ${}^{13}_{\Lambda}$C found in Ref. [IU95] is much lower but no details are given to understand the origin of this discrepancy. The same is true for their ${}^{5}_{\Lambda}$He result when compared with the present work value. However, combining their OPE result with $V_{(2\pi)/\rho}$ and $V_{(2\pi)/\sigma}$ the rates increase and lie very close to the experimental values. The OPE ${}^{5}_{\Lambda}$He results of Refs. [TT85,IU95] are slightly smaller than what is found in other references.

The inclusion of the ρ-meson has been done with the use of different models to generate the weak $\Lambda N\rho$ coupling and, therefore, a variety of quite different results have been obtained. Only the work of Dubach *et al.* [DF96] uses the same model as the present work and this is the reason why, in the following, their results are discussed in more detail. Their preliminary results appear to be very different in comparison with those obtained in the present work. Their uncorrelated OPE-only rate for ${}^{12}_{\Lambda}$C is listed as 3.4 which is about a factor of 2 larger than the one quoted in this work

while adding initial SRC, FF, and FSI reduce this rate to 0.5. This amounts to a reduction factor of almost 7, in contrast to the suppression of roughly a factor of two found here. Furthermore, their correlated rate for ${}^{5}_{\Lambda}$He is listed as 0.9, almost a factor of two larger than their ${}^{12}_{\Lambda}$C result. Unfortunately, no details are given in Ref. [DF96] that address these problems. Note, however, that there are some unexplained inconsistencies between their recent results of Ref. [DF96] and what was reported ten years before in Ref. [Du86], where the correlated π-exchange decay rate for ${}^{12}_{\Lambda}$C is 2.0 while the addition of the other mesons lowers this value to 1.2. In fact, these values are more consistent with their ${}^{5}_{\Lambda}$He results, as well as with the effect of short-range correlations found in almost all studies of the nonmesonic weak decay either in nuclear matter or finite nuclei. Finally, and even though they are not shown in the Table, a brief comparison between the values of the neutron-to-proton ratio and the asymmetry parameter reported in Ref. [DF96] and the ones given in this work, will be made. The present results for Γ_n/Γ_p again differ from what it is reported in Ref. [DF96], where a value $\Gamma_n/\Gamma_p = 0.2$ is obtained for π-exchange alone but 0.83 when all the mesons are included. However, their results in finite nuclei are, surprisingly, quite different from their nuclear matter results, namely $\Gamma_n/\Gamma_p = 0.06$ for π-exchange alone and 0.345 when all mesons are included. With regard to the asymmetry parameter, the nuclear matter results of Ref. [DF96] are qualitatively similar to the results of this work for the Nijmegen couplings. They obtain a value $a_\Lambda = -0.192$ for π-exchange alone and -0.443 when all the mesons are considered.

Table 3.8. Different published results, compared to the ones presented in this work, concerning the Λ nonmesonic weak decay rate in nuclear matter, ${}^{12}_{\Lambda}$C and ${}^{5}_{\Lambda}$He.

Ref.	Remarks	$\Gamma^{nm}/\Gamma_\Lambda$				
		OBE			QM	QM + OPE
		π	π,ρ	all mesons		
[This work]	${}^{12}_{\Lambda}$C	0.885	0.859	0.753		
	${}^{5}_{\Lambda}$He	0.486	0.474	0.414		
McKellar	nuc. matter	1.06	2.91 ($\pi+\rho$)			
[MG84]			0.11 ($\pi-\rho$)			
Takeuchi	${}^{5}_{\Lambda}$He	0.14	0.45 ($\pi+\rho$)			
[TT85]			0.03 ($\pi-\rho$)			
Oset	nuc. matter	2.1				
[OS85]	LDA ${}^{12}_{\Lambda}$C	1.45				
	LDA ${}^{5}_{\Lambda}$He	1.15				
Dubach	nuc. matter	1.85		1.38		
[DF96]	${}^{12}_{\Lambda}$C	0.5		0.2		
	${}^{5}_{\Lambda}$He	0.9		0.5		
Shinmura	${}^{5}_{\Lambda}$He	0.42				
[Sh97]						
Itonaga	${}^{5}_{\Lambda}$He	0.20	0.13†	0.44††		
[IU95]	${}^{13}_{\Lambda}$C	0.46		1.05††		
Heddle	nuc. matter	0.77			0.73	3.0
[HK86]	${}^{12}_{\Lambda}$C	0.41			0.24	1.28
Inoue	${}^{5}_{\Lambda}$He	0.333			0.381	0.574 (QM+OPE)
[IT96]						0.855 (QM−OPE)

† $\pi + 2\pi/\rho$

†† $\pi + 2\pi/\rho + 2\pi/\sigma$

Chapter 4

A Special Case: The Nonmesonic Weak Decay of the Hypertriton

The hypertriton (${}^{3}_{\Lambda}$H), consisting of a pnΛ bound state, is the bound nuclear system of lowest mass with one hyperon with which one can test YN forces, including the Λ-Σ conversion. All experimental information obtained for the hypertriton comes from early bubble chamber measurements and emulsion works more than 20 years ago and contains large uncertainties. However, different proposals exist (COSY, BNL and TJNL) devoted to measuring the lifetime of ${}^{3}_{\Lambda}$H. In the TJNL experiment [TJNL] the production of ${}^{3}_{\Lambda}$H would proceed via the kaon photoproduction reaction ^{3}He (γ,K^{+}) ${}^{3}_{\Lambda}$H, although it has to be kept in mind that the cross sections for this process are predicted to be very small [MT96] ($\approx$ 1 nb). On the other hand, in the COSY experiment [COSY] the hypertriton would be produced via a two step reaction leading to p+d $\rightarrow$ K^{+} + ${}^{3}_{\Lambda}$H, using an incident beam momentum of 1848 MeV/c, where an enhanced fusion probability of the deuteron and the Λ is expected. A more likely candidate is the experiment proposed at Brookhaven [BNL] where the ^{4}He (K^{-}, π^{0}) ${}^{4}_{\Lambda}$H reaction will be studied and where there exist plans to obtain the hypertriton.

The hypertriton lifetime is dominated by the non-suppressed mesonic decay mode, since there is not phase space restrictions and the momentum of the final nucleon (100 MeV/c) is sufficient to lift the nucleon above the Fermi sea. Theoretical estimates

[DR62] predict that this mesonic mode is about 5-10 % less than that of the free Λ. Even though the nonmesonic decay channel is not as important in ${}^{3}_{\Lambda}$H as for heavier hypernuclei, it is interesting to test this decay mechanism in the hypertriton, due to the fact that the wave function in the initial state can be calculated exactly using the Faddeev formalism.

When one uses a formalism which includes both Λ and Σ degrees of freedom, one handles a coupled channel problem between the ΛNN and ΣNN systems. This coupled channel incorporates a three-body force and leads to a modification of the YN force due to the presence of a second nucleon. This effect is the so-called dispersive effect. As we can see in Refs. [MG93,MK95], one can solve the Faddeev equations for the coupled ΛNN and ΣNN systems precisely using meson-theoretical NN and YN interactions. With the use of the Jülich hyperon-nucleon interaction in a one-boson-exchange potential parametrization combined with various realistic NN interactions, the hypertriton turns out to be unbound [MG93]. This is just the opposite to what happens when using the Nijmegen interaction with full inclusion of the Λ-Σ conversion: independently of the specific choice of the various realistic NN forces, the hypertriton turns out to be bound at the experimental binding energy (-2.35 ± 0.05 MeV). One reason for the unbound feature appearing when the Jülich interaction is used might be the weaker attraction of this potential at very low energies of up to a few MeV, which corresponds to the typical kinetic energy of the Λ particle in the hypertriton. Another explanation can be traced to the different Λ-Σ conversion potential obtained in the Jülich case.

As we have seen in previous chapters, the study of the nonmesonic decay of p-shell hypernuclei found that proper short-range correlations in the initial and final states are of major importance in predicting decay rates and asymmetry observables. The present work has been performed in a shell-model framework, including bound state wave functions, spectroscopic factors, short-range correlations and final state interactions in the weak decay mechanism. These ingredients do not all originate from the same underlying dynamics and, therefore, introduce approximations that may be difficult to quantify. The decay of few-body hypernuclei offers a window to extract information on hadronic weak vertices from the ΛN$\rightarrow$NN process, since all nuclear structure ingredients are derived from the same baryon-baryon interaction.

Previous calculations of the nonmesonic decay of the hypertriton [BRA92] used a simplified uncorrelated Λ-deuteron wave function, where the ${}^{3}_{\Lambda}$H is taken to be a deuteron and a Λ particle moving in an effective Λ-d potential and where the influence

of the lambda on the two nucleons was neglected. However, since the mesons emitted by the weak hyperon-nucleon transition are reabsorbed by the nucleons, one expects that correlations should play an important role. The resulting meson-exchange operator acts like a two-body force and consequently probes the hypertriton wave function in its dependence on the pair distance between a hyperon and a nucleon. Another ingredient neglected in Ref. [BRA92] is the strong interaction between the three final nucleons, fully incorporated here.

Troughout this chapter, the nonmesonic decay of the ${}^{3}_{\Lambda}$H hypernucleus will be studied using a hypertriton wave function and 3N scattering states which are rigorous solutions of 3-body Faddeev equations. The weak transition potential has been already described in § 2.1.3.

4.1 Formalism of the Weak Decay of Hypertriton

As for the other hypernuclei studied in this work, the exchange of the pion together with heavier mesons in the two-body ΛN→NN transition are considered. The form of the transition potential corresponding to these exchanges is not going to be repeated here, and only the expression for the nonrelativistic decay probabilities will be presented.

When analyzing the weak decay of the hypertriton, two different nonmesonic channels come into consideration. These channels differ in the final state, leading to n+d and n+n+p final systems. For each of these decays the nonrelativistic partial probabilities are given by [Go97]:

$$\begin{aligned} d\Gamma^{\mathrm{n+d}} &= \frac{1}{2} \sum_{m\, m_{\mathrm{N}}\, m_d} |< \Psi^{(-)}_{\vec{k}_{\mathrm{N}}\, \vec{k}_d\, m_{\mathrm{N}}\, m_d} \mid \hat{O} \mid \Psi_{{}^{3}_{\Lambda}\mathrm{H}\, m} >|^2 \\ &\times\ d\vec{k}_{\mathrm{N}}\, d\vec{k}_d\, 2\pi\, \delta(\vec{k}_{\mathrm{N}} + \vec{k}_d)\, \delta\left(M_{{}^{3}_{\Lambda}\mathrm{H}} - M_{\mathrm{N}} - M_d - \frac{\vec{k}_{\mathrm{N}}{}^2}{2M_{\mathrm{N}}} - \frac{\vec{k}_d{}^2}{2M_d} \right) \end{aligned} \tag{4.1}$$

and

$$\begin{aligned} d\Gamma^{\mathrm{n+n+p}} &= \frac{1}{2} \sum_{m\, m_1\, m_2\, m_3} |< \Psi^{(-)}_{\vec{k}_1\, \vec{k}_2\, \vec{k}_3\, m_1\, m_2\, m_3} \mid \hat{O} \mid \Psi_{{}^{3}_{\Lambda}\mathrm{H}\, m} >|^2 \\ &\times\ d\vec{k}_1\, d\vec{k}_2\, d\vec{k}_3\ 2\pi\, \delta(\vec{k}_1 + \vec{k}_2 + \vec{k}_3) \\ &\times\ \delta\left(M_{{}^{3}_{\Lambda}\mathrm{H}} - 3M_{\mathrm{N}} - \frac{\vec{k}_1{}^2}{2M_{\mathrm{N}}} - \frac{\vec{k}_2{}^2}{2M_{\mathrm{N}}} - \frac{\vec{k}_3{}^2}{2M_{\mathrm{N}}} \right), \end{aligned} \tag{4.2}$$

where $\Psi^{(-)}$ stands for the appropriate final nuclear scattering state, $\hat{O}$ for the transition operator and $\Psi_{^{3}_{\Lambda}\mathrm{H}}$ for the hypertriton wave function.

More details of the calculation and an extensive discussion on the results can be found in Ref. [Go97]. Here, only the basic ideas discussed in this reference will be presented.

After introducing the Jacobi momenta for the final 3N states:

$$\vec{p} = \frac{1}{2}(\vec{k}_1 - \vec{k}_2) \tag{4.3}$$

$$\vec{q} = \frac{2}{3}\left(\vec{k}_3 - \frac{1}{2}(\vec{k}_1 + \vec{k}_2)\right) \tag{4.4}$$

the decay probability for the nd breakup ($\vec{k}_3 = \vec{k}_{\mathrm{N}}$ and $\vec{k}_{\mathrm{d}} = \vec{k}_1 + \vec{k}_2$) reads:

$$d\Gamma^{\mathrm{n+d}} = \frac{1}{2}\sum_{m\, m_{\mathrm{N}}\, m_{\mathrm{d}}} |\langle \Psi^{(-)}_{\vec{q}_0\, m_{\mathrm{N}}\, m_{\mathrm{d}}} \mid \hat{O} \mid \Psi_{^{3}_{\Lambda}\mathrm{H}\, m}\rangle|^2\, 2\pi \frac{2M_{\mathrm{N}}}{3} q_0 d\hat{q}, \tag{4.5}$$

with

$$q_0 = \sqrt{\frac{4M_{\mathrm{N}}}{3}(M_\Lambda - M_{\mathrm{N}} + \epsilon - \epsilon_{\mathrm{d}})} \tag{4.6}$$

and where ϵ and ϵ_{d} stand for the hypernucleus and for the deuteron binding energies, respectively. When averaging over spin projections the squared matrix element of $d\Gamma^{\mathrm{n+d}}$ becomes independent on $\hat{q}$. The final formula for obtaining the total decay rate for the nd break up is given by:

$$\Gamma^{\mathrm{n+d}} = 8\pi^2 \frac{2M_{\mathrm{N}}}{3} q_0 \frac{1}{2} \sum_{m\, m_{\mathrm{N}}\, m_{\mathrm{d}}} |< \Psi^{(-)}_{\vec{q}_0\, m_{\mathrm{N}}\, m_{\mathrm{d}}} \mid \hat{O} \mid \Psi_{^{3}_{\Lambda}\mathrm{H}\, m} >|^2 . \tag{4.7}$$

Similarly, for the n+n+p decay one gets

$$d\Gamma^{\mathrm{n+n+p}} = \frac{1}{2} \sum_{m\, m_1\, m_2\, m_3} |< \Psi^{(-)}_{\vec{p}\,\vec{q}\, m_1\, m_2\, m_3} \mid \hat{O} \mid \Psi_{^{3}_{\Lambda}\mathrm{H}\, m} >|^2\, 2\pi \frac{2M_{\mathrm{N}}}{3} q d\hat{q}\, d\hat{p} p^2 dp \tag{4.8}$$

with

$$q = \sqrt{\frac{4M_{\mathrm{N}}}{3}\left(M_\Lambda - M_{\mathrm{N}} + \epsilon - \frac{\vec{p}^{\,2}}{M_{\mathrm{N}}}\right)}. \tag{4.9}$$

For the $d\Gamma^{\mathrm{n+n+p}}$ case, only a dependence on the angle θ between $\hat{p}$ and $\hat{q}$ remains, and the differential decay rate reads:

$$\begin{aligned} d\Gamma^{\mathrm{n+n+p}} &= 16\pi^3 \frac{2}{3} M_{\mathrm{N}}\, q\, p^2\, dp\, \sin\theta\, d\theta \frac{1}{2} \\ &\times \sum_{m\, m_1\, m_2\, m_3} |< \Psi^{(-)}_{\vec{p}\,\vec{q}\, m_1\, m_2\, m_3} \mid \hat{O} \mid \Psi_{^{3}_{\Lambda}\mathrm{H}\, m} >|^2 . \end{aligned} \tag{4.10}$$

This form is convenient for the integration to determine the total (nnp) decay rate. If one wants to display the angular and energy distribution of the three nucleons in the n+n+p channel, it is more convenient to use the following form:

$$d\Gamma^{\mathrm{n+n+p}} = \frac{1}{2} \sum_{m\, m_1\, m_2\, m_3} |< \Psi^{(-)}_{\vec{p}\,\vec{q}\, m_1\, m_2\, m_3} \mid \hat{O} \mid \Psi_{^3_\Lambda \mathrm{H}\, m} >|^2$$
$$\times\ 2\pi\, d\hat{k}_1\, d\hat{k}_2\, dS \frac{M_N^2\, k_1^2\, k_2^2}{\sqrt{k_1^2(2k_2 + \vec{k}_1 \cdot \hat{k}_2)^2 + k_2^2(2k_1 + \vec{k}_2 \cdot \hat{k}_1)^2}}\,, \quad (4.11)$$

with $\hat{k}_1$ and $\hat{k}_2$ denoting the directions of two detected nucleons and S the arclength along the kinematically allowed locus in the $E_1 - E_2$ energy plane for these nucleons (see Fig. 4.1).

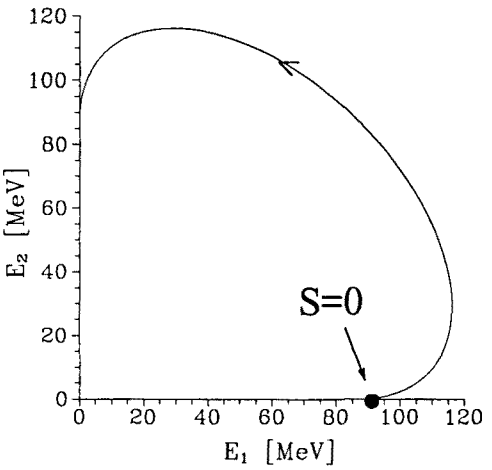

Figure 4.1. Locus for kinematically allowed events in the $E_1 - E_2$ plane and $\theta_{12} = 180°$. From the S=0 point on, S is evaluated for each point on the locus in the counterclockwise sense.

For the sake of simplifying the notation, Eq. (4.11) does not include the identification of the detected particles 1 and 2 as a proton-neutron pair or as two neutrons. One must keep in mind that the final scattering states should carry additional isotopic spin quantum numbers.

As we have seen in § 2, the $\hat{O}$ operator is of two-body character, acting between the Λ and one of the nucleons in the hypernucleus. Choosing the lambda to be particle 1, one gets:

$$\hat{O} = \sum_{i=2,3} \hat{O}(1,i) \tag{4.12}$$

where $i = 2,3$ represents each of the nucleons. Once one antisymmetrizes the initial and final states, the following expression for the hypernuclear matrix element holds:

$$\langle \Psi^{(-)} \mid \hat{O} \mid \Psi_{^{3}_{\Lambda}\mathrm{H}} \rangle = 2 \, \langle \Psi^{(-)} \mid \hat{O}(1,2) \mid \Psi_{^{3}_{\Lambda}\mathrm{H}} \rangle \; . \tag{4.13}$$

4.2 The Initial and Final States

In this section, a brief discussion on the initial and final wave functions used in this work will be given. For more details one is referred again to Ref. [Go97].

4.2.1 The Hypertriton Wave Function

In the following, a hypertriton wave function based on the Nijmegen93 NN potential [SK94] and the Nijmegen YN interaction [NR77] which includes the $\Lambda - \Sigma$ transitions, will be used. In order to keep both states for the hyperons, Λ and Σ, explicitly, the wave function of the hypertriton has to be built up of two orthogonal parts [MG93,MK95]:

$$|\Psi> = |\mathrm{NN}\Lambda> \Psi_{\mathrm{NN}\Lambda} + |\mathrm{NN}\Sigma> \Psi_{\mathrm{NN}\Sigma} \; . \tag{4.14}$$

The energy eigenvalue problem reads:

$$(E - \underline{H}_0) \, \underline{\Psi} = \underline{V} \, \underline{\Psi} \; , \tag{4.15}$$

where the underline stands for a compact matrix notation for H_0, V and Ψ, which can be found explicitly written in Ref. [MG93]. For instance, the function $\underline{\Psi}$ has two components, $\Psi_{\mathrm{NN}\Lambda}$ and $\Psi_{\mathrm{NN}\Sigma}$, as written explicitly in Eq. (4.14). Denoting the nucleons by 1 and 2 and the Λ or Σ by 3, the integral form of this energy eigenvalue problem provides the Faddeev decomposition:

$$\underline{\Psi} = \frac{1}{E - \underline{H}_0} \, \underline{V} \, \underline{\Psi} \equiv \underline{\psi}^{(12)} + \underline{\psi}^{(13)} + \underline{\psi}^{(23)} \; , \tag{4.16}$$

with

$$\underline{\psi}^{(ij)} \equiv \frac{1}{E - \underline{H}_0} \, \underline{V}_{ij} \underline{\Psi} \; . \tag{4.17}$$

Inserting the decomposition of Eq. (4.16) in Eq. (4.17) and summing up $\underline{V}_{ij}$ within the pair ij to infinite order yields the matrix Faddeev equations

$$\underline{\psi}^{(ij)} = \frac{1}{E - \underline{H}_0} \underline{T}_{ij} \sum_{kl \neq ij} \underline{\psi}^{(kl)} . \tag{4.18}$$

Assuming $\underline{\Psi}$ to be antisymmetrized in the two nucleons (1,2) it follows that:

$$P_{12}\underline{\psi}^{(13)} = -\underline{\psi}^{(23)} , \tag{4.19}$$

where P_{12} is the permutation operator acting between the two nucleons labelled by 1 and 2. Therefore it suffices to regard only two coupled (matrix) Faddeev equations:

$$\underline{\psi}^{(12)} = \frac{1}{E - \underline{H}_0} \underline{T}_{12} (1 - P_{12})\underline{\psi}^{(13)} \tag{4.20}$$

and

$$\underline{\psi}^{(13)} = \frac{1}{E - \underline{H}_0} \underline{T}_{13} (\underline{\psi}^{(12)} - P_{12}\underline{\psi}^{(13)}) , \tag{4.21}$$

where the two-body T matrices obey the (matrix) Lippmann-Schwinger equations:

$$\underline{T}_{ij} = \underline{V}_{ij} + \underline{V}_{ij} \frac{1}{E - \underline{H}_0} \underline{T}_{ij} , \tag{4.22}$$

with $ij, kl = 12, 13, 23$. Note that each of the two Faddeev amplitudes has two components:

$$\underline{\psi}^{(ij)} = \begin{bmatrix} \psi_\Lambda^{(ij)} \\ \psi_\Sigma^{(ij)} \end{bmatrix} . \tag{4.23}$$

In the case of the two-nucleon $\underline{T}$ operator, the 2×2 $\underline{T}_{12}$ matrix is diagonal and only the free propagator distinguishes the presence of a Λ or a Σ. For the hyperon-nucleon operator this is not the case, and one faces coupled Lippmann-Schwinger equations. This T-matrix incorporates the $\Lambda N \longleftrightarrow \Lambda N$, $\Sigma N \longleftrightarrow \Sigma N$ and the $\Lambda N \longleftrightarrow \Sigma N$ transitions. After solving the coupled equations (4.20) and (4.21) for $\underline{\psi}^{(12)}$ and $\underline{\psi}^{(13)}$, the two parts of the total wave function in Eq. (4.14) are given by:

$$\Psi_{NN\Lambda} = \psi_\Lambda^{(12)} + (1 - P_{12})\psi_\Lambda^{(13)} \tag{4.24}$$

$$\Psi_{NN\Sigma} = \psi_\Sigma^{(12)} + (1 - P_{12})\psi_\Sigma^{(13)} . \tag{4.25}$$

The antisymmetry in the two nucleons of the total wave function is guaranteed by choosing $\psi_{\Sigma,\Lambda}^{(12)}$ to be antisymmetric in 1 and 2.

Even though the $\Lambda - \Sigma$ conversion is crucial for the binding of the hypertriton, the ΣNN admixture in the hypertriton wave function is extremely small (with a 0.5 % of probability) and the contribution of the Σ decay can be neglected keeping only the ΛNN part.

For the evaluation of the transition operator matrix elements and for the solution of the Faddeev equation, a partial wave representation is used [MK95]. The number of channels used in the solution of the corresponding Faddeev equation is 102, which leads to a fully converged state which has the proper antisymmetrization among the nucleons built in.

For the hypertriton state it is convenient to take the form in which one of the nucleons acts as an spectator:

$$\mid \Psi_{^3_\Lambda\mathrm{H}} \rangle = \sum_\alpha \int dp\, p^2 \int dq\, q^2 \mid pq\alpha \rangle \, \Psi_\alpha(pq) \;, \tag{4.26}$$

where p and q are the magnitudes of the Jacobi momenta

$$\vec{p} = \frac{M_\mathrm{N}\vec{k}_1 - M_\Lambda \vec{k}_2}{M_\mathrm{N} + M_\Lambda} \tag{4.27}$$

$$\vec{q} = \frac{(M_\mathrm{N} + M_\Lambda)\,\vec{k}_3 - M_\mathrm{N}\,(\vec{k}_1 + \vec{k}_2)}{2M_\mathrm{N} + M_\Lambda} \;, \tag{4.28}$$

and α denotes the set of discrete quantum numbers $\alpha \equiv (ls)j\,(\lambda\frac{1}{2})I\,(jI)J\,(t\frac{1}{2})T$. The $(ls)j$ term describes the coupling of the orbital angular momentum l and the intrinsic spin s to the total two-body angular momentum j of the ΛN subsystem. The $(\lambda\frac{1}{2})I$ term refers to the same quantities for the other nucleon in the hypertriton. Both subsystems (ΛN and N) couple to a total angular momentum J and to a total isospin $T = 0$ (coming from the coupling of the $t_{\Lambda\mathrm{N}} = 1/2$ and the $t_\mathrm{N} = 1/2$ isospin values of each subsystem).

4.2.2 The Final 3N State

Two different final states can be obtained in the nonmesonic weak decay of $^3_\Lambda$H, the n+d state and the n+n+p three nucleon state. The deuteron and the final state interaction among the three nucleons is generated using the Nijmegen93 NN force, including the NN force components up to total two-body angular momentum $j = 2$. This is sufficient to get a converged result for the nuclear matrix element. Since the total 3-body angular momentum is conserved, the corresponding Faddeev equation

for the final state interaction (FSI) only has to be solved for total three-body angular momentum J=1/2, but for both parities due to the parity-violating transition potential.

It is briefly shown here, as an example, how to include the final state interactions among the three final nucleons for the nnp breakup process. The scattering state $\Psi^{(-)} \equiv \Psi^{(-)}_{\vec{p}\,\vec{q}}$ is Faddeev decomposed [Gl83] as:

$$\Psi^{(-)} = (1+P)\,\psi^{(-)} \;, \tag{4.29}$$

where P is the sum of a cyclical and anticyclical permutation of 3 objects and $\psi^{(-)}$ is one Faddeev component. This component obeys the Faddeev equation:

$$\psi^{(-)} = \phi^{(-)} + G_0^{(-)}\, t^{(-)}\, P\, \psi^{(-)} \;, \tag{4.30}$$

with

$$\phi^{(-)} = (1 + G_0^{(-)}\, t^{(-)})\, \phi_0^{\rm a} \tag{4.31}$$

and

$$\phi_0^{\rm a} = \frac{1}{\sqrt{3!}}\,(1-P_{12})\mid \phi_0\rangle \equiv \frac{1}{\sqrt{6}}\,(1-P_{12})\mid \vec{p}\,\rangle \mid \vec{q}\,\rangle \;. \tag{4.32}$$

In the last expressions, $G_0^{(-)}$ stands for the free three-nucleon propagator, $t^{(-)}$ for the NN (off-shell) t-matrix and $1/\sqrt{6}$ takes care of the identity of the three nucleons. The permutation operator P_{12} acts in the two-body susbsystem described by the relative momentum $\vec{p}$.

Inserting Eqs. (4.29), (4.30) and (4.31) into Eq. (4.13) and iterating (4.30), the hypernuclear matrix element can be put into the form:

$$\begin{aligned} \langle\, \Psi^{(-)}_{\vec{p}\,\vec{q}} \mid \hat{O}(1,2) \mid \Psi_{^3_\Lambda{\rm H}}\,\rangle \;&=\; \langle\, \phi_0^{\rm a} \mid (1+P)\,\hat{O}(1,2) \mid \Psi_{^3_\Lambda{\rm H}}\,\rangle \\ &+\; \langle\, \phi_0^{\rm a} \mid (1+P) \mid \mathcal{U}\,\rangle \;, \end{aligned} \tag{4.33}$$

where $\mid \mathcal{U}\rangle$ obeys the Faddeev equation:

$$\mid \mathcal{U}\,\rangle \;=\; t\,G_0\,(1+P)\,\hat{O}(1,2) \mid \Psi_{^3_\Lambda{\rm H}}\,\rangle + t\,G_0\,P \mid \mathcal{U}\,\rangle \;. \tag{4.34}$$

Keeping just the first term on the right hand side of Eq. (4.33) is equivalent to select the pure plane wave impulse approximation to solve the problem. Similar steps yield the corresponding expression for the nd breakup process, given by:

$$\langle\, \Psi^{(-)}_{\vec{q}_0} \mid \hat{O}(1,2) \mid \Psi_{^3_\Lambda{\rm H}}\,\rangle = \langle\, \phi \mid (1+P)\,\hat{O}(1,2) \mid \Psi_{^3_\Lambda{\rm H}}\,\rangle + \langle\, \phi \mid P \mid \mathcal{U}\,\rangle \;, \tag{4.35}$$

where now $\mid \phi\rangle$ contains the deuteron state $\mid \varphi_{\rm d}\rangle$:

$$\mid \phi\,\rangle = \mid \varphi_{\rm d}\,\rangle \mid \vec{q}_0\,\rangle \;. \tag{4.36}$$

4.3 Results

The total nonmesonic decay rate (in units of the free Λ decay rate, $\Gamma_\Lambda = 3.8 \times 10^9$ s^{-1}) obtained for the hypertriton within this model is $\Gamma/\Gamma_\Lambda = 5.58 \times 10^{-3}$, which is about one order of magnitude smaller than what has been found in Ref. [BRA92]. In Table 4.1 the individual contributions of the six mesons to the nonmesonic decay rate Γ_{nm}, and the way each of them contributes to the final result, are shown. As for the p-shell hypernuclei studied previously, the pion is found to provide the largest contribution. One can see that the K, the K* and the ω mesons also give large individual rates. When adding all the mesons in an arbitrary order, a varying sequence in the rates is observed. However, the final result, obtained with the exchange of the six mesons, is only 12% smaller than the corresponding rate for the π-only exchange.

Table 4.1. Decay rates in units of Γ_Λ for individual meson exchanges and for partially summed up exchanges.

	Γ^{meson}	$\Gamma^{\text{partially summed}}$	
π	6.35×10^{-3}	π	6.35×10^{-3}
η	0.13×10^{-3}	$\pi + \eta$	6.05×10^{-3}
K	1.43×10^{-3}	$\pi + \eta + \mathrm{K}$	2.44×10^{-3}
ρ	0.20×10^{-3}	$\pi + \eta + \mathrm{K} + \rho$	1.97×10^{-3}
ω	1.15×10^{-3}	$\pi + \eta + \mathrm{K} + \rho + \omega$	4.61×10^{-3}
K*	1.47×10^{-3}	$\pi + \eta + \mathrm{K} + \rho + \omega + \mathrm{K}^*$	5.58×10^{-3}

In § 4.2, the total decay rate was expressed as the sum of the partial rates for the nd and nnp decays. The four first rows in Table 4.2 show these partial rates when only the π-exchange contribution (first column) is considered, and the results obtained exchanging the whole set of mesons (second column). The nnp decay is clearly dominant in both cases. The symmetrized plane wave impulse approximation (PWIAS) is also shown, and the comparison of the PWIAS results to the full one underlines the relevance of the final state interaction, which produces a considerable reduction in the rate.

Table 4.2. Selected decay rates in units of Γ_Λ for π–exchange only and for exchange of all mesons.

	π–exchange only	Exchange of all mesons
Γ^{n+d}_{PWIAS}	1.553×10^{-3}	1.237×10^{-3}
Γ^{n+d}	0.395×10^{-3}	0.579×10^{-3}
Γ^{n+n+p}_{PWIAS}	12.105×10^{-3}	9.474×10^{-3}
Γ^{n+n+p}	6.053×10^{-3}	5.000×10^{-3}
Γ^{n+d}_{PC}	0.232×10^{-3}	0.579×10^{-3}
Γ^{n+d}_{PV}	0.155×10^{-3}	0.006×10^{-3}
Γ^{n+n+p}_{PC}	3.421×10^{-3}	3.158×10^{-3}
Γ^{n+n+p}_{PV}	2.421×10^{-3}	1.921×10^{-3}

In the last four rows, the parity-conserving (PC) and parity-violating (PV) parts of the transition are listed separately for completeness. The PC rate is dominant, specially in the nd decay.

It is well known that theoretically one can choose the Λ-particle to interact with a neutron or a proton in the hypernucleus, in order to separate the neutron and proton induced decay mechanisms, Γ_n and Γ_p, respectively. In Table 4.3 these Γ_n and Γ_p partial rates are shown for each nd and nnp channel, as well as for the total reaction including both channels. It is obvious that the n- and p-induced transitions add coherently in the evaluation of the total decay rate, and this is clearly evidenced in the same table, specially for the nd decay. However, in the 3N decay channel the total decay rate is very close to the sum of the individual rates for the n- and p-induced processes. Nevertheless these individual decay rates cannot be measured separately. In Fig. 4.2 the values for S and the angle between the two nucleon detectors, θ_{12}, under which the n- and p-induced decay events can be found, are shown. Those events are selected such that their sum corresponds to 60% and 90% of their respective total decay rates. Thereby the differential decay rates are summed up starting with the largest values downwards. The pictures refer to the detection of a neutron-proton pair. If one is satisfied to

Table 4.3. Proton- and neutron- induced decay rates in units of Γ_Λ for π–exchange only and for the exchange of all mesons in comparison to the total nd and nnp rates.

	π–exchange only	Exchange of all mesons
$\Gamma_{(n)}^{n+d}$	0.053×10^{-3}	0.168×10^{-3}
$\Gamma_{(p)}^{n+d}$	0.205×10^{-3}	0.184×10^{-3}
Γ^{n+d}	0.395×10^{-3}	0.579×10^{-3}
$\Gamma_{(n)}^{n+n+p}$	1.553×10^{-3}	1.500×10^{-3}
$\Gamma_{(p)}^{n+n+p}$	4.737×10^{-3}	3.421×10^{-3}
Γ^{n+n+p}	6.053×10^{-3}	5.000×10^{-3}

collect 60% of the n- and p-induced decay, the events occur in kinematically separated regions. For the 90% case however the two detectors receive events from both processes. Therefore, one has to conclude that despite the fact that Γ^{n+n+p} is rather close to the sum of $\Gamma_{(p)}^{n+n+p}$ and $\Gamma_{(n)}^{n+n+p}$, the latter values cannot be determined experimentally, only fractions, the smaller, the cleaner.

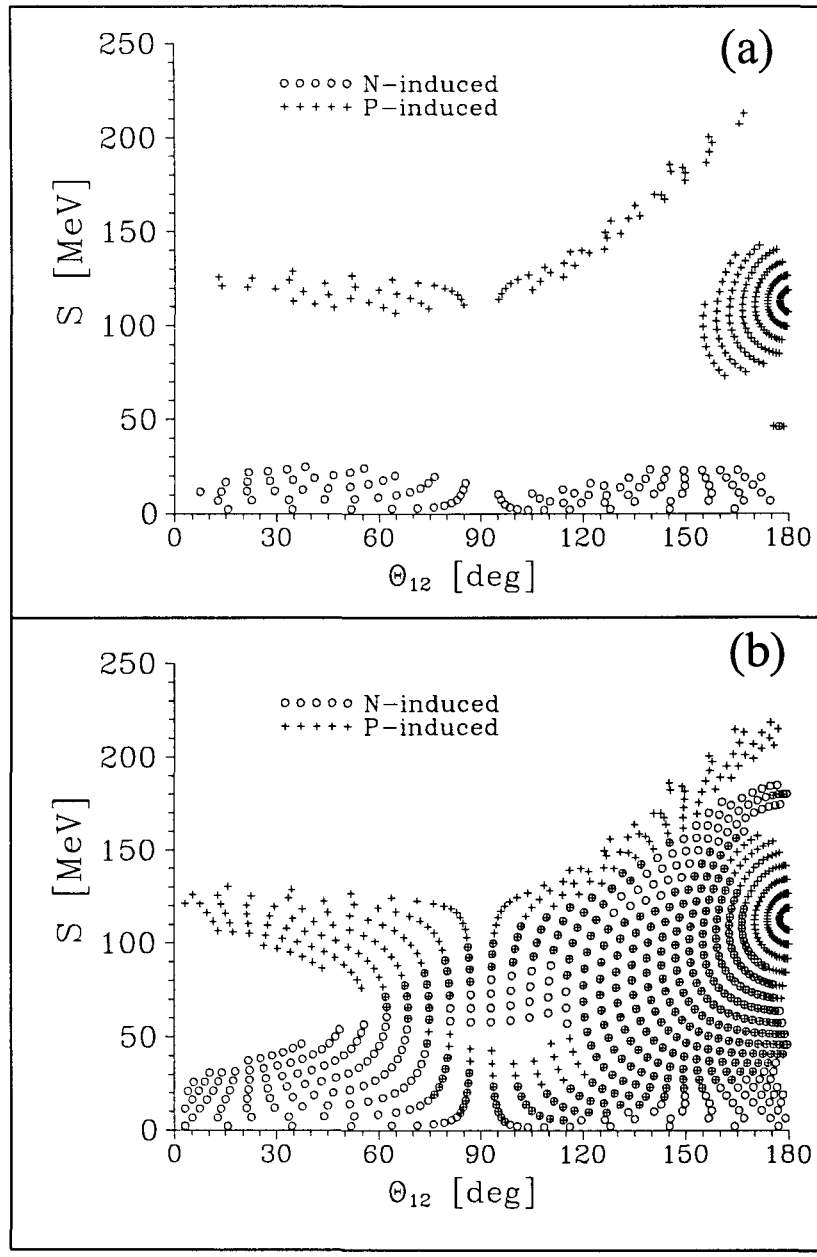

Figure 4.2. The separate regions in the $\theta_{12} - S$ plane contributing to (a) 60% and (b) 90% of the rates of n- and p-induced decays. Note the strong overlap of the different processes in phase space in case (b).

Chapter 5

Conclusions

The present work has analyzed the weak nonmesonic decay mode, $\Lambda N \rightarrow NN$, in Λ-hypernuclei, using a shell-model approach for the description of the hypernucleus. Many different ingredients have been considered for evaluating the hypernuclear weak decay, in order to treat the nuclear structure details with as few approximations and ambiguities as possible. One of these ingredients is the use of spectroscopic factors to describe the structure of the initial hypernuclear system, as well as the final nuclear system. Troughout this study, s-shell and p-shell hypernuclei have been explored, and all the possibilities for the initial and final relative angular momenta have been included in the calculation. The importance of short-range effects has been emphasized through the consideration of short-range correlations for the initial ΛN system as well as for the final NN system. This has been done via the inclusion of realistic ΛN and NN interactions based on the Nijmegen baryon-baryon potential.

The present calculations have been performed in a one-boson-exchange model that includes not only the long-ranged pion but also contributions from the other pseudoscalar mesons, the η and K, as well as the vector mesons ρ, ω and K*. The weak baryon-baryon-meson PV vertices have been obtained using SU(3) symmetry for pseudoscalar mesons, SU(6) symmetry for vector mesons and soft-meson theorems. For the evaluation of the weak PC vertices, the pole model has been used. The primary goal of this work was to reduce nuclear structure uncertainties as much as possible so

that our framework can be used to extract these weak baryon-baryon-meson couplings. However, the task of extracting these constants becomes difficult due to the sensitivity shown by our results to the different models used in the strong sector.

The conclusions of this work can be summarized as follows:

Total decay rate

- The OPE mechanism dominates the total nonmesonic decay rate in magnitude and in range.

- The rate is specially sensitive to the inclusion of strange mesons. Their influence is considerable not only in the rate but also in the neutron-to-proton ratio, due to their special isospin structure.

  The second-largest contribution to the rate comes from the K-meson, which amounts to 15% of the individual OPE rate but with a shorter range. The importance of kaon exchange makes it possible to see the effects of modifying the weak NNK couplings by loop contributions from next-to-leading order χPT. Including these loop graphs leads to a reduction of the NNK couplings from their tree-level value up to 30%, which in turns modifies the K-rate by a factor of 2. Future experiments should be able to verify this effect.

  The K meson contribution is followed by that of the K* which tends to partially cancel the effects of the kaon. It is imperative that future studies include both strange mesons simultaneously.

- The role of the ρ meson is found to be less relevant than expected. Our results for its contribution to the total decay rate differ substantially from the ones quoted by previous calculations, where the central potential in the ρ-exchange diagram was omitted and different models for the $\Lambda N\rho$ coupling constants were used.

- The combined effect of the isoscalar η and ω mesons in the rate is almost negligible.

- There is large interference between the different mesons contributing to the total decay rate, and the evaluation of the contribution of each isospin-like pair [(π,ρ), (K,K*) and (η,ω)] leads to destructive interference between both components of each pair.

- Due to the different ranges of the various mesons considered in the exchange, their contribution is modified differently when SRC and FF are included. Adding the heavier mesons to the pion-exchange mechanism leads to fluctuating accumulated rates, and end up reducing the π-exchange rate by only 15%.

- The decay process is very sensitive to short-range effects. It is therefore imperative to use appropriate short-range correlations for the initial and final two-body states.

  In this work the discrepancies between relativistic and nonrelativistic approaches on the effect of SRC have been understood. It has been shown that the appropriate method to include correlations is that followed by the nonrelativistic treatment.

- Due to the sensitivity of our results to the different models used for the vertices, a more accurate set of coupling constants is needed.

  Using the Nijmegen constants in the strong sector leads to a total rate (including all the mesons) which is 15% smaller than the OPE rate, while the use of Jülich constants leads to a total rate 15% larger than in the pion case. However, both results are consistent with the experimental value for the rate. Improved YN potentials which narrow the range of the strong coupling constants are required to reduce the uncertainty in their values.

  Once the breaking of SU(3) symmetry is taken into account via the use of NNK weak coupling constants derived in next-to-leading order χPT, the effect of the K meson is reduced, increasing the total rate by about 10% and bringing the result closer to the experimental value.

- When computing the nonmesonic weak decay rates for different hypernuclei, an overall agreement with the corresponding experimental values is obtained.

  In the case of the ${}^{12}_{\Lambda}$C and ${}^{11}_{\Lambda}$B hypernuclei, for which a mean field description of the wave function is a rather realistic picture, one can see a good agreement with the experimental data. For ${}^{5}_{\Lambda}$He, one should further consider dynamical effects tied to the short-range ΛN repulsion, which pushes the Λ wave function to the surface of the nucleus. This would reduce slightly the decay rate obtained in this work.

Calculations performed in nuclear matter and using the LDA can reproduce accurately the finite nucleus results presented throughout this work. The choice of an appropriate value of the Landau-Migdal parameter, which controls the amount of SRC in the LDA approach, is crucial to bring the results closer.

The neutron-to-proton induced decay ratio

- The Γ_n/Γ_p ratio is quite sensitive to the isospin structure of the exchanged mesons. The inclusion of the strange K and K* mesons modify strongly this ratio, as it has been suggested for many years. The K meson reduces this value by about a factor of three, while the K* meson adds constructively leading a value which is half the one corresponding to the pion, when the Nijmegen strong coupling constants are used.

  Even though the strange mesons considerably change the value of the Γ_n/Γ_p ratio, adding all the mesons reduces the value bringing it further away from all the experimental results obtained until now.

- Furthermore, this ratio turns out to be sensitive to the choice of strong coupling constants as well. Using the Nijmegen strong couplings reduces the ratio by 30% from its pion-only value while the use of the Jülich strong couplings leads to a change of only a few percent.

- The present model predicts Γ_n/Γ_p values that are much smaller than the central experimental ones. However, due to the large experimental error bars, one can not draw definite conclusions about the evaluation of this ratio. More precise experiments are needed in order to correct possible deficiencies present in the theoretical results obtained until now.

- It is worth noticing that while the individual Γ_n and Γ_p disagree with the data their sum conspires to a total rate which reproduces the measurements quite well.

The intrinsic lambda asymmetry parameter

- The intrinsic lambda asymmetry parameter, a_Λ, is also quite sensitive to the inclusion of additional mesons in the weak mechanism.

  In contrast to the previous observables we found the proton asymmetry to be very sensitive to the ρ-exchange while the influence of the kaon is more moderate. The strongest modification in the value of this parameter is caused by the

addition of the ρ and ω mesons. The final value obtained when the whole set of mesons is included is 30% or 50% larger than the value corresponding to the OPE mechanism, depending of the strong coupling constants used.

The asymmetry is therefore an important addition to the set of observables since its sensitivity to the various ingredients is different from the total and partial rates.

- There is a considerable level of uncertainty in the experiments concerning the measure of the asymmetry parameter. It is again this uncertainty which prevents one from using the asymmetry as an observable that can select between the different models for the weak decay at this stage.

5.1 Future Perspectives

This study clearly indicates that further theoretical effort must be invested to understand the dynamics of the nonmesonic weak hypernuclear decay. At present, it appears to be impossible to reconcile the discrepancies observed in the partial rates when using the different available models for the coupling constants within a one-boson-exchange potential. In order to approach the present experimental values, the weak couplings of the heavier mesons would have to be unreasonably large which would yield very large total rates incompatible with the data. The sensitivity shown by the Γ_n/Γ_p ratio and the asymmetry to the values of the weak coupling constants is an indication that these observables could be used to discriminate between different theoretical models, as soon as new data with reduced statistical errors are available. Within the one-meson exchange picture it would be desirable to use weak coupling constants developed with more sophisticated approaches. A beginning has been made by Savage and Springer [SS96] in their evaluation of the weak NNK couplings in next-to-leading order χPT and the effect has been found to be important. However, an understanding of the weak $\Lambda N\pi$ and $\Sigma N\pi$ couplings within the framework of chiral lagrangians is still missing. Furthermore, due to the importance of the K*-meson it would be desirable to recalculate its weak NNK* couplings in improved models as well.

Several recent studies [IT96] have gone beyond the conventional picture of meson exchange and have developed mechanisms based purely on quark degrees of freedom. These works [IT96,CH83,HK86], although promising, are still at an early stage. The

obtained results depend upon the relative sign between the pion contribution and the one from quarks, which are assumed to be independent. One should keep in mind, however, that such models have not always been able to reproduce the experimentally measured free hyperon decays. Efforts continue in this direction trying to establish the connection between the effective quark hamiltonian and the empirical $\Lambda \rightarrow N\pi$ vertex.

Another avenue that is currently being pursued is the validity of the $\Delta T = 1/2$ rule in the $\Lambda N \rightarrow NN$ process. While this empirical rule is well established for the free hyperon and kaon decays there is some indication that it could be violated for the $\Lambda N \rightarrow NN$ process. Within the framework of SU(3) and soft-meson theorems the weak NNK and $\Lambda N\eta$ vertices are related to the observable $\Lambda N\pi$ decay and, therefore, one would expect small $\Delta T = 3/2$ contributions for these mesons. On the other hand, the vector meson vertices can receive substantial contributions from factorization terms which have been shown not to fulfil the $\Delta T = 1/2$ rule [MS94]. The attractive feature of these additional terms is their strong influence on the ratio Γ_n/Γ_p.

On the level of implanting the basic $\Lambda N \rightarrow NN$ amplitude into the nucleus, uncertainties have been minimized in this study by treating each ingredient as well as possible. Nevertheless, within the framework of the impulse approximation and the use of a shell-model description for the nuclear systems, the short-range correlations, the spectroscopic factors and the single particle wavefunctions still come from separate sources. This dilemma can be avoided in rigorous few-body calculations with realistic wave functions. The nonmesonic decay of the hypertriton has been calculated using correlated three-body hypernuclear wave functions for the initial hypertriton state and continuum Faddeev solutions for the three-nucleon scattering state [Go97]. Thus, all nuclear structure input is generated from the same underlying YN- and NN-potentials, eliminating the ambiguities of the shell-model approach. It is therefore of utmost importance to pursue experimental measurements of the nonmesonic decay of this light hypernucleus.

Other works [IU95,Sh94] incorporate, in addition to the pion, the exchanges of the σ and the ρ mesons. In these new potentials ($V_{2\pi/\sigma}$ and $V_{2\pi/\rho}$), two pions are coupled to each of these mesons and the intermediate baryon is allowed to be a Σ or a nucleon, the weak process taking place at the $\Lambda \rightarrow N\pi$ or $\Sigma \rightarrow N\pi$ vertex. However, it was found that this inclusion increases the value of the Γ_n/Γ_p ratio to values around 0.2, which, although going in the right direction, are still far from the empirical values.

On the experimental side, it is critical to obtain new high accuracy data soon.

Improved partial rates for the proton- and neutron-induced decay modes are specially important. Of help would be to not only measure rates but also exclusive spectra of the decay products. Such distributions would be significant to disentangle the effects of the $\Lambda NN \rightarrow NNN$ process from the two-body process discussed here. Recent works [RO94,RV97] studied this 2N induced Λ decay channel and analyzed the possible repercussions of this mechanism in extracting the neutron-to-proton induced ratio from the measured data. After the calculation of the spectra of neutrons and protons following the decay of the Λ in several hypernuclei, through the one- and two-nucleon induced mechanisms, it was found that the two-nucleon channel was relevant specially in the determination of the Γ_n/Γ_p ratio. The fraction of this decay channel was found to be only 30% of the free Λ width, or 20% of the total Λ width in the nucleus, but the error band in Γ_n/Γ_p was actually enlarged with respect to a determination omitting this channel in the analysis. It was also pointed out that the ratio Γ_n/Γ_p can be determined reliably provided one can measure the number of emitted protons and neutrons with sufficient precision.

Beyond improving the present data base for the weak decay of Λ-hypernuclei, there are two more avenues which would aid our understanding of the weak $\Delta S = 1$ hadronic interaction.

First, with the advent of new, high precision proton accelerators such as COSY in Jülich, it may become possible to perform a direct study of the time-reversed process $pn \rightarrow \Lambda p$ [Ha95]. While the very low cross sections will make this direct investigation of the $\Delta S = 1$ baryon-baryon interaction difficult to measure, high efficiency detection schemes should allow determining a branching ratio of 10^{-13}. Thus, the strangeness changing hadronic weak interaction could be studied similarly to the weak parity-violating NN interaction. The asymmetry of this reaction has been measured at several kinematics which are sensitive to different parts of the meson-exchange potential. Furthermore, measuring the $p\,n \rightarrow \Lambda\,p$ process directly would give access to a number of polarization observables since the Λ is self-analyzing.

Secondly, the hypernuclear weak decay studies should be extended to double-Λ hypernuclei. Very few events involving these exotic objects — whose very existence would place stringent constraints on the existence of the elusive H-dibaryon — have been reported. Studying the weak decay of these objects would open the door to a number of new exotic Λ-induced decays: $\Lambda\Lambda \rightarrow \Lambda N$ and $\Lambda\Lambda \rightarrow \Sigma N$. Both of these decays would involve hyperons in the final state and should be distinguishable from

the ordinary $\Lambda N \rightarrow NN$ mode. Specially the $\Lambda\Lambda \rightarrow \Lambda N$ channel would be intruiging since the dominant pion exchange is forbidden, thus this reaction would have to occur mostly through kaon exchange. One would therefore gain access to the $\Lambda\Lambda K$ vertex.

The promising efforts at KEK with an improved measurement of the ${}^{5}_{\Lambda}\mathrm{He}$ decay, the continuing program at BNL, and the advent of the hypernuclear physics program (FINUDA) at DAΦNE represent excellent opportunities to obtain new valuable information that will shed light onto the still unresolved problems of the weak decay of hypernuclei.

Appendix A

Coefficients $\langle (L'S)JM_J|\hat{O}_\alpha|(L_rS_0)JM_J\rangle$

In this Appendix the explicit expressions for the $\langle (L'S)JM_J|\hat{O}_\alpha|(L_rS_0)JM_J\rangle$ coefficients appearing in the evaluation of the relative ΛN $\rightarrow$ NN amplitude ($t_{\rm rel}$ in § 2.3), will be given. The quantum numbers L_r, S_0, J and M_J stand for the initial ΛN state, while the numbers L', S, J and M_J correspond to the final NN system. Note that due to the scalar nature of the spin-space $\hat{O}_\alpha$ operator, the values of the total angular momentum and its projection, J and M_J respectively, are conserved by the transition.

A.1 Central Transition

$$\hat{O}_\alpha = \hat{1}$$
$$\langle (L'S)JM_J|\hat{O}_\alpha|(L_rS_0)JM_J\rangle = \delta_{L_rL'}\ \delta_{S_0S} \qquad \text{(A.1)}$$

A.2 Spin-Spin Transition

$$\hat{O}_\alpha = \vec{\sigma}_1\vec{\sigma}_2$$
$$\langle (L'S)JM_J|\hat{O}_\alpha|(L_rS_0)JM_J\rangle = (2S(S+1)-3)\ \delta_{L_rL'}\ \delta_{S_0S} \qquad \text{(A.2)}$$

A.3 Tensor Transition

$$\begin{aligned}\hat{O}_\alpha &= S_{12}(\hat{r}) = 3\vec{\sigma}_1\hat{r}\vec{\sigma}_2\hat{r} - \vec{\sigma}_1\vec{\sigma}_2 \\ \langle (L'S)JM_J|\hat{O}_\alpha|(L_rS_0)JM_J\rangle &= S^J_{L_rL'}\ \delta_{S_0S}\ \delta_{S1}\ ,\end{aligned} \tag{A.3}$$

where the coefficients $S^J_{L_rL'}$ are given in Table A.1.

A.4 Parity-Violating Transition

A.4.1 Pseudoscalar Mesons

$$\begin{aligned}&\hat{O}_\alpha = \vec{\sigma}_2\hat{r} \\ &\langle (L'S)JM_J|\hat{O}_\alpha|(L_rS_0)JM_J\rangle \\ &\qquad = (-1)^{J+1-L'}\sqrt{6}\sqrt{2S_0+1}\sqrt{2L_r+1}\sqrt{2S+1} \\ &\qquad \times \langle 10L_r0|L'0\rangle \begin{pmatrix} \frac{1}{2} & \frac{1}{2} & S_0 \\ S & 1 & \frac{1}{2} \end{pmatrix} \begin{pmatrix} L' & L_r & 1 \\ S_0 & S & J \end{pmatrix}\end{aligned} \tag{A.4}$$

A.4.2 Vector Mesons

$$\begin{aligned}&\hat{O}_\alpha = [\vec{\sigma}_1 \times \vec{\sigma}_2]\,\hat{r} \\ &\langle (L'S)JM_J|\hat{O}_\alpha|(L_rS_0)JM_J\rangle \\ &\qquad = \mathrm{i}(-1)^{J-L'+S}6\sqrt{6}\sqrt{2S_0+1}\sqrt{2L_r+1}\sqrt{2S+1} \\ &\qquad \times \langle 10L_r0|L'0\rangle \begin{pmatrix} L' & L_r & 1 \\ S_0 & S & J \end{pmatrix} \begin{pmatrix} 1 & 1 & 1 \\ \frac{1}{2} & \frac{1}{2} & S \\ \frac{1}{2} & \frac{1}{2} & S_0 \end{pmatrix}\end{aligned} \tag{A.5}$$

Table A.1. Matrix elements of the tensor operator evaluated between generalized spherical harmonic states of definite J,L and S

$S^J_{L_r L'}$	$L' = J+1$	$L' = J$	$L' = J-1$
$L_r = J+1$	$\frac{-2(J+2)}{2J+1}$	0	$\frac{6\sqrt{J(J+1)}}{2J+1}$
$L_r = J$	0	2	0
$L_r = J-1$	$\frac{6\sqrt{J(J+1)}}{2J+1}$	0	$\frac{-2(J-1)}{2J+1}$

Appendix B
PV amplitudes. An example

Ref. [D82] gives the necessary steps for obtaining the unphysical PV amplitudes via the use of soft-meson techniques and SU(3) symmetry. The point is to relate these quantities to the physical PV amplitudes for the nonleptonic hyperon decays B $\rightarrow$ B' + π. As an example, the $\langle nK^+ \mid H_{pv} \mid p \rangle$ amplitude will be derived in this section. To obtain this quantity the following tools will be necessary:

- The definition of the K^+-meson as a member of the pseudoscalar-meson octet ($\pi^{\pm}, \pi^0$, $K^{\pm}$, $K^0, \overline{K}^{\,0}, \eta$) and the definition of the proton and the neutron as members of the spin 1/2 octet ($\Sigma^{\pm}, \Sigma^0, p, \Xi^-, n, \Xi^0, \Lambda$).

$$K^+ = \frac{1}{\sqrt{2}}(M_4 + iM_5) \tag{B.1}$$

$$p = \frac{1}{\sqrt{2}}(B_4 + iB_5) \tag{B.2}$$

$$n = \frac{1}{\sqrt{2}}(B_6 + iB_7) \tag{B.3}$$

- The soft-meson reduction theorem given in Eq. (2.65).
- The action of the SU(3) generator F_i on a baryon B_j given by Eq. (2.66).
- The coupling defined in Eq. (2.67).

- The values of the f_{ijk} (completely antisymmetric) and d_{ijk} (completely symmetric) SU(3) coefficients shown in Table B.1.

Let us write the desired PV amplitude explicitely as:

$$\langle \mathrm{nK}^+ \mid H_{\mathrm{pv}} \mid \mathrm{p} \rangle = \frac{1}{2\sqrt{2}} \langle (\mathrm{B}_6 - \mathrm{i}\mathrm{B}_7)\ (\mathrm{M}_4 - \mathrm{i}\mathrm{M}_5) \mid H_{\mathrm{pv}} \mid (\mathrm{B}_4 + \mathrm{i}\mathrm{B}_5) \rangle\ . \tag{B.4}$$

Applying the soft-meson reduction theorem to the last equation one gets the following expression for the loww energy limit,

$$\begin{aligned} \lim_{q\to 0} \langle \mathrm{nK}^+ \mid H_{\mathrm{pv}} \mid \mathrm{p} \rangle \ = \ & -\frac{\mathrm{i}}{F_\pi}\ \frac{1}{2\sqrt{2}}\ \Big\{ \langle \mathrm{B}_6 \mid F_4 H^6 - H^6 F_4 \mid \mathrm{B}_4 \rangle \\ & -\mathrm{i}\ \langle \mathrm{B}_6 \mid F_5 H^6 - H^6 F_5 \mid \mathrm{B}_4 \rangle\ -\mathrm{i}\ \langle \mathrm{B}_7 \mid F_4 H^6 - H^6 F_4 \mid \mathrm{B}_4 \rangle \\ & -\ \langle \mathrm{B}_7 \mid F_5 H^6 - H^6 F_5 \mid \mathrm{B}_4 \rangle\ +\mathrm{i}\ \langle \mathrm{B}_6 \mid F_4 H^6 - H^6 F_4 \mid \mathrm{B}_5 \rangle \\ & +\ \langle \mathrm{B}_6 \mid F_5 H^6 - H^6 F_5 \mid \mathrm{B}_5 \rangle\ +\ \langle \mathrm{B}_7 \mid F_4 H^6 - H^6 F_4 \mid \mathrm{B}_5 \rangle \\ & -\mathrm{i}\ \langle \mathrm{B}_7 \mid F_5 H^6 - H^6 F_5 \mid \mathrm{B}_5 \rangle \Big\}\ . \end{aligned} \tag{B.5}$$

Taking into account that:

$$F_4 \mid \mathrm{B}_4 \rangle = 0 \tag{B.6}$$

$$F_4 \mid \mathrm{B}_5 \rangle = \frac{\mathrm{i}}{2} \mid \mathrm{B}_3 \rangle + \frac{\sqrt{3}\mathrm{i}}{2} \mid \mathrm{B}_8 \rangle \tag{B.7}$$

$$F_4 \mid \mathrm{B}_6 \rangle = \frac{\mathrm{i}}{2} \mid \mathrm{B}_2 \rangle \tag{B.8}$$

$$F_4 \mid \mathrm{B}_7 \rangle = \frac{\mathrm{i}}{2} \mid \mathrm{B}_1 \rangle \tag{B.9}$$

$$F_5 \mid \mathrm{B}_4 \rangle = -\frac{\mathrm{i}}{2} \mid \mathrm{B}_3 \rangle - \frac{\sqrt{3}\mathrm{i}}{2} \mid \mathrm{B}_8 \rangle \tag{B.10}$$

$$F_5 \mid \mathrm{B}_5 \rangle = 0 \tag{B.11}$$

$$F_5 \mid \mathrm{B}_6 \rangle = -\frac{\mathrm{i}}{2} \mid \mathrm{B}_1 \rangle \tag{B.12}$$

$$F_5 \mid \mathrm{B}_7 \rangle = \frac{\mathrm{i}}{2} \mid \mathrm{B}_2 \rangle\ , \tag{B.13}$$

the limit of the amplitude takes the form:

$$\begin{aligned} \lim_{q\to 0} \langle \mathrm{nK}^+ \mid H_{\mathrm{pv}} \mid \mathrm{p} \rangle \ = \ & -\frac{\mathrm{i}}{F_\pi}\ \frac{1}{2\sqrt{2}}\ \Big\{ \langle \mathrm{B}_6 \mid H^6 \mid \mathrm{B}_3 \rangle + \sqrt{3}\ \langle \mathrm{B}_6 \mid H^6 \mid \mathrm{B}_8 \rangle \\ & -\mathrm{i}\ \langle \mathrm{B}_7 \mid H^6 \mid \mathrm{B}_3 \rangle - \sqrt{3}\mathrm{i}\ \langle \mathrm{B}_7 \mid H^6 \mid \mathrm{B}_8 \rangle \Big\}\ , \end{aligned} \tag{B.14}$$

with

$$\langle \mathrm{B}_6 \mid H^6 \mid \mathrm{B}_3 \rangle = \mathrm{i}\mathrm{A} f_{636} + \mathrm{B} d_{636} = -\frac{1}{2}\mathrm{B} \tag{B.15}$$

$$\langle \mathrm{B}_6 \mid H^6 \mid \mathrm{B}_8 \rangle = \mathrm{i}\mathrm{A} f_{686} + \mathrm{B} d_{686} = -\frac{1}{2\sqrt{3}}\mathrm{B} \tag{B.16}$$

$$\langle \mathrm{B}_7 \mid H^6 \mid \mathrm{B}_3 \rangle = \mathrm{i}\mathrm{A} f_{637} + \mathrm{B} d_{637} = \frac{1}{2}\mathrm{i}\mathrm{A} \tag{B.17}$$

$$\langle \mathrm{B}_7 \mid H^6 \mid \mathrm{B}_8 \rangle = \mathrm{i}\mathrm{A} f_{687} + \mathrm{B} d_{687} = -\frac{\sqrt{3}}{2}\mathrm{i}\mathrm{A} \,. \tag{B.18}$$

Finally one can express the limit of the PV amplitude in terms of the reduced matrix elements A and B in the following way:

$$\lim_{q\to 0} \langle \mathrm{n}\mathrm{K}^+ \mid H_{\mathrm{pv}} \mid \mathrm{p} \rangle = -\frac{\mathrm{i}}{F_\pi} \frac{1}{2\sqrt{2}} (-\mathrm{A} - \mathrm{B}) \,. \tag{B.19}$$

Let us now relate this quantity to the physical amplitudes for the Λ^0_- ($\Lambda \to \pi^- + \mathrm{p}$) and Σ^+_0 ($\Sigma \to \pi^0 + \mathrm{p}$) decays. Once again Ref. [D82] is used to get:

$$\Lambda^0_- = -\frac{\mathrm{i}}{F_\pi} \frac{-3\mathrm{A} - \mathrm{B}}{4\sqrt{3}} \tag{B.20}$$

$$\Sigma^+_0 = -\frac{\mathrm{i}}{F_\pi} \frac{\mathrm{A} - \mathrm{B}}{4} \,. \tag{B.21}$$

From these relations one can solve A and B in terms of Λ^0_- and Σ^+_0:

$$-\frac{\mathrm{i}}{F_\pi}\mathrm{A} = -\sqrt{3}\,\Lambda^0_- + \Sigma^+_0 \tag{B.22}$$

$$-\frac{\mathrm{i}}{F_\pi}\mathrm{B} = -\sqrt{3}\,\Lambda^0_- - 3\,\Sigma^+_0 \tag{B.23}$$

and substitute their corresponding expressions in Eq. (B.19) getting the final result:

$$\lim_{q\to 0} \langle \mathrm{n}\mathrm{K}^+ \mid H_{\mathrm{pv}} \mid \mathrm{p} \rangle = \sqrt{\frac{3}{2}}\,\Lambda^0_- + \frac{1}{\sqrt{2}}\,\Sigma^+_0 \,. \tag{B.24}$$

Table B.1. Non-zero elements of the SU(3) coefficients f_{ijk} and d_{ijk}

ijk	f_{ijk}	ijk	d_{ijk}
123	1	118	$\sqrt{\frac{1}{3}}$
147	$\frac{1}{2}$	146	$\frac{1}{2}$
156	$-\frac{1}{2}$	157	$\frac{1}{2}$
246	$\frac{1}{2}$	228	$\sqrt{\frac{1}{3}}$
257	$\frac{1}{2}$	247	$-\frac{1}{2}$
345	$\frac{1}{2}$	256	$\frac{1}{2}$
367	$-\frac{1}{2}$	338	$\sqrt{\frac{1}{3}}$
458	$\frac{1}{2}\sqrt{3}$	344	$\frac{1}{2}$
678	$\frac{1}{2}\sqrt{3}$	355	$\frac{1}{2}$
		366	$-\frac{1}{2}$
		377	$-\frac{1}{2}$
		448	$-\frac{1}{2\sqrt{3}}$
		558	$-\frac{1}{2\sqrt{3}}$
		668	$-\frac{1}{2\sqrt{3}}$
		778	$-\frac{1}{2\sqrt{3}}$
		888	$-\sqrt{\frac{1}{3}}$